











Effects of trophic status, water level, and temperature on shallow lake metabolism and metabolic balance: A standardized pan-European mesocosm experiment

Ulrike Scharfenberger  <https://orcid.org/0000-0001-9564-5327>, Erik Jeppesen, Meryem Beklioğlu, Martin Søndergaard  <https://orcid.org/0000-0002-1514-0482>, David G. Angeler, Ayşe İdil Çakıroğlu, Stina Drakare  <https://orcid.org/0000-0002-7389-2105>, Josef Hejzlar  <https://orcid.org/0000-0002-7186-4776>, Aldoushy Mahdy, Eva Papastergiadou  <https://orcid.org/0000-0003-4430-878X>, Michal Šorf  <https://orcid.org/0000-0002-9368-6421>, Konstantinos Stefanidis  <https://orcid.org/0000-0002-9121-3188>, Arvo Tuvikene  <https://orcid.org/0000-0001-5520-1166>, Priit Zingel  <https://orcid.org/0000-0003-1629-2063>, Rita Adrian  <https://orcid.org/0000-0002-6318-7189>

DOI

[10.1002/lno.11064](https://doi.org/10.1002/lno.11064)

Original publication date

02 November 2018

Document version

Accepted version

Published in

Limnology and Oceanography

Citation (Vancouver)

Scharfenberger U, Jeppesen E, Beklioğlu M, Søndergaard M, Angeler DG, Çakıroğlu Aİ, et al. Effects of trophic status, water level, and temperature on shallow lake metabolism and metabolic balance: A standardized pan-European mesocosm experiment. *Limnology and Oceanography*. 2019;64(2):616-31.

Disclaimer

This is the peer reviewed version of the following article: Scharfenberger U, Jeppesen E, Beklioğlu M, Søndergaard M, Angeler DG, Çakıroğlu Aİ, et al. Effects of trophic status, water level, and temperature on shallow lake metabolism and metabolic balance: A standardized pan-European mesocosm experiment. *Limnology and Oceanography*. 2019;64(2):616-31 which has been published in final form at <https://doi.org/10.1002/lno.11064>. This article may be used for non-commercial purposes in accordance with Wiley Terms and Conditions for Use of Self-Archived Versions.

Title: Effects of trophic status, water level, and temperature on shallow lake metabolism and metabolic balance: A standardized pan-European mesocosm experiment

Running head: Shallow lakes metabolism

List of authors: Ulrike Scharfenberger^{1,2}, Erik Jeppesen^{3,4}, Meryem Beklioğlu^{5,6}, Martin Søndergaard³, David G. Angeler⁷, Ayşe İdil Çakıroğlu⁸, Stina Drakare⁷, Josef Hejzlar⁹, Aldoushy Mahdy¹⁰, Eva Papastergiadou¹¹, Michal Šorř^{9,12}, Konstantinos Stefanidis¹³, Arvo Tuvikene¹⁴, Priit Zingel¹⁴, Rita Adrian^{1,2}

Institute of origin:

¹Department of Ecosystem Research, Leibniz Institute of Freshwater Ecology and Inland Fisheries, (IGB), Müggelseedamm 310, 12587 Berlin, Germany

²Department of Biology, Chemistry, Pharmacy, Freie Universität Berlin, Takustr. 3, 14195 Berlin, Germany

³Department of Bioscience and the Arctic Research Centre, Aarhus University, Silkeborg, Denmark

⁴Sino-Danish Centre for Education and Research (SDC), Beijing, China

⁵Department of Biology, Limnology Laboratory, Üniversiteler Mahallesi, Middle East Technical University, Dumlupınar Bulvarı, 06800, Çankaya, Ankara, Turkey

⁶Kemal Kurdas, Ecological Research and Training Station, Lake Eymir, Middle East Technical University, Oran Mahallesi, 06400 Çankaya, Ankara, Turkey

23 ⁷Department of Aquatic Sciences and Assessment, Swedish University of Agricultural Sciences,
24 Uppsala, Sweden

25 ⁸Mechanical Engineering Department, Koc University, Rumelifeneri Yolu, 34450 Sarıyer
26 Istanbul, Turkey

27 ⁹Institute of Hydrobiology, Biology Centre of the Czech Academy of Sciences, Na Sádkách 7,
28 37005 České Budějovice, Czech Republic

29 ¹⁰Department of Zoology, Faculty of Science, Al-Azhar University (Assiut Branch), Assiut
30 71524, Egypt

31 ¹¹Department of Biology, University of Patras, University campus, 26504, Rio, Greece.

32 ¹²Faculty of Science, University of South Bohemia, Branišovská 31, 370 05 České Budějovice,
33 Czech Republic

34 ¹³Department of Water Resources and Environmental Engineering, School of Civil Engineering,
35 National Technical University of Athens, 5, Iroon Politechniou Street, Zografou, Athens, Greece

36 ¹⁴Centre for Limnology, Institute of Agricultural and Environmental Sciences, Estonian
37 University of Life Sciences, Tartumaa, 61117 Rannu, Estonia

38

39 **List of institutional email address for each author:**

40 Ulrike Scharfenberger^{1,2} – scharfenberger@igb-berlin.de,

41 Erik Jeppesen^{3,4} – ej@dmu.dk

42 Meryem Beklioğlu^{5,6} – meryem@metu.edu.tr

43 Martin Søndergaard³ – ms@dmu.dk

44 David G. Angeler⁷ – david.angeler@slu.se

45 Ayşe İdil Çakıroğlu⁸ – acakiroglu@ku.edu.tr

46 Stina Drakare⁷ – Stina.Drakare@slu.se

47 Josef Hejzlar⁹ – Josef.Hejzlar@seznam.cz

48 Aldoushy Mahdy¹⁰ – aldoushy@azhar.edu.eg

49 Eva Papastergiadou¹¹ – evapap@upatras.gr

50 Michal Šorf^{9,12} – michal.sorf@centrum.cz

51 Konstantinos Stefanidis¹³ – kstefani@chi.civil.ntua.gr

52 Arvo Tuvikene¹⁴ – arvo.tuvikene@emu.ee

53 Priit Zingel¹⁴ – priit.zingel@emu.ee

54 Rita Adrian^{1,2} – adrian@igb-berlin.de

55

56 **Corresponding author:** Ulrike Scharfenberger, Telephone: +49 30 64 181 690, Fax: +49 30 64

57 181 663, email: scharfenberger@igb-berlin.de

58

59 **Keywords:** Metabolism, shallow lakes, trophic state, water level change, temperature threshold,

60 climate change

Abstract

Important drivers of gross primary production (GPP) and ecosystem respiration (ER) in lakes are temperature, nutrients, and light availability, which are predicted to be affected by climate change. Little is known about how these three factors jointly influence shallow lakes metabolism and metabolic status as net heterotrophic or autotrophic. We conducted a pan-European standardized mesocosm experiment covering a temperature gradient from Sweden to Greece to test the differential temperature sensitivity of GPP and ER at two nutrient levels (mesotrophic or eutrophic) crossed with two water levels (1 and 2 m) to simulate different light regimes. The findings from our experiment were compared with predictions made according the metabolic theory of ecology (MTE). GPP and ER were significantly higher in eutrophic mesocosms than in mesotrophic ones, and in shallow mesocosms compared to deep ones, while nutrient status and depth did not interact. The estimated temperature gains for ER of ~ 0.62 eV were comparable with those predicted by MTE. Temperature sensitivity for GPP was slightly higher than expected ~ 0.54 eV, but when corrected for daylight length, it was more consistent with predictions from MTE ~ 0.31 eV. The threshold temperature for the switch from autotrophy to heterotrophy was lower under mesotrophic (~ 11 °C) than eutrophic conditions (~ 20 °C). Therefore, despite a lack of significant temperature-treatment interactions in driving metabolism, the mesocosm's nutrient level proved to be crucial for how much warming a system can tolerate before it switches from net autotrophy to net heterotrophy.

Introduction

The balance between gross primary production (GPP) and ecosystem respiration (ER) determines the metabolic status of lakes and has a decisive influence on their role in regional/global matter and energy cycles (Andersson & Sobek, 2006; Brothers et al., 2013; Pacheco et al., 2013). Shallow lakes are the most numerous lake type on Earth (Cael et al., 2017), and have been recognized as hotspots of carbon turnover (Cole et al., 2007; Tranvik et al., 2009). While oligotrophic lakes with high allochthonous carbon inputs tend to be predominantly net heterotrophic ($GPP < ER$), many eutrophied lakes have been found to be net autotrophic ($GPP > ER$) (del Giorgio & Peter, 1994; Cole et al., 2000; Balmer & Downing 2011). Lakes can switch between net autotrophy and net heterotrophy across multiple timescales (i.e. daily, weekly, or seasonal) (Staehr & Sand-Jensen 2007; Coloso et al., 2011; Sadro et al., 2011; Laas et al., 2012); in temperate lakes, the extent of net autotrophy in spring and summer can be a determining factor for the annual metabolic status of lakes (Staehr et al., 2010; Laas et al., 2012). Autotrophic and heterotrophic metabolic pathways are susceptible to changes in light regime, nutrient status, and temperature. All these drivers are predicted to be affected by climate change due to alterations in water levels, nutrient cycling and run-off from the catchment (Coops et al., 2003; Nickus et al., 2010; Jeppesen et al., 2015).

The metabolic theory of ecology (MTE) provides a comprehensive theoretical framework to investigate metabolic rates' dependence on temperature (Brown et al., 2004). Based on first principles the MTE allows the scaling of metabolic rates from individual biochemical reactions up to the level of ecosystems (Enquist et al., 2003; Allen et al., 2005; Yvon-Durocher et al., 2010b). Independent of temperature, the absolute metabolic rate at the ecosystem level is

primarily determined by the size and abundance distribution of the constituting community of the ecosystem. On the other hand, the physiological dependence of metabolic rates on temperature, approximated by the Arrhenius equation, is still governed by the rate-limiting biochemical process of the cellular level, even at the ecosystem level (Bernacchi et al., 2001; Gillooly et al., 2001; Allen et al., 2005). Under non-limiting conditions, the MTE assumes activation energies of ≈ 0.3 eV (photosynthesis) and ≈ 0.6 eV (respiration). Therefore, in a warming world the MTE predicts a shift towards heterotrophy (as temperatures increase) or even a switch from net autotrophy to net heterotrophy if stored or allochthonous carbon sources are available (Yvon-Durocher et al., 2010a; Laas et al., 2012; Weyhenmeyer et al., 2015). A shift towards heterotrophy would imply a reduction in the carbon sequestration capacity or even loss of this important ecosystem service as a carbon sink, unless offset by sedimentation rates. The temperature at which a net autotrophic system switches to net heterotrophy depends, however, not only on the differential temperature sensitivity of GPP and ER, but also on the ratio of the absolute GPP and ER rates. Theoretically, the more GPP exceeds ER at a given reference temperature, the more warming a lake can tolerate before switching from net autotrophy to net heterotrophy.

Since temperature and eutrophication are regarded as the two major stressors for lake ecosystems, several studies have documented their effects on GPP, ER, and the balance between them. Several of these studies have confirmed the occurrence of positive effects of temperature on both ER and GPP, but negative effects on net ecosystem production ($NEP = GPP - ER$) (Kosten et al., 2010; Moss 2010, Yvon-Durocher et al., 2010a,b, 2012). Moreover, there is general agreement that elevated nutrient concentrations promote metabolic rates, but have greater impact on GPP

than ER, causing increases in NEP, or decreases in ER/GPP ratios (del Giorgio & Peters, 1994; Hanson et al., 2003; Duarte et al., 2004; Staehr et al., 2010) as well as a stronger coupling between ER and GPP in oligotrophic than in eutrophic lakes (Solomon et al., 2013). However, the interacting effects of temperature and trophic state on ecosystem metabolism within the context of already observed and predicted changes in lake water levels, and thus light conditions, are not well understood (Anderson-Teixeira & Vitousek, 2012; Cross et al., 2015; Welter et al., 2015), and results from experiments on nutrient-temperature interactions are ambiguous (Berggren et al., 2010, Moss 2010, Liboriussen et al., 2011).

In particular, it is unclear how interactions between temperature, nutrients, and light availability can modify the MTE predicted values for the activation energy resulting in deviations of the apparent temperature sensitivity at ecosystem level from the physiological one (Cross et al., 2015), thereby modifying the MTE-predicted shift towards heterotrophy with increasing temperature. Models combining Arrhenius and Michaelis-Menten kinetics have shown, for instance, that substrate limitation and trophic structure can dampen the apparent temperature sensitivity (Davidson et al., 2012; Davidson et al., 2015). In addition, both the maximum rate and the half-saturation constant were found to increase with increasing temperature in photosynthesis-irradiance relations (Kirk, 2010). However, temperature-dependent increases in the photosynthetic rate might be subdued if phosphorus limits the process (Wykoff et al., 1998; Kirk, 2010). In accordance with this, Staehr & Sand-Jensen (2006) found a reduced metabolic response in a natural algae assembly to increased temperatures under nutrient-limiting conditions. Reduced light and nutrient conditions may affect ER either due to substrate limitation or changes in food quality (McFetters & Frost, 2011). However, results from laboratory experiments are difficult to

scale to the ecosystem level, where covariation of temperature with factors such as water level, daylight length, nutrient cycling, and N₂ fixation, as well as acclimation and adaptation at species or community levels can all influence the apparent temperature sensitivity (Atkin & Tjoelker, 2003; Anderson-Teixeira & Vitousek, 2012; Welter et al., 2015).

Based on a standardized pan-European mesocosm experiment, this study aims to improve the understanding of how the combined effects of water temperature, water level, and nutrient status affect metabolic rates in shallow lake ecosystems. Specifically, we investigated temperature effects on GPP, ER, and the ratio of ER/GPP under eutrophic and mesotrophic nutrient conditions and at two depth levels, simulating different light conditions. The findings from our experiment were compared with predictions made according to the theoretical framework of the MTE. We tested the following hypotheses: (1) Metabolic rates are lower with reduced nutrient availability, but increase at lower water levels due to higher light availability; (2) a shift towards heterotrophy occurs with increasing temperature due to a higher physiological temperature sensitivity of ER compared with GPP; (3) the apparent temperature sensitivity of ER and GPP will differ between treatments due to interactions between temperature, the availability of light and nutrients; (4) switching between auto- and heterotrophy occur at lower temperatures if the magnitude of ER and GPP is more similar (NEP near zero). We expect this situation under low-nutrient and low-light conditions that sustain a generally lower lake GPP.

Material and Methods

Experimental design and sampling – The mesocosm experiment was conducted in six European countries, encompassing a climate gradient from Sweden to Greece (Table 1) from May until November 2011. The fiberglass mesocosms used were produced by the same manufacturer, and had a diameter of 1.2 m and heights of 1.2 or 2.2 m. The mesocosms were set up within the lakes to ensure a natural and ambient water temperature regime, but were otherwise isolated from the surrounding water. In each country, the experiment involved a 2 x 2 factorial design with four replicates; measurements were taken monthly. The first factor involved two different water levels: 1 m (shallow – S) and 2 m (deep – D) deep mesocosms. These two depths coincided with different mixing depths, since the water in the mesocosms was constantly circulated from bottom to top by standard aquarium pumps, entailing different light conditions (S3 Figure 1). Water levels were allowed to fluctuate with precipitation and evaporation. The second factor involved nutrient manipulation to simulate mesotrophic (low – L) and eutrophic (high – H) conditions. Nutrients were adjusted to the two conditions by monthly nutrient addition aiming at initial concentrations after loading of 25 μg phosphate (P) L^{-1} (Na_2HPO_4) and 0.5 mg nitrogen (N) L^{-1} ($\text{Ca}(\text{NO}_3)_2$) in the mesotrophic and 200 μg P L^{-1} and 2 mg N L^{-1} in the eutrophic treatment. The experiment was synchronized using a common protocol to facilitate comparability (Landkildehus et al., 2014).

The mesocosms contained a 10 cm sediment layer of 90% washed sand and 10% natural sediment from an oligotrophic lake, situated near the respective experimental site. To prevent prolonged internal P loading (low nutrient conditions) or P retention (high nutrient conditions) at the start of the experiment, the sediment was acclimatized to the desired phosphate

concentrations for at least two months in the laboratory beforehand. Filtered (500 µm mesh) lake water was used in the mesocosms in all countries except Germany and the Czech Republic, where tap water was used because the P level exceeded the 25 µg TP L⁻¹ threshold of the low-nutrient treatment. The initial P and N loadings were adjusted in all high-nutrient mesocosms to obtain the desired nutrient concentration.

The ability of natural flora and fauna to adapt to the specific climate and nutrient conditions was ensured by using an inoculum of plankton and sediment collected from five different local lakes, covering a nutrient gradient from 25 to 200 µg TP L⁻¹ in each country. Macrophytes (*Myriophyllum spicatum*) and planktivorous fish were added to all mesocosms. Monthly samples were analyzed for water chemistry and chlorophyll *a* (Chl *a*) in laboratories and on site by using comparable, standard methods (see S2 Table 1). Concomitantly, macrophyte biomass was quantified as plant volume inhabited (PVI [%]). After each sampling event, 24-hour measurement of dissolved oxygen and water temperature was conducted at two-hour intervals using a multi-parameter probe (for sampling dates, see S1 Table 1). In addition, light profiles of the water column were measured at midday at 10 cm intervals. For details on the design and sampling, see Landkildehus et al. (2014).

Data preparation – The study utilized the data collected between July and November, under the assumption that all systems would have had enough time to adjust to the experimental manipulation by then. Seven mesocosms were excluded from the analysis (2 DH, 1 DL and 1 SH mesocosm in Germany and 2 SH and 1 SL mesocosm in the Czech Republic) as they were lost during storm events. The analysis is thus based on five measurements, including data from 89

mesocosms per measurement occasion. In Greece, massive water loss due to evaporation prevented sampling in the shallow mesocosms, involving light profiles (from September onwards), water chemistry (from October onwards) and the 24-hour measurement in November. Since visual inspection of these shallow mesocosms indicated high light attenuation, we assumed the same high attenuation for the remaining sampling occasions. Light profiles were also missing for August and September for the Estonian mesocosms. Here, the missing attenuation coefficients were linearly interpolated since none of the attenuation coefficients from the other countries indicated strong seasonality.

All data were visually inspected at the raw data level and outliers were identified using boxplots. Only extreme outliers (larger than 3 times the interquartile range) were removed from the data (O_2 : 36 values (1%) and water temperature: 4 values (0.1%)) and replaced by interpolated values. Single gaps in the 24-hour data were substituted by values from a polynomial model of degree 4 of time; for all other data linear interpolation were used. Reported average values (e.g. average air temperature) correspond to the sampling periods listed in S1 Table 1.

Estimation of reaeration coefficient ($K_{a,20} [h^{-1}]$) at 20 °C for O_2 – To ensure minimal influence from respiration, gas exchange was measured when water temperatures were low and after the last sampling in late October, or early November. Under continuous mixing, oxygen saturation was lowered to approx. 30% by bubbling N_2 into two randomly chosen shallow and deep mesocosms. At nightfall, oxygen reduction was completed and oxygen recovery was monitored overnight (reaeration). For each mesocosm, a transport coefficient $K_{L,20}$ was estimated following Liboriussen et al. (2011). Two different respiration models were tested: $R_{20^{\circ}C} \cdot 1.047^{(T-20)}$ (Erlandsen & Thyseen, 1983) and $R_{20^{\circ}C} \cdot 1.07^{(T-20)}$ (Streeter & Phelps, 1925; De Matos et al.,

2014). The model outputs did not differ systematically and differences were generally low. Since both models are plausible representations of the temperature effect on respiration, we synthesized the results into an average $K_{L,20}$ value (0.0218 m h^{-1}). However, values from the Czech mesocosms were excluded because the O_2 reductions were too low to permit proper calculations. Averaging was chosen to appropriately reflect modeling uncertainty, which is in line with the idea of ensemble modeling. $K_{a,20}$ values were then derived by dividing by the mixing depth.

Estimation of GPP and ER – Metabolic rates were estimated based on the 24-hour O_2 measurements using the free-water method following Jeppesen et al. (2012). Since the main focus of the investigation was to analyze the temperature response of the metabolic rate, Arrhenius-type corrections based on *a priori* Q_{10} values from the literature were avoided.

To assess the uncertainty of the estimated metabolic rates, we used a bootstrap approach similar to the one described in Solomon et al. (2013). Estimates with standard errors larger than the estimate itself, and estimates explaining $< 5\%$ of the variability of the 24-hour dissolved oxygen curve, were excluded from further analysis, totaling 14% of the values. Overall, 374 data points remained. For an overview of the distribution of data points per country, month, and treatment, see Table 2 in S1. To obtain daylight length-corrected GPP values, $\text{GPP}_{\text{dl}} [\text{mg m}^{-3} \text{ hd}^{-1}]$, GPP per day was divided by the average daylight period, LP (hd^{-1}), according to month and country. For further details on the estimation of metabolic rates and the meteorological data used, see Supplement S2.

Estimation of light attenuation coefficient, K_d , mean available light and effective light period –

For each light profile, an attenuation coefficient, K_d , was estimated based on the Beer-Lambert law. Mean available light over the water column (MAL) was estimated following Staehr et al. (2010). The effective light period (LP_{eff}), describing the effective light period due to mixing, was calculated following Shatwell et al. (2012). For more details, see Supplement S2.

Hypotheses generation based on MTE – We used the framework of the MTE to formally derive the expected temperature dependence of the measured metabolic rates and the ratio between them, which we tested against our experimental findings. Following the MTE, the temperature dependence of metabolic rates can be approximated by the Arrhenius equation within a temperature range of 0 to 30 °C (Gillooly et al., 2001; Brown et al., 2004; Allen et al., 2005). At the ecosystem level, the MTE is formulated as:

$$M(T) = M_0 \exp\left(\frac{-E}{kT}\right) \quad (1)$$

where $M(T)$ is the temperature-dependent metabolic rate; M_0 at the ecosystem level can be interpreted as the size-dependent basic metabolic flux summed over all autotrophs or heterotrophs, respectively, per unit volume (Allen et al., 2005); E is the activation energy and expresses the strength of the temperature effect on the metabolic rate; k is the Boltzmann constant ($8.62 \times 10^{-5} \text{ eVK}^{-1}$); and T is the absolute temperature in Kelvin. The above temperature effect can be conveniently analyzed and plotted with Arrhenius plots based on the logarithmized version of equation (1). In Arrhenius plots, the natural logarithm of the metabolic rate is plotted against the inverse and scaled temperature $1/(kT)$ so that the slope of this linear relationship represents the activation energy and the intercept the absolute metabolic rate of a particular

283 metabolic process. The absolute metabolic rate is usually shifted to a biological meaningful
 284 reference temperature (T_c), here to 15 °C, following Yvon-Durocher et al. (2010b), and Demars
 285 et al. (2011). Thus, the MTE equation used to analyze the temperature dependence of metabolic
 286 rates reads:

$$\ln M(T) = \ln M_{T_c} + E \frac{1}{k} \left(\frac{1}{T_c} - \frac{1}{T} \right) \quad (2)$$

287 At the ecosystem level, resource availability could either affect the absolute metabolic rate or the
 288 apparent activation energy, E .

289

290 To derive the expected temperature effects for the ER/GPP ratio, we assumed, following Yvon-
 291 Durocher et al. (2010b), that our systems were in a non-steady state and that ecosystem
 292 respiration is mainly driven by heterotrophic metabolism, unconstrained by net primary
 293 production (for data-driven justification of the assumption, see S6). Thus, the temperature-driven
 294 change of the ratio between ER and GPP can be simplified to:

$$\frac{ER}{GPP}(T) = \frac{ER_0}{GPP_0} \exp \left(\frac{E_p - E_r}{kT} \right) \quad (3)$$

295 where $ER/GPP(T)$ is the temperature-dependent metabolic ratio; ER_0 and GPP_0 are the absolute
 296 metabolic rates according to the definition of M_0 ; and E_p and E_r are the activation energies for
 297 GPP and ER, respectively.

298

299 Again, the Arrhenius plot together with a shift to a biological meaningful reference temperature
 300 can be used to analyze and depict the relationship in logarithmic terms:

$$\ln \frac{ER}{GPP}(T) = \ln \frac{ER_{Tc}}{GPP_{Tc}} - \frac{E_p - E_r}{k} \left(\frac{1}{Tc} - \frac{1}{T} \right) \quad (4)$$

where GPP_{Tc} and ER_{Tc} are the GPP and ER rate at the reference temperature, Tc ; and E_p and E_r are the activation energies for GPP and ER, respectively. Equations (2) and (4) explicitly state that changes in the metabolic balance with changing temperature, and thus its influence on the carbon sequestration capacity, depend solely on the amount of differential temperature sensitivity between ER and GPP

Based on the MTE, we derived an expectation about the temperature at which the switch from autotrophy to heterotrophy occurs. Formally, this is the point of equality between GPP and ER, given by:

$$T = \frac{1}{\frac{k \ln \frac{GPP_{Tc}}{ER_{Tc}}}{E_p - E_r} + \frac{1}{Tc}} \quad (5)$$

For fixed E_p and E_r , the switch point depends solely on the ratio between GPP_{Tc} and ER_{Tc} , i.e. the smaller the ER_{Tc} relative to GPP_{Tc} , the higher the temperature at which the system switches from autotrophy to heterotrophy. Thus, assuming resource-dependent absolute ER_{Tc}/GPP_{Tc} values, the switch point from autotrophy to heterotrophy should be lower in nutrient-reduced environments.

Statistical analysis – All statistical analyses were conducted using R version 3.1.3 (R Core Team, 2015). We analyzed temperature and treatment effects based on monthly data from all countries using linear mixed effect models (“lme4” package, Bates et al., 2014). The following basic model was applied:

$\ln M_{c,(s,m),i}^{(D \times N)}(T) = \overline{\ln M_{Tc}^{(D \times N)}} + \epsilon_R^c + \epsilon_R^{c,s} + \epsilon_R^{c,m} + \left(\overline{E^{(D \times N)}} + \epsilon_E^c + \epsilon_E^{c,m} \right) \frac{1}{k} \left(\frac{1}{T_c} - \frac{1}{T} \right) + \epsilon_{c,(s,m),i}$	(6)
--	-----

319 where $\ln M_{c,(s,m),i}^{(D \times N)}$ and $\epsilon_{c,(s,m),i}$ are the temperature-dependent metabolic rate and associated
 320 random error for measurement i of mesocosm m in month s and country c; k is the Boltzmann
 321 constant; and T_c is the reference temperature set to 15 °C as in Equations (2) and (4).
 322 $\overline{\ln M_{Tc}^{(D \times N)}}$ and $\overline{E^{(D \times N)}}$ are the logarithmic average metabolic rate at T_c , and the average apparent
 323 activation energy, respectively, for each treatment. For the average metabolic rate at 15 °C,
 324 random effects at the level of country (ϵ_R^c), month ($\epsilon_R^{c,s}$), and mesocosm ($\epsilon_R^{c,m}$) were considered,
 325 where both month and mesocosm are nested within country. For the average apparent activation
 326 energy, random effects on the level of country (ϵ_E^c) and mesocosm ($\epsilon_E^{c,m}$) were taken into account
 327 as well. The random effect on the level of mesocosm was nested within country. Following
 328 Yvon-Durocher et al. (2012), the random effect of month was added to control for confounding
 329 effects on apparent activation energy, which a potential covariation between monthly absolute
 330 metabolic rates and temperature may cause. With this modeling approach, we assumed a generic
 331 activation energy as suggested by MTE, with an additional possibility of random variation
 332 between countries and mesocosms due to interactions and covariation with factors other than
 333 those controlled for experimentally. These assumptions are justified, since country-specific
 334 activation energies and absolute metabolic rates at 15 °C did not reveal systematic changes in
 335 relation to average temperature (S4). In this situation, the mixed-effect models approach that we
 336 chose is reliably capable of estimating the average activation energy as well as the absolute

metabolic rate, as validated in a simulation approach emulating the structure and random structure of our experimental data (S8).

The same basic model as in Equation (6) was used for the analysis of GPP, daylight length-corrected GPP_{dl} , ER, and the ER/GPP ratio. Model selection of random and fixed effects was done based on likelihood ratio tests by stepwise backward elimination (“lmerTest” package, Kuznetsova et al., 2014; “step” function). However, we retained the main effects of depth, nutrients, and temperature as a minimum, since we – apart from significance – sought to describe effect size and to conduct comparisons between estimated and predicted values based on the MTE. Effect sizes were calculated using standardized predictors following Gelman (2008).

Model validation was conducted by graphical inspection of the Pearson residuals, including their relation to all predictor variables. The model fit was assessed by conditional (variance explained by fixed effects) and marginal (variance explained by fixed and random effects) coefficients of determination (“MuMIn” package, Bartoń 2015; “r.squaredGLMM” function). Treatment-specific confidence intervals were computed based on a “t” statistic with degrees of freedom established by the Kenward & Rogers method (“lsmeans” package, Lenth & Hervé 2015; function “lsmeans”).

Covariation of temperature, depth, and nutrient levels with TP, TN, K_d , MAL, LP_{eff} , Chl a , and PVI was assessed with the same basic mixed effects model as in Equation (6). However, rather than the scaled inverse water temperature, a centered water temperature of 15 °C was used. Box-Cox transformation was applied for the dependent variable to meet model assumptions (“MASS” package, Ripley et al., 2015; “boxcox” function). Factor covariate interaction was probed using two-tailed t tests for pairwise comparisons of least-square-means over the temperature gradients

360 at one degree intervals (“lsmeans” package; Lenth & Hervé 2015). Reported treatment-wise
361 adjusted means (“phia” package, Rosario-Martinez 2015; “InteractionMeans” function) as well as
362 the direction and amount of average change between 7 °C and 29 °C (the temperature range we
363 tested) were estimated based on these models.

364

365 Using semi-partial Spearman correlation, we assessed the differential influence of MAL, LP_{eff} ,
366 daylight length, Chl a , PVI, and inverse and scaled water temperatures on GPP, ER, and the
367 ER/GPP ratio (“ppcor” package, Kim, 2012 ; “spcor” function). Semi-partial Spearman
368 correlation coefficient r and percentile 95% confidence intervals were bootstrapped over
369 mesocosms (“boot” package, Canty & Ripley, 2015; “boot” and “boot.ci” function). To further
370 disentangle the influence of daylight lengths from the effect of temperature on GPP, we
371 compared the results from two separate regression models based on standardized variables,
372 conducted a residual regression analysis (see S7), and analyzed daylight length-corrected GPP
373 (Allen et al., 2005).

Results

Water temperatures revealed a distinct seasonal pattern in all countries (Table 1, Figure 1a). From July to November 2011, water temperature ranged from 6.8 to 29.1 °C (all countries included).

Water temperatures were highly correlated with monthly mean air temperatures ($r = 0.88$ with a 95% confidence interval of 0.85 – 0.90), confirming that the monthly point measurements in our enclosures represented the overall seasonal temperature conditions (Table 1).

The water level decreased drastically in the two southern countries during autumn, while changes were modest in the central and northern European countries (Figure 1b).

The differential monthly loading of phosphate resulted in significantly (< 0.05) different TP levels between the high-nutrient and low-nutrient mesocosms over the entire temperature gradient (Figure 2a, S3 Table 1). TN levels between deep eutrophic mesocosms and both low-nutrient treatments were not significant for temperatures above ~ 25 °C (Figure 2b, S3 Table 1). Light availability, as measured by the mean available light (MAL) and the effective light period (LP_{eff}), was highest in the shallow mesotrophic followed by the shallow eutrophic mesocosms, and the deep mesotrophic mesocosms; it was lowest in the deep eutrophic mesocosms (S3 Figure 1b, c). Over the entire temperature gradient, MAL differed significantly (< 0.05) between all treatments (for DL – SH above 9 °C). LP_{eff} was significantly shorter in the deep eutrophic mesocosms compared to all other treatments. The deep mesotrophic mesocosm had shorter LP_{eff} compared with the shallow mesocosms for temperatures above 15 °C (SL) and 21 °C (SH), while at no point did LP_{eff} values differ significantly among the shallow mesocosms (S3 Figure 1, S3 Table 1).

Nutrient and light effects on average metabolic rates (Hypothesis (1)) – On average, GPP and ER were significantly higher in the eutrophic than in the mesotrophic systems, and significantly higher in the shallow than in the deep mesocosms (Table 2, Figure 3). In line with our expectations, the eutrophic shallow mesocosms with ample light had the highest metabolic rates, followed by eutrophic deep systems with reduced light availability, shallow mesotrophic systems with ample light, and deep mesotrophic light-reduced systems.

Temperature and interaction effects (Hypotheses (2) and (3)) – Both log-transformed GPP and ER increased significantly with increasing temperatures as predicted by the Arrhenius Equations (1) and (2) (Figure 4, Table 2). Contrary to our expectations, we found no significant interacting effects between water temperature and the different light and nutrient regimes on GPP and ER. The average temperature sensitivity of ER in all treatments was 0.62, predicting a 13.5-fold increase in ER over a temperature range from 0 to 30 °C. The average temperature sensitivity of GPP amounted to 0.54 (Figure 4, Table 3), predicting a 9.7-fold increase in GPP over a temperature range from 0 to 30 °C. Thus, as predicted from the metabolic theory, ER increased more with temperature than did GPP. Consequently, according to Equations (3) and (4), the activation energy of the ER/GPP ratio was expected to average 0.08 eV. This corresponds to a predicted 1.4-fold increase in the ratio over a temperature range from 0 to 30 °C. Although close to the theoretically predicted value, the actual estimated average activation energy of 0.13 eV for the ER/GPP ratio was not significant (Figure 5a, Table 3). However, due to lower absolute ER/GPP ratios in eutrophic compared with mesotrophic systems, the mesotrophic mesocosms had, on average, a 10% lower metabolic-driven carbon sequestration capacity than the eutrophic mesocosms over a temperature range from 0 to 30 °C.

420

421 *The effect of covariates on metabolic rates* – The average temperature sensitivity for daylight
422 length-corrected GPP had an estimated average activation energy of 0.31 eV, and was thus close
423 to the canonical temperature dependence of photosynthesis. However, it was not significant at the
424 0.05 percent level (Table 2).

425 Results from semi-partial Spearman correlations confirmed the importance of temperature for
426 metabolic rates independent of light-related factors (Table 4). As expected, however, light-related
427 factors were also significantly correlated with GPP, except in shallow mesotrophic systems.
428 Significant correlations between GPP and Chl *a* or PVI were observed in systems in which these
429 drivers were highest, i.e. in the eutrophic and mesotrophic shallow mesocosms (S3 Figure 2,
430 Table 4). In addition to temperature, ER was strongly correlated with GPP.

431

432 *Temperature-specific switch from autotrophy to heterotrophy (Hypothesis (4))* – In the
433 mesotrophic mesocosms, based on Equation (5) and average values from the mixed effects
434 regression for GPP and ER (Table 3), the switch from autotrophy to heterotrophy generally
435 occurred at lower temperatures (12 °C and 10 °C) than in the eutrophic mesocosms (21 °C and
436 19 °C) (Figure 5b). This is in line with our prediction. In contrast, light regime and mixing depth
437 had only a minor impact on the switch point. This is confirmed by a significant nutrient effect (p
438 = 0.05), but an insignificant depth effect (p = 0.85) for the ER/GPP ratio (Figure 5a, Table 2).

439

440

441 **Discussion**

It is anticipated that climate change will affect shallow lake metabolism and thereby the ability of such lakes to sequester carbon due to direct and indirect impacts on major drivers such as temperature, nutrients, water level, and light conditions (Tranvik et al., 2009; Nickus et al., 2010; Jeppesen et al., 2015). We confirmed the existence of a positive relationship between nutrient concentrations, light availability, temperature, and metabolic rates in shallow lakes.

The observed apparent differential temperature sensitivity between GPP and ER adds support to the anticipated shift (Cole et al., 2000; Staehr & Sand-Jensen, 2006; Yvon-Durocher et al., 2010a, 2010b) towards an increasing degree of heterotrophy in shallow lake ecosystems with increasing temperatures. Since the observed activation energy for ER was higher than for GPP, ecosystem respiration increased more than production, leading to a predicted increase in ER/GPP over the tested temperature gradient. The average temperature sensitivity of the ER/GPP ratio itself was not significant, perhaps due to the inherent variance of both the GPP and the ER estimates. Nonetheless, the estimated average activation energy of 0.13 eV is in accordance with the predicted values of 0.08 eV based on equation (4) (Figure 5b). The established apparent average temperature sensitivities of the metabolic rates of 0.62 eV and 0.31 eV for ER and GPP per daylight hour, respectively, match well with predictions for the physiological temperature dependence for respiration (0.6 eV) and photosynthesis (0.3 eV) predicted by the metabolic theory (Allen et al., 2005). With a value of 0.54 eV, the observed activation energy of GPP per day exceeds the predicted physiological temperature dependence, but closely conforms to findings from other aquatic environments: 0.50 ± 0.18 eV (Wilken et al., 2013); 0.54 ± 0.24 eV (Demars et al., 2011); and 0.45 eV (95% CI 0.38-0.53) (Yvon-Durocher et al., 2010b).

Most algae and cyanobacteria have carbon-concentration mechanisms (CCMs) to prevent the oxygenase activity of Rubisco, particularly under low $p\text{CO}_2$ and high alkalinity conditions (Raven et al. 2011; Falkowski & Raven, 2013; Demars et al., 2016). CCMs are assumed to be the cause of the systematic higher activation energy for GPP found in freshwater systems compared with the activation energy derived for terrestrial C3 plants (Demars et al. 2015, 2016). The alkalinity in our systems was at intermediate levels on average (mean $1363 \pm 27 \text{ mol L}^{-1} \text{ eq HCl}$). $p\text{CO}_2$ levels, estimated from midday alkalinity and daily average pH (Trolle et al., 2012), indicate the potential of low $p\text{CO}_2$ episodes (mean $\text{epCO}_2 \approx 0.55 \pm 0.07$ times atmospheric pressure), making the active operation of CCMs likely. However, in our systems, high positive correlations between daylight length and temperature serve as a reasonable explanation for the higher-than-expected activation energy, as daylight length-corrected estimates led to the physiologically predicted temperature sensitivity of 0.31 eV. Interestingly, regions with seasonal temperature fluctuations exhibit a natural correlation between daylight length and temperature, possibly mitigating the expected shift towards heterotrophy.

The expected temperature at which a system switches from autotrophy to heterotrophy can be modeled in the framework of MTE according to Equation 5. The model suggests that the temperature threshold at which a system switches from net autotrophic to net heterotrophic depends on the extent of the differential temperature sensitivity between GPP and ER (E_{GPP} and E_{ER} , respectively) and on the log ratio between GPP and ER at a reference temperature, T_c (here, 15°C). This temperature threshold turned out to be affected by trophic state (Figure 5a): higher nutrient availability in the eutrophic mesocosms led not only to significantly higher GPP and ER,

but also to significantly lower ER to GPP ratios (0.9 (DH) and 0.91 (SH)) than under mesotrophic conditions (0.98 (DL) and 0.99 (SL)). This apparently small difference was, however, large enough to cause an average temperature threshold increase of approximately 5 °C (based on ER/GPP ratio). Thus, under the predicted warming scenarios of 1.5 to 5 °C by 2100 (Rogelj et al., 2012; Stocker et al., 2013), high-nutrient systems are likely to have a lower risk of becoming net heterotrophic than systems with lower nutrient concentrations (Figure 5b, Table 3). The direct effect of water depth on the ER/GPP ratio was not significant, and the effect of depth on the threshold temperature was low, indicating that a reduced water level is of minor importance for the switch from autotrophy to heterotrophy in these generally shallow systems.

In our experiment the confirmation of the MTE was strong when aggregating data from all countries and seasons, while at the same time, temperature sensitivity exhibited a relatively high idiosyncrasy between countries (S4 Table 2). This is in line with findings from other studies, where single systems tend to deviate from the MTE predictions (De Castro & Gaedke, 2008, Davidson et al., 2015), while larger-scale studies are often in good agreement with the predictions (López-Urrutia et al., 2006, Yvon-Durocher et al., 2012). Potential mechanisms behind this variation include acclimatization and adaptation processes, which are hypothesized to induce reduced temperature sensitivity with increasing average temperature (Atkin & Tjoelker, 2003; Hikosaka et al., 2006; Hartley et al., 2008; Angilletta, 2009; Smith & Dukes, 2012). In this study, we found no evidence for a systematic change in activation energy with average temperature (S4 Table 2), which is in line with Perkins et al. (2012), who reported consistent Q10 temperature coefficient values for ER regardless of the thermal history or community composition of

biofilms, as well as with a global survey of activation energies based on satellite data by Kraemer et al. (2016).

Furthermore, contrary to our expectations, we observed no significant interactions between the temperature sensitivity of both GPP and ER and nutrient levels, or depth. We can only speculate about the underlying mechanisms. Perhaps the missing depth-temperature interaction reflects light adaptation, rendering photosynthesis primarily dependent on the maximum photosynthetic rate. The lack of TP-temperature interaction indicates that either TP affinity was not a function of temperature, or that shifts in community composition in the mesotrophic mesocosms towards species with higher phosphate affinity prevented limitation of photosynthesis by phosphorus (Domis et al., 2014). However, lack of sensitivity to depth and nutrients may also reflect the relatively modest variations in these experimental variables.

Therefore, a better understanding of the factors leading to deviations from MTE-predicted temperature sensitivity remains an important area of research.

A decline in water level, as already reported and further anticipated within the context of global warming for lakes in the Mediterranean region (Coops et al., 2003; Beklioglu et al., 2006, 2007; Jeppesen et al., 2015), affects mixing depth and light availability. We found a significantly lower GPP and ER in deep than in shallow mesocosms (Table 3). The difference in production levels was most likely generated by the influence of depth on the light availability, while impacts on gas exchange due to a lower surface-to-volume ratio were most likely negligible since all mesocosms were fully mixed. Light saturation for photosynthesis is specific to each algal species and ranges from around 60 to 100 $\mu\text{mol m}^{-2} \text{s}^{-1}$ (Lampert & Sommer, 1999). This confines deep mesocosms to the lower end of the range, and makes them more prone to being light-limited, while the

shallow mesocosms are close to, or above, the upper end of the range (S3 Table 1), and thus most likely light-saturated. Additionally, only in the eutrophic deep systems was the sediment layer generally below the euphotic zone; thus, only these mesocosms had a considerably shorter average LP_{eff} compared with all other treatments (S3 Table 1). Therefore, a reduction in water level considerably improves light availability, and might allow benthic primary production where it was not possible before.

The linear mixed effect regression approach is an optimal method for analyzing our data as long as we can reasonably assume a generic temperature sensitivity of metabolic rates or random variation in temperature sensitivity due to interactions with factors randomly varying between countries (see Supplement S8). Since the between-country comparison of systematic changes in temperature sensitivity with average temperature indicated no systematic change (see Supplement S4), there is solid justification for the approach used in this study. Furthermore, this approach would be sensitive to interactions between average temperature sensitivity and nutrients, or between average temperature sensitivity and water level. However, the use of this approach also implies that we must analyze temperature sensitivity, as it responds to seasonal temperature changes, as opposed to controlled experimental temperature manipulation. The temperature response of ecosystem level metabolic rates based on seasonal data captures the apparent temperature sensitivity towards relatively short-termed temperature changes and cannot replace a true experimental test of the effect of global warming (therefore, we use “apparent” temperature sensitivity). This is a limitation, but the response to seasonal temperature changes is of scientific interest, since seasonal temperature changes are the dimension along which the property of temperature sensitivity takes effect in ecosystems. Like all experimental approaches, mesocosm

experiments come with inherent abstractions from the natural complexity, as well as their own challenges, which restrict a direct generalization of results to natural systems. In our experimental design, the constant mixing by aquarium pumps creates ideal constant mixing conditions, which prevents the natural variability in mixing intensity, including micro- and short-term stratification events. Mixing-induced fluctuation in light conditions has been shown to influence phytoplankton growth rates (Shatwell et al. 2012, Köhler et al. 2017), and stratification influences the availability of nutrients and oxygen (Wilhelm & Adrian, 2008). In turn, phytoplankton growth impacts water transparency and thus water temperature and the mixing regime (Shatwell et al. 2016). However, differential warming of our mesocosms due to differences in water transparency was prevented, since water temperature in the mesocosms was mainly determined by the surrounding lake. Another well-known general problem in mesocosm studies is periphyton growth on the walls of the enclosures, forming in part a micro-environment. There is limited knowledge about the influence of periphyton on nutrient cycling and metabolic rates in the open water column, which prevents quantification (Wetzel, 2001; Petersen, 2009). Furthermore, our experimental design may have influenced the proportion of GPP to ER, as we included sediment, which contained foreign organic matter that may have enhanced ER at higher temperatures and, thus, the ratio. While this may potentially affect the absolute values (if not in equilibrium with the current conditions in the mesocosm) of thresholds regarding the shift to heterotrophy, it does not affect the observed direction of changes and the overall conclusions. However, the absolute thresholds should be interpreted with caution.

Research indicates that shallow lakes play an important role in local and global carbon cycling, as they are the most numerous type of lake in the world (Cael et al., 2017; Tranvik et al., 2009).

578 Given that a differential temperature sensitivity of ER and GPP poses a potential feedback
579 mechanism to atmospheric CO₂ levels in a warming scenario, understanding the metabolic
580 processes of shallow lake ecosystems, and how they will be affected by a changing climate, is not
581 only of basic but also of applied ecological interest. The results of this study confirmed and
582 quantified the varying apparent temperature sensitivity of GPP and ER and showed that trophic
583 state is important for the question of how much warming a shallow lake system can tolerate
584 before it switches from net autotrophy to net heterotrophy.

585 We linked our experimental findings with the framework of the MTE and tested theoretically
586 derived predictions on our data. In line with earlier studies, we found good agreement between
587 theory and practice, which affirmed the potential of the MTE also in the context of shallow lakes.
588 Furthermore, we found that the balance between ER and GPP depends not only on the energy
589 supply, as in the MTE, but also on the availability of nitrogen and phosphorus. Thus, we
590 conclude that quantitative inclusion of these nutrients in the MTE, as suggested for instance by
591 Allen & Gillooly, 2009, Anderson-Teixeira & Vitousek, 2012 and Davidson et al., 2012, could
592 greatly add to its predictive power for shallow lakes.

593 **Acknowledgements**

594 We thank the technical staff at the various experimental sites for their support. We thank Alena S.
595 Gesell, Deniz Özkundakci, Jan-Hendrik Schleimer, Silke Schmidt, Torsten Seltmann, and Tom
596 Shatwell for their helpful discussions during the preparation of this manuscript. We thank Anne
597 Mette Poulsen, Adam Wilkins, and Michael Thayne for their valuable editing of the manuscript.
598 We are also grateful to reviewers for their valuable comments on the manuscript. This study was
599 supported by FP-7 REFRESH (Adaptive strategies to Mitigate the Impacts of Climate Change on
600 European Freshwater Ecosystems, Contract No.: 244121) and the MARS project (Managing
601 Aquatic ecosystems and water Resources under multiple Stress), funded under the 7th EU
602 Framework Programme, Theme 6 (Environment including Climate Change), Contract No.:
603 603378 (<http://www.mars-project.eu>), TUBITAK- ÇAYDAG (projects no.: 105Y332 and
604 110Y125), the Middle East Technical University (METU)-BAP program of Turkey. EJ was
605 further supported by AU Centre for Water Technology and AİÇ was also supported by
606 TUBITAK (project 296 nos.: 105Y332 and 110Y125).

References

- Allen, A. P., J. F. Gillooly, and J. H. Brown. 2005. Linking the global carbon cycle to individual metabolism. *Funct. ecol.* 19: 202–213.
- Allen, A. P., and Gillooly. 2009. Towards an integration of ecological stoichiometry and the metabolic theory of ecology to better understand nutrient cycling. *Ecol. let.* 12: 369–384.
- Anderson-Teixeira, K. J., and P. M. Vitousek. 2012. Ecosystems, p. 99–111. In R. M. Sibly, J. H. Brown, A. Kodric-Brown [eds.], *Metabolic Ecology*. Wiley-Blackwell.
- Andersson, E., and S. Sobek. 2006. Comparison of a mass balance and an ecosystem model approach when evaluating the carbon cycling in a lake ecosystem. *Ambio* 35: 476–483.
- Angilletta, M. J. J. 2009. *Thermal Adaptation - A Theoretical and Empirical Synthesis*, Oxford University Press, Oxford.
- Atkin, O. K., and M. G. Tjoelker. 2003. Thermal acclimation and the dynamic response of plant respiration to temperature. *Trends plant sci.* 8: 343–51.
- Balmer, M. B., and J. A. Downing. 2011. Carbon dioxide concentrations in eutrophic lakes: undersaturation implies atmospheric uptake. *Inland Waters* 1: 125–132.
- Bartoń, K. 2015. MuMIn: Multi-Model Inference. R package version 1.13.4, <http://cran.r-project.org/package=MuMIn>.
- Bates, D., M. Maechler, B. Bolker, and S. Walker. 2014. lme4: Linear mixed-effects models using Eigen and S4. R package version 1.1-7, <http://cran.r-project.org/package=lme4>.
- Beklioglu, M., G. Altınayar, and C. T. Tan. 2006. Water level control over submerged macrophyte development in five Mediterranean Turkey. *Arch. hydrobiol.* 166 (4): 535–556.

630 Beklioglu, M., S. Romo, I. Kagalou, X. Quintana, and E. Bécares. 2007. State of the art in the
631 functioning of shallow Mediterranean Lakes: workshop conclusion. *Hydrobiologia* 196:
632 317–326.

633 Berggren, M., H. Laudon, A. Jonsson, and M. Jansson. 2010. Nutrient constraints on
634 metabolism affect the temperature regulation of aquatic bacterial growth efficiency.
635 *Microb. ecol.* 60: 894–902.

636 Bernacchi, C. J., E. L. Singsaas, C. Pimentel, A. R. Portis Jr., and S. P. Long. 2001. Improved
637 temperature response functions for models of Rubisco-limited photosynthesis. *Plant cell*
638 *environ.* 24: 253–259.

639 Brothers, S. M., S. Hilt, K. Attermeyer, H. P. Grossart, S. Kosten, B. Lischke, T. Mehner, N.
640 Meyer, K. Scharnweber, and J. Köhler. 2013. A regime shift from macrophyte to
641 phytoplankton dominance enhances carbon burial in a shallow, eutrophic lake. *Ecosphere*
642 4: 1–17.

643 Brown, J.H., J. F. Gillooly J. F., A. P. Allen, V. M. Savage, and G. B. West. 2004. Toward a
644 metabolic theory of ecology. *Ecology* 85: 1771–1789.

645 Cael, B.B., A.J. Heathcoate and D.A. Seekell. 2017. The volume and mean depth of Earth's
646 lakes. *Geophys. Res. Lett.* 44: 209–218.

647 Canty, A., and B. Ripley. 2015. boot: Bootstrap R (S-Plus) Functions. R package version 1.3-
648 15, <http://cran.r-project.org/package=boot>.

649 De Castro, F., and U. Gaedke. 2008. The metabolism of lake plankton does not support the
650 metabolic theory of ecology. *Oikos* 117: 1218–1226.

- Cole, J. J., M. L. Pace, S. R. Carpenter, and J. F. Kitchell. 2000. Persistence of net heterotrophy in lakes during nutrient addition and food web manipulations. *Limnol. oceanogr.* 45: 1718–1730.
- Cole, J. J., Y. T. Prairie, N. F. Caraco, W. H. McDowell, L. J. Tranvik, R. G. Striegl, C. M. Duarte, P. Kortelainen, J. A. Downing, J. J. Middelburg, and J. Melack. 2007. Plumbing the global carbon cycle: Integrating Inland waters into the terrestrial carbon budget. *Ecosystems* 10: 172–185.
- Coloso, J. J., J. J. Cole, and M. L. Pace. 2011. Difficulty in discerning drivers of lake ecosystem metabolism with high frequency data. *Ecosystems* 14: 935–948.
- Coops, H., M. Beklioglu, and T. L. Crisman. 2003. The role of water-level fluctuations in shallow lake ecosystems – workshop conclusions. *Hydrobiologia* 506: 23–27.
- Cross, W., J. Hood, J. Benstead, A. Huryn, and D. Nelson. 2015. Interactions between temperature and nutrients across levels of ecological organization. *Glob. chang. biol.* 21: 1025–1040.
- Davidson, E. A., S. Samanta, S. C. Samantha, and K. Savage. 2012. The Dual Arrhenius and Michaelis-Menten kinetics model for decomposition of soil organic matter at hourly to seasonal time scales. *Glob. chang. biol.* 18: 371–384.
- Davidson, T. A., J. Audet, J.-C. Svenning, T. L. Lauridsen, M. Søndergaard, F. Landkildehus, S. E. Larsen, and E. Jeppesen. 2015. Eutrophication effects on greenhouse gas fluxes from shallow-lake mesocosms override those of climate warming. *Glob. chang. biol.* 21: 4449–4463.
- Del Giorgio, P. A., and R. H. Peters. 1994. Patterns in planktonic P:R ratios in lakes: Influence of lake trophic and dissolved organic carbon. *Limnol. oceanogr.* 39: 772–787.

- Demars, B. O. L., J. Russell Manson, J. S. Ólafsson, G. M. Gíslason, R. Gudmundsdóttir, G. Woodward, J. Reiss, D. E. Pichler, J. J. Rasmussen, and N. Friberg. 2011. Temperature and the metabolic balance of streams. *Freshwater biol.* 56: 1106–1121.
- Demars, B. O. L., J. Thompson, and J. R. Manson. 2015. Stream metabolism and the open diel oxygen method: Principles, practice, and perspectives. *Limnol. oceanogr., methods* 13: 356–374.
- Demars, B. O. L., G. M. Gíslason, J. S. Ólafsson, J. R. Manson, N. Friberg, J. M. Hood, J. J. D. Thompson, and T. E. Freitag. 2016. Impact of warming on CO₂ emission from streams countered by aquatic photosynthesis. *Nat. geosci.* 9: 758–761.
- Duarte, C. M., S. Agustí, and D. Vaqué. 2004. Controls on planktonic metabolism in the Bay of Blanes, northwestern Mediterranean littoral. *Limnol. oceanogr.* 49: 2162–2170.
- Enquist, B. J., E. P. Economo, T. E. Huxman, A. P. Allen, D. D. Ignace, and J. F. Gillooly. 2003. Scaling metabolism from organisms to ecosystems. *Nature* 423: 639–42.
- Erlandsen, M., and N. Thyseen. 1983. Modelling the community oxygen production in lowland streams dominated by submerged macrophytes, p. 855-860. In W. K. Lauenroth, and G. V. Skogerboe [eds.], *Analysis of Ecological Systems: State-of-the art in Ecological Modelling*, Volume 5. Elsevier.
- Falkowski, J. A., and A. Raven. 2013. *Aquatic Photosynthesis*, Princeton University Press, New Jersey.
- Gelman, A. 2008. Scaling regression inputs by dividing by two standard deviations. *Stat. med.* 27: 2865–2873.
- Gillooly, J. F., J. H. Brown, G. B. West, V. M. Savage, and E. L. Charnov. 2001. Effects of size and temperature on metabolic rate. *Sci.* 293: 2248–2251.

Hanson, P. C., D. L. Bade, S. R. Carpenter, and T. K. Kratz. 2003. Lake metabolism: Relationships with dissolved organic carbon and phosphorus. *Limnol. oceanogr.* 48: 1112–1119.

Hartley, I. P., D. W. Hopkins, M. H. Garnett, M. Sommerkorn, and P. A. Wookey. 2008. Soil microbial respiration in arctic soil does not acclimate to temperature. *Ecol. let.* 11: 1092–1100.

Hikosaka, K., K. Ishikawa, A. Borjigidai, O. Muller, and Y. Onoda. 2006. Temperature acclimation of photosynthesis: Mechanisms involved in the changes in temperature dependence of photosynthetic rate. *J. exp. bot.* 57: 291–302.

Jeppesen, E., M. Søndergaard, T. L. Lauridsen, T. A. Davidson, Z. Liu, N. Mazzeo, C. Trochine, K. Özkan, H. S. Jensen, D. Trolle, F. Starling, X. Lazzaro, L. S. Johansson, R. Bjerring, L. Liboriussen, S. E. Larsen, F. Landkildehus, S. Egemose, and M. Meerhoff. 2012. Biomanipulation as a restoration tool to combat eutrophication: Recent advances and future challenges. *Adv. ecol. res.* 47: 411–488.

Jeppesen, E., S. Brucet, L. Naselli-Flores, E. Papastergiadou, K. Stefanidis, T. Nöges, P. Nöges, J. L. Attayde, T. Zohary, J. Coppens, T. Bucak, R. F. Menezes, F. R. Sousa Freitas, M. Kernan, M. Søndergaard, and M. Beklioğlu. 2015. Ecological impacts of global warming and water abstraction on lakes and reservoirs due to changes in water level and related changes in salinity. *Hydrobiologia* 750: 201–227.

Kim, S. 2012. ppcor: Partial and Semi-partial (Part) correlation. R package version 1.0, <http://cran.r-project.org/package=ppcor>.

Kirk, J. T. O. 2010. *Light and Photosynthesis in Aquatic Ecosystems*, 3rd ed.. Cambridge University Press.

720 Köhler J., L. Wang, A. Guislan and T. Shatwell. 2018. Influence of vertical mixing on light-
721 dependency of phytoplankton growth. *Limnol. oceanogr.* 63: 1156–1167.

722 Kosten, S., F. Roland, D. M. L. Da Motta Marques, E. H. van Nes, N. Mazzeo, L. da S. L.
723 Sternberg, and Marten Scheffer. 2010. Climate-dependent CO₂ emissions from lakes.
724 *Glob. biogeochem. cycles* 24: 1–7.

725 Kraemer B. M., S. Chandra, A. I. Dell, M. Dix, E. Kuusisto, D. M. Livingstone, S. G.
726 Schladow, E. Silow, L. M. Sitoki, R. Tamatamah and P. B. McIntyre. 2016. Global patterns
727 in lake ecosystem responses to warming based on the temperature dependence of
728 metabolism. *Glob. chang. biol.* 56: 1447–1455.

729 Kuznetsova, A., P. B. Brockhoff, and R. H. Bojesen. 2014. lmerTest: Tests in Linear Mixed
730 Effects Models. R package version 2.0-20, <http://cran.r-project.org/package=lmerTest>.

731 Laas, A., P. Nöges, T. Kõiv, T. Nöges. 2012. High-frequency metabolism study in a large and
732 shallow temperate lake reveals seasonal switching between net autotrophy and net
733 heterotrophy. *Hydrobiologia* 694: 57–74.

734 Lampert, W. and U. Sommer. 1999. *Limnoökologie*, 2nd ed. Georg Thieme Verlag, Stuttgart,
735 New York.

736 Landkildehus, F., M. Søndergaard, M. Beklioglu, R. Adrian, D. G. Angeler, J. Hejzlar, E.
737 Papastergiadou, P. Zingel, A. I. Çakiroğlu, U. Scharfenberger, S. Drakare, T. Nöges, M.
738 Šorf, K. Stefanidis, Ü. N. Tavşanoğlu, C. Trigal, A. Mahdy, C. Papadaki, L. Tuvikene, S.
739 E. Larsen, M. Kernan, and E. Jeppesen. 2014. Climate change effects on shallow lakes:
740 design and preliminary results of a cross-European climate gradient mesocosm experiment.
741 *Est. j. ecol.* 63: 71–89.

- Lenth, R. V., and M. Hervé. 2015. Least-Squares Means. R package version 2.16, <http://cran.r-project.org/package=lsmeans>
- Liboriussen, L., T. L. Lauridsen, M. Søndergaard, F. Landkildehus, M. Søndergaard, S. E. Larsen, and E. Jeppesen. 2011. Effects of warming and nutrients on sediment community respiration in shallow lakes: an outdoor mesocosm experiment. *Freshw. biol.* 56: 437–447.
- López-Urrutia, Á, E. San Martín, R. P. Harris, and X. Irigoien. 2006. Scaling the metabolic balance of the oceans. *PNAS* 103: 8739–8744.
- De Matos, M. P., A. C. Borges, A. T. de Matos, E. F. da Silva, and M. A. Martinez. 2014. Effect of time-temperature binomial in obtaining biochemical oxygen demand of different wastewaters. *Eng. agric.* 34: 332–340.
- McFeeters, B. J., and P. C. Frost. 2011. Temperature and the effects of elemental food quality on *Daphnia*. *Freshw. biol.* 56: 1447–1455.
- Moss, B. 2010. Climate change, nutrient pollution and the bargain of Dr Faustus. *Freshw. biol.* 55: 175–187.
- Nickus, U., K. Bishop, M. Erlandsson, C. D. Evans, M. Forsius, H. Laudon, D. M. Livingstone, D. Monteith, and H. Thies. 2010. Direct Impacts of climate change on Freshwater Ecosystems, p. 38–64. In M. Kernan, R. W. Battarbee and B. Moss [eds.], *Climate Change Impacts on Freshwater Ecosystems*. Wiley-Blackwell.
- Pacheco, F., and F. Roland. 2014. Eutrophication reverses whole-lake carbon budgets. *Inland Waters* 4: 41–48.
- Perkins, D. M., G. Yvon-Durocher, B. O. L. Demars, J. Reiss, D. E. Pichler, N. Friberg, M. Trimmer, and G. Woodward. 2012. Consistent temperature dependence of respiration across ecosystems contrasting in thermal history. *Glob. chang. biol.* 18: 1300–1311.

- Petersen, J. 2009. Enclosed Experimental Ecosystems and Scale: Tools for Understanding and Managing Coastal Ecosystems. Springer.
- R Core Team. 2015. R: A Language and Environment for Statistical Computing.
<http://www.R-project.org/>.
- Raven, J. A., and M. Giordano, J. Beardall, S. C. Maberly. 2011. Algal and aquatic plant carbon concentration mechanisms in relation to environmental change. *Photosyn. res.* 109: 281–296.
- Ripley, B., B. Venables, D. M. Bates, K. Hornik, A. Gebhardt, and D. Firth. 2015 MASS: Modern Applied Statistics with S. R package version 7.3-40, <http://cran.r-project.org/package=MASS>.
- Rogelj, J., M. Meinshausen, and R. Knutti. 2012. Global warming under old and new scenarios using IPCC climate sensitivity range estimates. *Nat. clim. chang.* 2: 248–253.
- De Rosario-Martinez, H. 2015. phia: Post-Hoc Interaction Analysis. R package version 0.2-0, <http://cran.r-project.org/package=phia>.
- Sadro, S., J. M. Melack, and S. MacIntyre. 2011. Spatial and temporal variability in the ecosystem metabolism of a high-elevation lake: Integrating benthic and pelagic habitats. *Ecosystems* 14: 1123–1140.
- de Senerpont Domis, L. N., D. B. van de Waal, N. R. Helmsing, E. van Donk, and W. M. Mooij. 2014. Community stoichiometry in a changing world: combined effects of warming and eutrophication on phytoplankton dynamics. *Ecology* 95: 1485–1495.
- Shatwell, T., A. Nicklisch, and J. Köhler. 2012. Temperature and photoperiod effects on phytoplankton growing under simulated mixed layer light fluctuations. *Limnol. oceanogr.* 57: 541–553.

788 Shatwell, T., R. Adrian, and G. Kirillin. 2016. Planktonic events may cause polymictic-
789 dimictic regime shifts in temperate lakes. *Sci. Rep.* 6: 24361.

790 Smith, N. G., and J. S. Dukes. 2012. Plant respiration and photosynthesis in global-scale
791 models: Incorporating acclimation to temperature and CO₂. *Glob. chang. biol.* 19: 45–63.

792 Solomon, C. T., D. A. Bruesewitz, D. C. Richardson, K. C. Rose, M. C. van de Bogert, P. C.
793 Hanson, T. K. Katz, B. Larget, R. Adrian, B. L. Babin, C.-Y. Chiu, D. P. Hamilton, E. E.
794 Gaiser, S. Hendricks, V. Istvánovics, A. Laas, D. M. O'Donnell, M. L. Pace, E. Ryder, P.
795 A. Staehr, T. Torgersen, M. J. Vanni, K. C. Weathers, and G. Zhu. 2013. Ecosystem
796 respiration: Drivers of daily variability and background respiration in lakes around the
797 globe. *Limnol. oceanogr.* 58: 849–866.

798 Staehr, P. A., and K. Sand-Jensen. 2006. Seasonal changes in temperature and nutrient control
799 of photosynthesis, respiration and growth of natural phytoplankton communities. *Freshw.*
800 *biol.* 51: 249–262.

801 Staehr, P. A., and K. Sand-Jensen. 2007. Temporal dynamics and regulation of lake
802 metabolism. *Limnol. oceanogr.* 52: 108–120.

803 Staehr, P. A., K. Sand-Jensen, A. L. Raun, B. Nilsson, and J. Kidmose. 2010. Drivers of
804 metabolism and net heterotrophy in contrasting lakes. *Limnol. oceanogr.* 55: 817–830.

805 Stocker, T. F., Q. Dahe, and G.-K. Plattner. 2013. Technical Summary, p. 33–116. In *Climate*
806 *Change 2013: The Physical Science Basis. Contribution of Working Group I to the Fifth*
807 *Assessment Report of the Intergovernmental Panel on Climate Change.*

808 Streeter, H. W., and E. B. Phelps. 1925. A study of the natural purification of the Ohio River.
809 Public Health Bulletin 146: U.S. Public Health Service, Washington DC, 1925.

Tranvik, L. J., J. A. Downing, J. B. Cotner, S. A. Loiselle, R. G. Striegl, T. J. Ballatore, P. Dillon, K. Finlay, K. Fortino, L. B. Knoll, P. L. Kortelainen, T. Kutser, S. Larsen, I. Laurion, D. M. Leech, S. L. McCallister, D. M. McKnight, J. M. Melack, E. Overholt, J. A. Porter, Y. Prairie, W. H. Renwick, F. Roland, B. S. Sherman, D. W. Schindler, S. Sobek, A. Tremblay, M. J. Vanni, A. M. Verschoor, E. von Wachenfeldt, and G. A. Weyhenmeyer. 2009. Lakes and reservoirs as regulators of carbon cycling and climate. *Limnol. oceanogr.* 54: 2298–2314.

Trolle, D., P. A. Staehr, T. A. Davidson, R. Bjerring, T. L. Lauridsen, M. Søndergaard, and E. Jeppesen. 2012. Seasonal dynamics of CO₂ flux across the surface of shallow temperate lakes. *Ecosystems* 15: 336–347.

Welter, J. R., P. B. Jonathan, W. F. Cross, J. M. Hood, A. D. Huryn, P. W. Johnson, and T. J. Williamson. 2015. Does N₂ fixation amplify the temperature dependence of ecosystem metabolism? *Ecology* 93: 603–610.

Wetzel, R. G. 2001. *Limnology: Lake and river ecosystems*, 3rd ed. Academic Press.

Weyhenmeyer, G. A., S. Kosten, M. B. Wallin, L. J. Tranvik, E. Jeppesen, and R. Fabio. 2015. Significant fraction of CO₂ emissions from boreal lakes derived from hydrologic inorganic carbon inputs. *Nat. geosci.* 8: 933–936.

Wilhelm, S., and R. Adrian. 2008. Impact of summer warming on the thermal characteristics of a polymictic lake and consequences for oxygen, nutrients and phytoplankton. *Freshw. biol.* 53: 226–237.

Wilken, S., J. Huisman, S. Naus-Wiezer, and E. van Donk. 2013. Mixotrophic organisms become more heterotrophic with rising temperature. *Ecol. lett.* 16: 225–233.

Wykoff, D. D., J. P. Davies, A. Melis, A. R. Grossman. 1998. The regulation of photosynthetic electron transport during nutrient deprivation in *Chlamydomonas reinhardtii*. Plant physiol. 117: 129–139.

Yvon-Durocher, G., A. P. Allen, J. M. Montoya, M. Trimmer, and G. Woodward. 2010a. The temperature dependence of the carbon cycle in aquatic ecosystems, pp. 267–313. In G. Woodward [ed.], Advances in Ecological Research, Vol. 43. Elsevier.

Yvon-Durocher, G., J. I. Jones, M. Trimmer, G. Woodward, and J. M. Montoya. 2010b. Warming alters the metabolic balance of ecosystems. Philos. trans. –R. Soc., Biol. Sci. 365: 2117–26.

Yvon-Durocher, G., J. M. Caffrey, A. Cescatti, M. Dossena, P. del Giorgio, J. M. Gasol, J. M. Montoya, J. Pumpanen, P. A. Staehr, M. Trimmer, G. Woodward, and A. P. Allen. 2012. Reconciling the temperature dependence of respiration across timescales and ecosystem types. Nature 487: 472–476.

Figure legends

Figure 1: a) Development of water temperature and b) change in water level due to evaporation losses and precipitation gains over the experimental period from June to November by country. SE = Sweden, EE = Estonia, CZ = Czech Republic, GE = Germany, TR = Turkey, GR = Greece.

Figure 2: Covariation of nutrients with water temperature. Covariation of monthly a) total phosphorus (TP) and b) total nitrogen (TN) levels with water temperature by treatment. Main images show treatment-specific least-square means over the temperature gradient with 95% confidence intervals at the scale of the transformed variable. The insets depict TP and TN at original scale with treatment-specific average TP or TN concentrations as estimated by mixed effects regression (S3 Table 1). DH = deep high nutrient, SH = shallow high nutrient, DL = deep low nutrient and SL = shallow low nutrient treatment.

Figure 3: Treatment-wise metabolic rates at 15 °C as estimated by mixed effects regression. Values were back transformed to original scale, depicting the geometric mean (Table 3). Error bars represent the 95% confidence interval of the geometric mean. DH = deep high nutrient, SH = shallow high nutrient, DL = deep low nutrient and SL = shallow low nutrient treatment.

Figure 4: Arrhenius plot of GPP and ER for each treatment (DH = deep high nutrient, SH = shallow high nutrient, DL = deep low nutrient and SL = shallow low nutrient). The plot is based on monthly measurements from July to November along a temperature gradient from Sweden to Greece. The solid line is the estimated average GPP; the dotted line is the average ER as estimated by mixed effects regression. Note that the actual units of the x-axis of the Arrhenius

plot are $1/k (1/T_c - 1/T)$ in units of electron volts and a reference temperature, T_c , of 15 °C; for easier interpretation, corresponding temperatures in degrees Celsius are depicted.

Figure 5: Water temperature-dependent switch from net autotrophy to net heterotrophy. a) Average treatment-specific change in ER/GPP ratio over the temperature gradient as estimated by mixed effect model (Table 3). b) Theoretically predicted switch point temperatures from autotrophy to heterotrophy depending on the ER/GPP ratio at a reference temperature of 15 °C (Equation 5). The solid line depicts the switch point temperature for activation energies of 0.54 eV and 0.62 eV for GPP and ER, respectively. The dashed line represents the relation at an activation energy of 0.31 eV for GPP, as suggested by the metabolic theory of ecology and established as the average apparent activation energy for daylight length-corrected primary production. Superimposed are the treatment-wise average switch point temperatures as established by mixed effects regression (Table 3). DH = deep high nutrient, SH = shallow high nutrient, DL = deep low nutrient and SL = shallow low nutrient treatment.

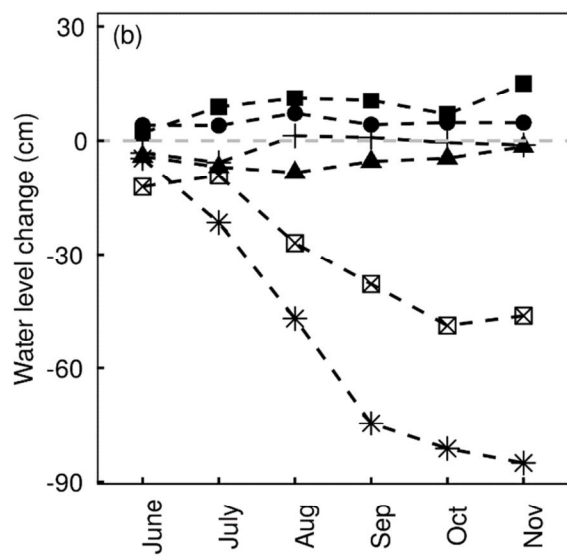
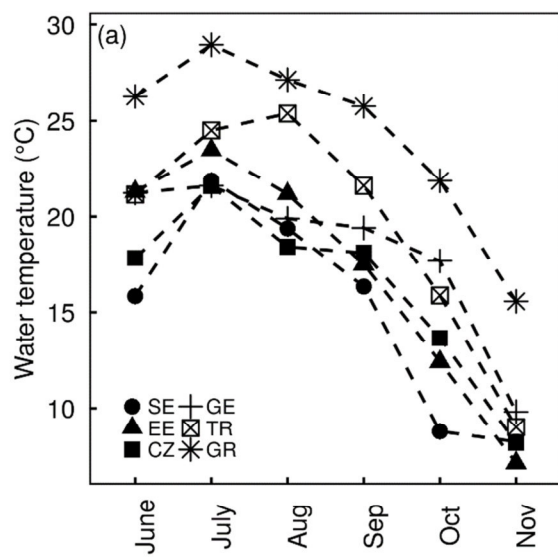
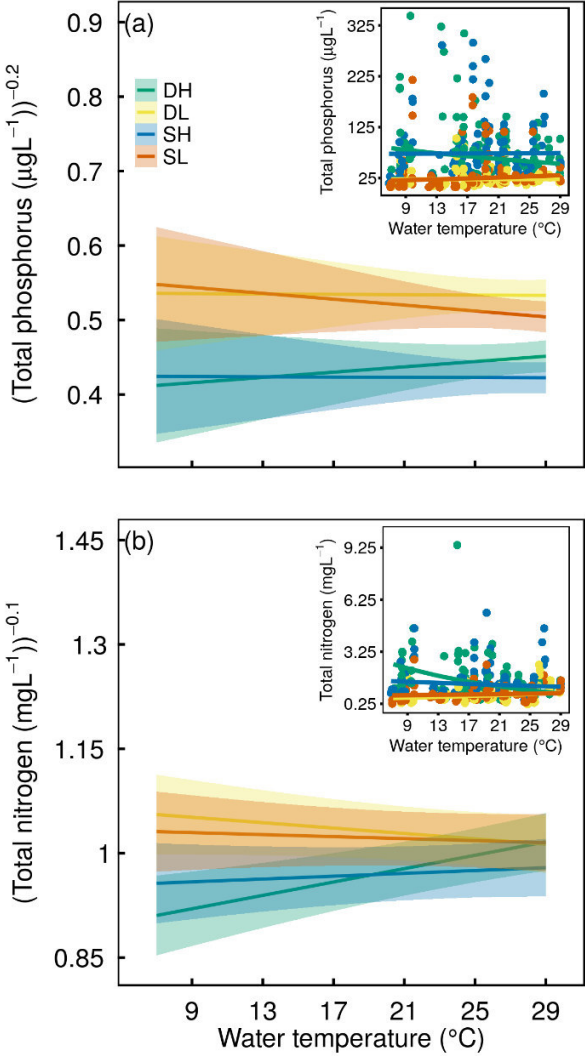
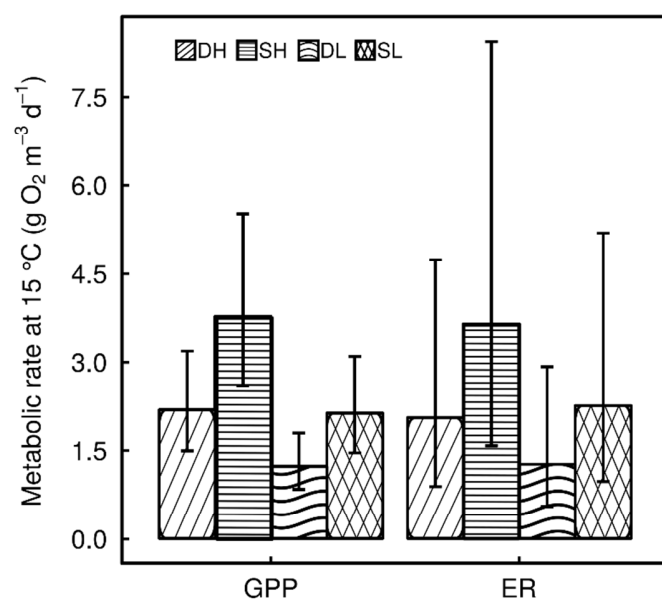


Figure 1

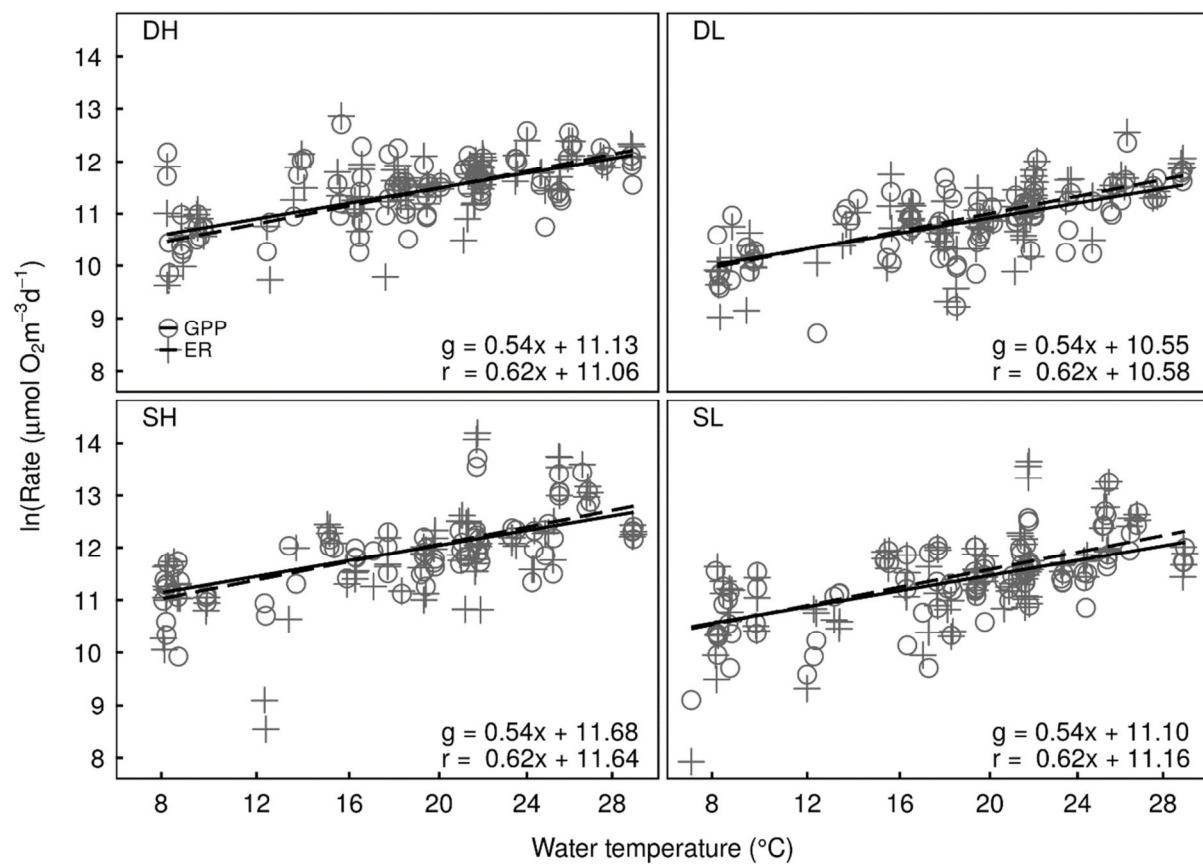




47

48 Figure 3

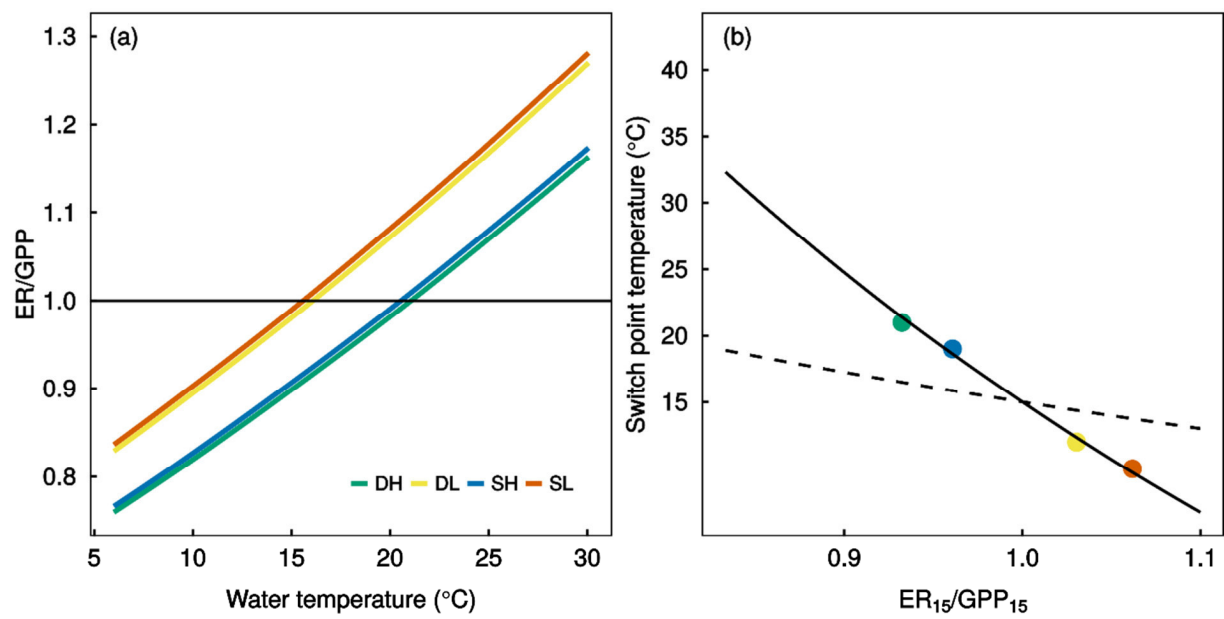
49



50

51 Figure 4

52



53

54 Figure 5

1 **Table 1:** Location of experimental sites and average temperatures. Average air temperatures were
2 calculated based on daily average air temperatures of the periods leading up to the 24-hour
3 measurements as defined in S1 Table 1. Water temperatures are daily averages based on 24-hour
4 point measurements (S1 Table 1).

Experimental site	Coordinates	Altitude (m a.s.l.)	Air temperature (°C)			Water temperature (°C)		
			Mean	Min	Max	Mean	Min	Max
Sweden (SE) - Erken	59°49'59"N 18°33'55"E	11	14.5	8.7	18.8	14.9	8.1	22.0
Estonia (EE) - Võrtsjärv	58°12'17" N 26°06'16" E	35	15.1	7.5	19.9	16.3	6.8	24.0
Germany (GE) - Müggelsee	52°26'0" N 13°39'0" E	32	16.0	9.6	18.4	17.7	9.7	21.7
Czech Republic (CZ) - Vodňany	49°09'14"N 14°10'11"E	395	15.2	7.5	18.8	16.0	8.1	22.0
Turkey (TR) - ODTÜ-DSİ Gölet	39°52'38" N 32°46'32" E	998	20.0	10.4	26.2	19.3	8.2	25.6
Greece (GR) - Lysimachia	38°33'40" N 21°22'10" E	16	23.8	15.0	27.9	24.8	15.4	29.1

Table 2: Results from minimal linear mixed effect regressions. The effects of inverse scaled temperature (invT), depth (D) and nutrients (N), as well as their interactions, were tested on: gross primary production per day (GPP), ecosystem respiration per day (ER), primary production per daylight hour (GPP_{dl}), and the ratio between ecosystem respiration and gross primary production (ER/GPP). Effect size is given as regression coefficients from standardized predictors (Shallow = -0.5, Deep = 0.5, Low = -0.5, High = 0.5). The first R² value refers to the marginal R² (variance explained by fixed factors) and the second to the conditional R² (variance explained by fixed and random factors).

Response	Predictor	Effect size	Std. error	T-value	P-value	R ²
ln(GPP)	Int	11.34	0.14	77.99	<0.01	0.50, 0.8
	invT	-0.91	0.16	-3.29	0.02	
	D	-0.55	0.03	-9.93	<0.01	
	N	0.58	0.03	10.52	<0.01	
ln(ER)	Int	11.37	0.32	34.99	<0.01	0.33, 0.88
	invT	-1.05	0.24	-2.54	0.06	
	D	-0.58	0.03	-9.37	<0.01	
	N	0.48	0.03	7.91	<0.01	
ln(GPP _{dl})	Int	8.71	0.18	46.68	<0.01	0.34, 0.78
	invT	-0.53	0.15	-2.03	0.10	
	D	-0.54	0.03	-9.74	<0.01	
	N	0.58	0.03	10.49	<0.01	
	N	0.48	0.03	9.29	<0.01	
ln(ER/GPP)	Int	- 0.01	0.14	-0.41	0.71	0.04, 0.60
	invT	-0.22	0.10	-1.27	0.27	
	D	-0.01	0.02	-0.20	0.85	
	N	-0.09	0.02	-1.99	0.05	

Table 3: Slope (activation energy), intercept (average metabolic rate at 15 °C), and temperature at which the systems switch from autotrophy to heterotrophy. Slope and intercept values are derived from minimal mixed effect models, i.e. models from which all insignificant terms are removed, but which contain at least the inverse scaled temperature and the main effects of the depth and nutrient treatment (Table 2). 95% confidence intervals are given in brackets. Confidence intervals for activation energies were computed based on likelihood profiles (“confint.merMod” function of the “lme4” package). Treatment-specific confidence intervals for the intercepts were computed based on t-statistics with degrees of freedom determined by the Kenward & Rogers method (“lsmeans” function of the “lsmeans” package). DH = deep high nutrient, SH = shallow high nutrient, DL = deep low nutrient and SL = shallow low nutrient treatment.

		GPP	ER	GPP _{dl}	ER/GPP
Activation energy [eV]	DH				
	SH	0.54	0.62	0.31	0.13
	DL	(0.9 – 0.2)	(1.14 – 0.11)	(0.65 – -0.01)	(0.36 – -0.08)
	SL				
Intercept at 15 °C ln[μmol O ₂ m ⁻³ d ⁻¹] or ln[μmol O ₂ m ⁻³ LP ⁻¹]	DH	11.13 (10.78 – 11.47)	11.06 (10.30 – 11.83)	8.60 (8.15 – 9.06)	-0.11 (-0.47 – 0.26)
	SH	11.68 (11.33 – 12.02)	11.64 (10.87 – 12.41)	9.14 (8.69 – 9.60)	-0.10 (-0.46 – 0.27)
	DL	10.55 (10.20 – 10.90)	10.58 (9.81 – 11.35)	8.03 (7.57 – 8.48)	-0.02 (-0.38 – 0.35)
	SL	11.10 (10.75 – 11.45)	11.16 (10.39 – 11.92)	8.57 (8.11 – 9.03)	-0.01 (-0.38 – 0.35)
Switch point temperature [°C]	DH	21			21
	SH	19			21
	DL	12			16
	SL	10			16

Table 4: Bootstrapped semi-partial Spearman correlation coefficient r over all treatments (all) and treatment-specific (S = shallow, D = deep, H = high nutrient, L = low nutrient) for the three criterion variables GPP, ER, and ER/GPP and the following predictor variables: inverse-scaled temperature (invT), chlorophyll a (Chl a), PVI (plant volume inhabited), effective light period (LP_{eff}), mean available light (MAL), daylight length (DayL), ER/GPP ratio, GPP, and ER. Only r values ≥ 0.10 are reported, “*” denotes values where the 95% confidence interval did not include zero, “-” denotes cells of variables not used as predictors for the particular variable.

		invT	Chl a	PVI	LP_{eff}	MAL	DayL	GPP
GPP	all	-0.23*	0.33*		-0.12*	0.24*		-
	DH	-0.22	0.28*		-0.15*	0.16	0.15	-
	SH	-0.40*	0.23*	0.12			0.25*	-
	DL	-0.41*			-0.18*	0.13		-
	SL	-0.28*		0.27*				-
ER	all	-0.19*			-	-	-	0.52*
	DH	-0.27*			-	-	-	0.43*
	SH	-0.19*	0.1	0.14*	-	-	-	0.32*
	DL	-0.28*		0.12	-	-	-	0.38*
	SL	-0.19*			-	-	-	0.38*
ER/GPP	all	-0.23*					-0.10*	-
	DH	-0.16	-0.12			-0.14		-
	SH	-0.20*			-0.12			-
	DL	-0.29*				-0.16	-0.11	-
	SL	-0.25*			-0.16			-

Appendix S1

S1 Table 1: Country-wise measurement dates for the 24-h measurement and associated month and period of analysis. Monthly 24-h measurements for measurement 3 – 7 were planned to take place on 12.07, 09.08, 06.09, 04.10 and 1.11. However, the actual measurements deviated slightly from this date; thus, average values for each country, for instance monthly air temperature, are calculated over the individual period for each country leading up to a 24-h measurement.

		Sweden		Estonia		Germany		Czech Republic		Turkey		Greece	
Measurement no.	Associated month	Date	Period	Date	Period	Date	Period	Date	Period	Date	Period	Date	Period
3	July	11.07 12.07	14.06 – 11.07	12.07 13.07	09.06 – 12.07	11.07 12.07	15.06 – 11.07	11.07 12.07	14.06 – 11.07	12.07 13.07	15.06 – 12.07	15.07 16.07	16.06 – 15.07
4	August	15.08 16.08	12.07 – 15.08	09.08 10.08	13.07 – 09.08	08.08 09.08	12.07 – 08.08	08.08 09.08	12.07 – 08.08	08.08 09.08	13.07 – 08.08	13.08 14.08	16.07 - 13.08
5	September	13.09 14.09	16.08 - 13.09	05.09 06.09	10.08 – 05.09	05.09 06.09	09.08 – 06.09	05.09 06.09	09.08 – 05.09	06.09 07.09	09.08 – 06.09	11.09 12.09	14.08 – 11.09
6	October	18.10 19.10	14.09 - 18.10	03.10 04.10	06.09 – 03.10	04.10 05.10	07.09 – 04.10	03.10 04.10	06.09 – 03.10	04.10 05.10	07.09 – 04.10	10.10 11.10	12.09 – 10.10
7	November	07.11 08.11	19.10 - 07.11	31.10 01.11	04.10 – 31.10	31.10. 01.11	05.10 – 31.10	30.10 31.10	04.10 – 31.10	01.11 02.11	05.10 - 01.11	08.11 09.11	11.10 - 31.10

S1 Table 2: Available data points for the statistical analysis of GPP, ER and metabolic balance (ER/GPP) and their distribution over countries, months and treatments. Imbalance in the data is due to loss of mesocosms during storm events and removal of GPP and ER estimates with standard errors larger than the estimated value or less than 5% explained variability by the model.

Country	Treatment	June	July	Aug	Sep	Oct	Total
SE	DH	4	4	4	4	3	76
	DL	4	4	4	2	4	
	SH	4	4	4	3	4	
	SL	4	4	4	4	4	
EE	DH	4	3	4	2	0	50
	DL	4	4	3	1	0	
	SH	4	3	1	2	0	
	SL	4	4	3	3	1	
GE	DH	2	2	2	2	2	60
	DL	3	3	3	3	3	
	SH	3	3	3	3	3	
	SL	4	4	4	4	4	
CZ	DH	4	4	3	4	2	46
	DL	1	3	3	4	1	
	SH	1	1	0	2	2	
	SL	3	3	1	3	1	
TR	DH	3	4	4	4	4	73
	DL	2	3	4	4	3	
	SH	3	4	4	4	4	
	SL	4	4	4	4	3	
GR	DH	4	4	4	4	4	69
	DL	4	4	4	4	4	
	SH	4	4	4	2	0	
	SL	4	4	4	3	0	
Total		81	84	78	75	56	374

S1 Table 3: Country- and month-wise average air temperature. For each month, column 5 shows the temperature range in regard to the warmest and the coldest country along the climate gradient, as well as the standard deviation between countries.

Month	Country	Average air temperature [°C]	Monthly average air temperature [°C]	Range [°C]/Std [°C]
July	SE	16.86	20.01	9.56/ 3.52
	EE	18.75		
	GE	18.43		
	CZ	17.98		
	TR	21.64		
	GR	26.42		
August	SE	18.81	21.29	10.11/ 4.33
	EE	19.92		
	GE	18.37		
	CZ	17.16		
	TR	26.23		
	GR	27.27		
September	SE	16.7	20.18	11.51/ 4.44
	EE	16.35		
	GE	18.4		
	CZ	18.79		
	TR	22.99		
	GR	27.86		
October	SE	11.64	16.01	11.04/ 4.04
	EE	13.2		
	GE	15.32		
	CZ	14.49		
	TR	18.74		
	GR	22.68		
November	SE	8.71	9.78	7.50/ 2.79
	EE	7.47		
	GE	9.61		
	CZ	7.5		
	TR	10.44		
	GR	14.97		

Appendix S2: Methods

S2.1 Estimation of primary production (GPP) and ecosystem respiration (ER) rates

Temporal dynamics of dissolved oxygen were modelled according to Jeppesen et al. (2012):

$$\frac{dDO}{dt} = K_{a,20} \Phi^{(T_t-20)} (DO_{sat} - O_2) + \rho \frac{I_t}{\eta + I_t} - \pi$$

where DO [mg L⁻¹] is the measured dissolved oxygen concentration, t [h] is time, K_{a,20} [h⁻¹] is the reaeration coefficient as established in the gas exchange experiment, T [°C] is the water temperature, I_t [mol photons m⁻²s⁻¹] is the surface photosynthetically active radiation, Φ_K=1.0241 is the coefficient for the Arrhenius type temperature dependence of the reaeration coefficient and DO_{sat} [mg L⁻¹] is the saturation concentration of dissolved oxygen estimated following Benson & Krause (1980, 1984). Corrections for atmospheric pressure were made based on monthly mean air pressure data for each experimental site. The model uses a Michaelis Menten type relation to describe light saturation of primary production. We did not use the Arrhenius type temperature model suggested by Jeppesen et al. (2012) since we were particularly interested in investigating the temperature responses of the metabolic rates to the climate gradient. The parameter ρ [mg l⁻¹h⁻¹] is interpreted as the maximum obtainable production rate, η [mol photons m⁻²s⁻¹] is the light intensity at which the primary production reaches half its maximum (half saturation constant) and π [mg l⁻¹h⁻¹] is the average rate of ecosystem respiration. GPP and ER per day are then calculated as follows:

$$GPP \left[\frac{mg}{ld} \right] = \rho \sum_t \frac{I_t}{\eta + I_t} \Delta t$$

$$ER \left[\frac{mg}{ld} \right] = \pi \cdot 24$$

where Δt [h] is the time difference between two consecutive measurements.

For estimation of ρ, π and η, we used the shuffled complex evolution optimisation algorithm (SCE) as implemented in the R package "hydromad" (Andrews & Guillaume, 2014) to minimise the sum of the squared residuals. Starting values for all three parameters were found using a brute force grid search within the range 0.0001 to 5 applying the nls2 R package (Grothendieck, 2013). To assess the uncertainty of the estimated production and respiration rates, we used a bootstrap approach similar to that in Solomon et al. (2013) where the autocorrelation of lag 1 and the variance from the residuals of the original data are used to construct bootstrapped residuals with the same autocorrelation and variance as the original data. Those bootstrapped residuals are then added to the fitted values and the estimation, using the same starting values, is repeated for the so generated pseudo dDO replicates.

Estimates with standard errors larger than the estimate itself:

$$\frac{\sqrt{\left(\frac{1}{500} \sum_i^{500} (e_i - e)^2 \right)}}{e} > 1$$

where e_i are the bootstrapped estimates and e is the estimate from the raw data and estimates explaining less than 5% of the variability of the 24-h dissolved oxygen curve were excluded

from further analysis. Overall, 374 data points remained. For an overview of the distribution of data points per country, month and treatment, see S1 Table 2. To obtain day length-corrected GPP values, $GPP_{dl} [mg L^{-1} hd^{-1}]$, GPP per day was divided by the average daylight period, LP (hd^{-1}), per month and country.

S2.2 Estimation of light attenuation coefficient, K_d , mean available light and effective light period

Global radiation was converted to PAR using the transformation given in Kirk (2010):

$$PAR \approx E \cdot \gamma \cdot 0.45$$

where PAR is given in $\mu mol m^{-2} s^{-1}$ and E in $W m^{-2}$; $\gamma = 4.6 \mu mol J^{-1}$ is a conversion factor based on the centre wavelength of 550 nm of the 400 – 700 nm waveband (McCree, 1981). For each light profile (d) and each concurrent light intensity measurement (i), the attenuation coefficient $K_{di} (m^{-1})$ was estimated based on the Beer-Lambert law:

$$K_{di} = \frac{\ln \frac{I_i}{I_{i+1}}}{z_{i+1} - z_i}$$

, where I_i and I_{i+1} are PAR values at depth z_i and z_{i+1} . Values with $I_{i+1} > I_i$ were removed. $K_d (m^{-1})$ was then taken as the mean of all K_{di} .

Mean available light (\bar{I} , $\mu mol photons m^{-2} s^{-1}$) was estimated as:

$$\bar{I} = \frac{I_0}{z \cdot K_d} (1 - e^{-K_d \cdot z})$$

, where I_0 is the incident light just beneath the surface. If only incident light measurements were available, we corrected values for 10% backscatter (Kirk, 2010; Staehr et al., 2010). Effective light period, LP_{eff} , was calculated as described in Shatwell et al. (2012):

$$LP_{eff} = \frac{z_{1\%}}{z_{mix}} \cdot LP$$

, where $z_{1\%}$ (m) is the euphotic depth (depth at which 1% of surface light intensity is left), z_{mix} is the mixing depth, coinciding in our fully mixed mesocosms with the water column height, and LP is the mean light period (hd^{-1}) per month and country. Values were limited to one since the experienced LP cannot be larger than the actual LP. If $z_{1\%}$ is lower than z_{mix} , the effective day length is shorter than the actual LP due to mixing.

S2 Table 1: Overview of the used methods for water chemistry and chlorophyll a analysis.

	TP	TN	Ch a
Sweden	EN ISO 6878	EN ISO 11905-1 Tecator AN 5202-SE with a FIAstar 5000 system	Spectrophotometrically at a wavelength of 665 nm from acetone extraction. Material gained on GF/F glass microfiber filters by filtering of the water samples.
Estonia	ISO 15681-2	ISO 29441	Spectrophotometrically (Edler 1979) at a wavelength of 665 nm from 96% ethanol extracts. Material gained on GF/F glass microfiber filters by filtering of the water samples.
Germany	EN ISO 6878 (DEV, D11)	EN 12260 (DEV, H 34)	High-performance liquid chromatography (Waters, USA) following Fietz & Nicklish (2004).
Czech Republic	TP was determined spectrophotometrically with a molybdate method after perchloric acid digestion according to Kopáček J. and Hejzlar J. (1993) Semi-micro determination of total phosphorus in fresh waters with perchloric acid digestion. Int. J. Environ. Anal. Chem. 53, 173-183.	EN 12260 (DEV, H 34) Elementar vario TOC cube analyser (Elementar Analysensysteme GmbH, Germany).	Spectrophotometrically (Edler 1979) at a wavelength of 665 nm from 96% ethanol extracts. Material gained on glass-fibre filters of 0.4-µm nominal pore size (GF-5, Macherey-Nagel, Düren, Germany) by filtering of the water samples.
Turkey	ISO 6878:2004	ISO 29441:2010	Spectrophotometrically (Edler 1979) at a wavelength of 665 nm from 96% ethanol extracts. Material gained on GF/F glass microfiber filters by filtering of the water samples.
Greece	ISO 6878:2004	ISO 11905-1 and then use of a Shimadzu TOC- VCS/CP analyzer, equipped with TNM-1 TN unit.	Spectrophotometrically (Edler 1979) at a wavelength of 665 nm from 96% ethanol extracts. Material gained on GF/F glass microfiber filters by filtering of the water samples.

S2 Table 2: Overview of the used meteorological data and data providers. Global radiation was converted to PAR using the transformation given in Kirk (2010).

Country/ Variable	Air temperature (AT)	Air pressure (AP)	Photosynthetically active radiation (PAR) or Global radiation (GlobR)
Sweden	Laboratory Weather Station at Lake Erken, Department of Ecology and Genetics, Uppsala University. Measured at Lake Erken.	Swedish Meteorological and Hydrological Institute. Measured at Lake Erken.	Swedish Meteorological and Hydrological Institute. GlobR was measured at Norrköping.
Estonia	Centre of Limnology of the Estonian University of Life Sciences. Measured at Lake Võrtsjärv.		
Germany	Leibniz-Institute of Freshwater Ecology and Inland Fisheries (IGB). Measured at Lake Müggelsee.		
Czech Republic	České Budějovice - Institute of Hydrobiology. Measured at the the Římov Reservoir.	České Budějovice – Czech Hydrometeorological Institute. Measured at the the Římov Reservoir	České Budějovice - Institute of Hydrobiology. GlobR was measured at the the Římov Reservoir.
Turkey	Turkish State Meteorology Service (Ankara)		
Greece	Hellenic National Meteorological Service		

S2 References

- Andrews F, Guillaume J (2014) hydromad: Hydrological Model Assessment and Development.
- Benson BB, Krause DJ (1980) The concentration and isotopic fractionation of gases dissolved in freshwater in equilibrium with the atmosphere. 1. Oxygen. *Limnology and Oceanography*, **24**, 662–671.
- Benson BB, Krause D (1984) The concentration and isotopic fractionation of oxygen dissolved in freshwater and seawater in equilibrium with the atmosphere. *Limnology and Oceanography*, **29**, 620–632.
- Edler L (1979) Recommendations for marine biological studies in the Baltic Sea. Phytoplankton and Chlorophyll. *The Baltic Marine Biologists*, 5, 1–38
- Fietz S and Nicklish A (2004) An HPLC analysis of the summer phytoplankton assemblage in Lake Baikal. *Freshwater Biology*, 49, 332–345
- Grothendieck G (2013) nls2: Non-linear regression with brute force.
- Jeppesen E, Lauridsen TL, Davidson TA et al. (2012) Biomanipulation as a restoration tool to combat eutrophication: Recent advances and future challenges. *Advances in Ecological Research*, **47**, 411–488.
- Kirk JTO (2010) *Light and Photosynthesis in Aquatic Ecosystems*, 3rd edn. Cambridge University Press, 649 pp.
- McCree KJ (1981) Photosynthetically active radiation. In: *Physiological plant ecology*. Lang OL, Nobel P, Osmond B, Ziegler (ed). Vol. 12A, *Encyclopedia of plant physiology (new series)*. Springer-Verlag. Berlin, Heidelberg, New York.
- Shatwell T, Nicklisch A, Köhler J (2012) Temperature and photoperiod effects on phytoplankton growing under simulated mixed layer light fluctuations. *Limnology and Oceanography*, **57**, 541–553.
- Solomon CT, Bruesewitz DA, Richardson DC et al. (2013) Ecosystem respiration: Drivers of daily variability and background respiration in lakes around the globe. *Limnology and Oceanography*, **58**, 849–866.
- Staehr PA, Sand-Jensen K, Raun AL, Nilsson B, Kidmose J (2010) Drivers of metabolism and net heterotrophy in contrasting lakes. *Limnology and Oceanography*, 55, 817–830.

Appendix S3: Treatment differences in nutrients, light conditions, chlorophyll a and PVI and covariation with temperature

Proxies to assess the effects of the differential monthly loading of phosphate and nitrogen are TP and TN levels. Average TP levels in deep mesotrophic and shallow eutrophic mesocosms were almost constant over the entire temperature gradient. Whereas TP concentrations in shallow mesotrophic mesocosms increased with temperature (on average $10.2 \mu\text{g L}^{-1}$ over 7 to 29 °C), and decreased in the deep eutrophic mesocosms (on average $30.6 \mu\text{g TP L}^{-1}$ over 7 to 29 °C). Despite these dynamics, all treatments exhibited significantly different TP levels over the entire temperature gradient (Figure 2, S3 Table 1).

The average TN concentration showed only slight changes over the temperature gradient for all treatments except in the deep eutrophic mesocosms where they decreased with, on average, 1.5 mg TN L^{-1} along the whole temperature gradient from 7 to 29 °C. Due to these differences in dynamics, TN levels between deep eutrophic and both mesotrophic treatments were no longer significantly different for temperatures above 25 °C (SL) and 26 °C (DL) (Figure 2, S3 Table 1).

Average light attenuation (K_d) was significantly higher in the eutrophic than in the mesotrophic mesocosms. For the contrast between shallow mesotrophic and deep eutrophic mesocosms, this is, however, only true for temperatures above 10 °C. Generally, average light attenuation showed only small changes over the temperature gradient, with the exception of the shallow eutrophic mesocosms where attenuation decreased with increasing temperatures (1.1 m^{-1} from 7 to 29 °C) (S3 Figure 1a, S3 Table 1).

Average mean available light (MAL) was highest in the shallow mesotrophic mesocosms (adjusted mean: $111 \mu\text{mol photons m}^{-2} \text{ s}^{-1}$) along the entire temperature gradient, followed by the shallow eutrophic, deep mesotrophic mesocosms and, finally, the deep eutrophic mesocosms (adjusted mean: $41 \mu\text{mol photons m}^{-2} \text{ s}^{-1}$). MAL increased strongly with temperature for the shallow mesocosms and slightly less for the deep mesocosms, leading to more pronounced differences between treatments with increasing temperature. MAL differed significantly for all pairwise treatment comparisons over the temperature gradient. However, for the deep mesotrophic and shallow eutrophic mesocosms, this was only true for temperatures higher than 9 °C (S3 Figure 1b, S3 Table 1).

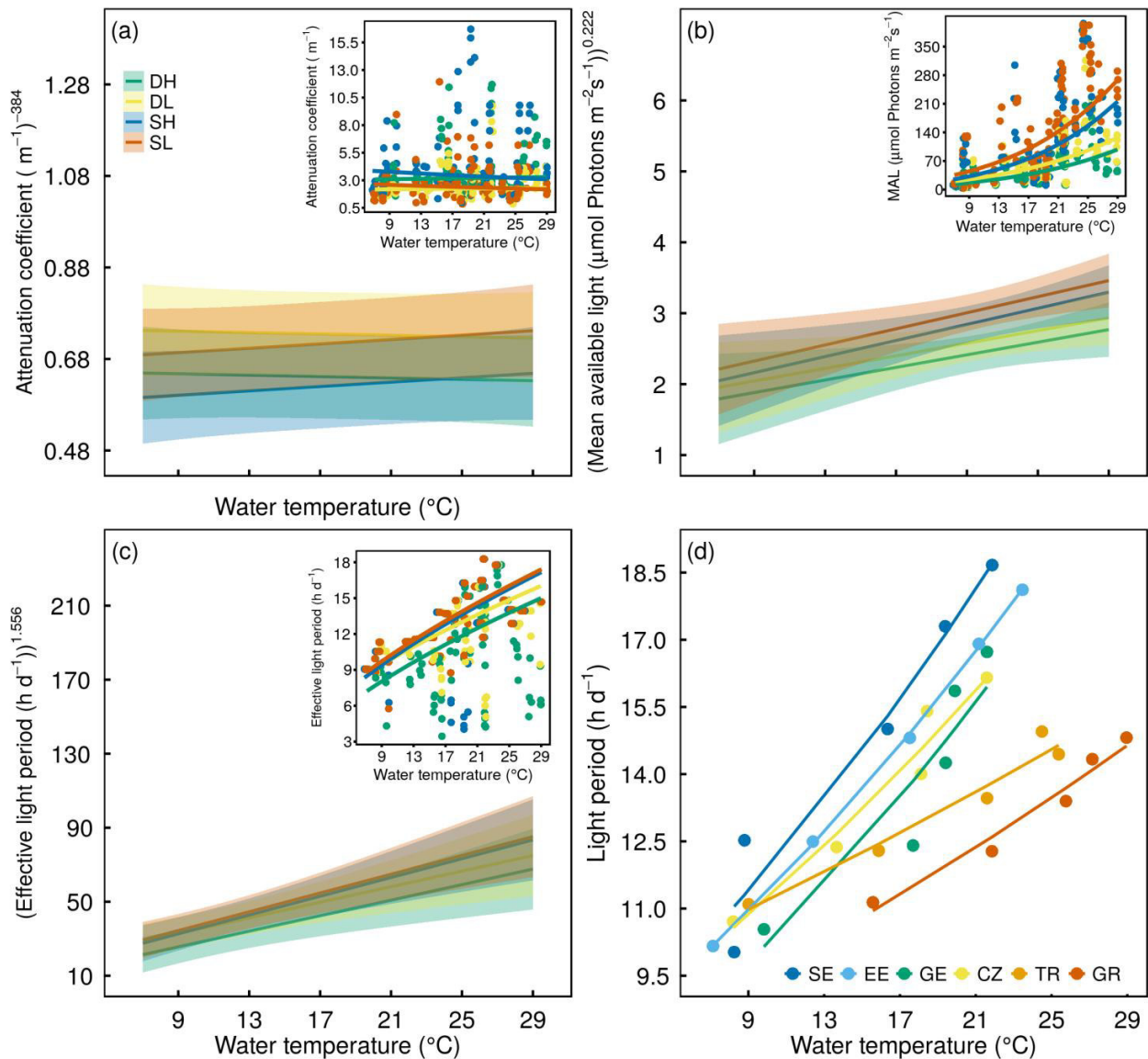
The average effective light period (LP_{eff}) was longest in the shallow mesotrophic mesocosms (adjusted mean: 13.6 h d^{-1}); however, LP_{eff} in the shallow eutrophic and deep mesotrophic mesocosms was only slightly shorter. LP_{eff} in the deep mesotrophic mesocosms was only significantly shorter than in the shallow mesocosms for temperatures above 15 °C (SL) and 21 °C (SH). Along the entire temperature gradient, the deep eutrophic mesocosms had a significantly shorter LP_{eff} (adjusted mean: $11.47 \text{ h LP}_{\text{eff}} \text{ h d}^{-1}$) (S3 Figure 1c, S3 Table 1).

The coinciding increase in temperature with daylight hours was more pronounced in the northern and mid-European than in the southern European countries (S3 Figure 1d).

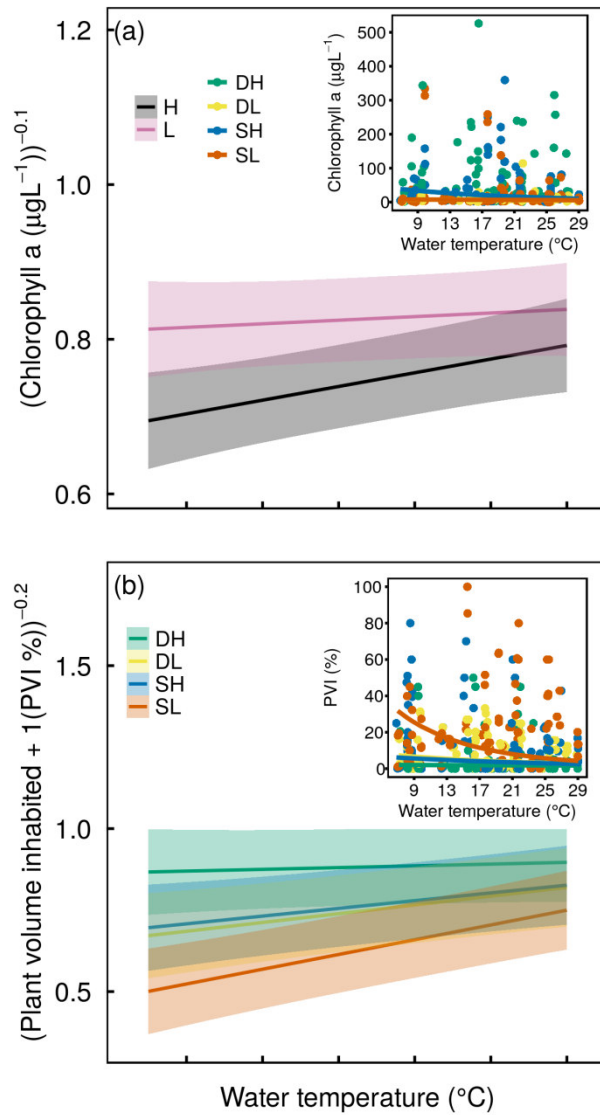
Average chlorophyll a levels were significantly higher under eutrophic (adjusted mean: 25.35 (DH) and 15.57 (SH) $\mu\text{g L}^{-1}$) than mesotrophic (6.54 (DL), 7.25 (SL) $\mu\text{g L}^{-1}$) conditions. In the eutrophic mesocosms, chlorophyll a decreased significantly along the temperature gradient but remained almost constant in the mesotrophic mesocosms. Despite these dynamics, average chlorophyll a levels remained significantly higher in the eutrophic than in the mesotrophic mesocosms along the entire temperature gradient (S3 Figure 2a, S3 Table 1).

PVI levels showed a trend opposite to that of chlorophyll a and were highest in the shallow mesotrophic mesocosm (adjusted mean: 8.09%), followed by the shallow eutrophic and deep mesotrophic mesocosms with comparable values (adjusted mean: 3.51% (SH) and 3.89% (DL)) and, finally, the deep eutrophic mesocosms (0.71%). PVI decreased strongly with increasing temperatures in all treatments but the deep, eutrophic mesocosms where similar low average values

were observed along the entire temperature gradient (S3 Figure 2b, S3 Table 1).



S3 Figure 1: Co-variation of light conditions with water temperature. Treatment-wise co-variation of a) attenuation coefficient (K_d), b) mean availability light (MAL) and c) effective light period (LP_{eff}). Main images in a), b) and c) show treatment-wise least square means with 95% confidence intervals at the scale of the transformed variable. The insets depict the same variable at original scale with treatment-wise average values as estimated by mixed effects regression (S3 Table 1). Lines in d) depict country-wise average monthly daylight hours per day estimated by linear regression. DH = deep high nutrient, SH = shallow high nutrient, DL = deep low nutrient and SL = shallow low nutrient treatment.



S3 Figure 2: Co-variation of primary producers with water temperature (S3 Table 1). Main image shows least-square means of significant factors with 95% confidence intervals on the scale of the transformed variable. The inserts depict values at original scale with average values transformed to original scale. Treatment-wise co-variation of a) phytoplankton measured as chlorophyll a and b) macrophytes measured as plant volume inhabited (PVI). DH = deep high nutrient, SH = shallow high nutrient, DL= deep low nutrient and SL = shallow low nutrient.

S3 Table 1: Mixed effects regression for potential covariates. The influences of water temperature (T), depth (D) and nutrients (N), as well as their interactions, were tested on: total phosphorus (TP), total nitrogen (TN), attenuation coefficient (K_d), mean available light (MAL), effective light period (LP_{eff}), chlorophyll a (Chl a) and plant volume inhabited (PVI). Only p-values ≤ 0.05 are reported. The first R^2 value refers to the marginal R^2 (variance explained by fixed factors) and the second to the conditional R^2 (variance explained by fixed and random factors). The next four columns show treatment-wise adjusted means and average differences over the water temperature gradient, i.e. the difference between average values at 7 °C and 29 °C. The last 6 columns show the results of pairwise comparison of least-square means over the temperature gradient in one degree intervals. Temperatures in brackets indicate temperatures from where on significant treatment differences were found at a 0.05 significance level.

	T	D	N	T x D	T x N	D x N	T x D x N	R^2	Adjusted mean and gradient difference				Contrasts over temperature gradient					
									SH	DH	SL	DL	SL-SH	DL-DH	SL - DH	DL - SH	SL - DL	DH - SH
TP [μgL^{-1}]			< 0.01	0.03	0.02			0.39, 0.88	68.92, 0.43	71.02, -30.63	26.32, 10.24	21.90, 0.30	p = < 0.05	p = < 0.05	p = < 0.05	p = < 0.05	p = < 0.05	p = < 0.05
TN [mgL^{-1}]			< 0.01	0.03	< 0.01		< 0.01	0.31, 0.88	1.37, -0.29	1.43, -1.54	0.79, 0.11	0.71, 0.28	p = < 0.05	p = < 0.05 (< 26 °C)	p = < 0.05 (< 25 °C)	p = < 0.05	n.s.	p = < 0.05 (< 13 °C, > 24 °C)
K_d [m^{-1}]			< 0.01	0.01				0.12, 0.76	3.45, -1.12	3.17, 0.03	2.38, -0.18	2.25, 0.22	p = < 0.05	p = < 0.05	p = < 0.05 (> 10 °C)	p = < 0.05	p = < 0.05 (< 14 °C)	p = < 0.05 (< 14 °C)
MAL [$\mu\text{mol Photons m}^{-2}\text{s}^{-1}$]	0.02	< 0.01	< 0.01	< 0.01				0.43, 0.94	85.90, 177.41	41.29, 76.95	110.56, 213.53	57.30, 100.48	p = < 0.05	p = < 0.05	p = < 0.05	p = < 0.05 (> 9 °C)	p = < 0.05	p = < 0.05
LP_{eff} [hd^{-1}]	< 0.01	< 0.01	< 0.01	0.01		0.03		0.45, 0.89	13.23, 7.74	11.47, 6.89	13.60, 8.20	12.76, 7.07	n.s.	p = < 0.05	p = < 0.05	p = < 0.05 (> 21 °C)	p = < 0.05 (> 15 °C)	p = < 0.05
Chl a [μgL^{-1}]			< 0.01		0.02			0.19, 0.76	15.57, -20.21	25.35, -32.57	7.25, -2.33	6.54, -2.03	p = < 0.05 for H - L (depth was not in the final model)					
PVI [%]	0.01	< 0.01	< 0.01	0.02	0.01			0.22, 0.86	3.51, -4.98	0.71, -0.04	8.09, -16.86	3.89, -5.83	p = < 0.05	p = < 0.05	p = < 0.05	n.s.	p = < 0.05	p = < 0.05

Appendix S4: Country-wise temperature and treatment effects of metabolism

To obtain an idea of the variability between countries for absolute metabolism at 15 °C and the activation energy, we included the factor country and the interaction between country and inverse-scaled temperature in the fixed effects of the model (6). The country-wise analysis for GPP, ER and ER/GPP ratio was based on the following mixed effect model:

$$\ln(\text{Parameter}) = \text{invT} + \text{D} + \text{N} + \text{Country} + \text{invT} \times \text{Country} + (\text{invT}|\text{Country}:\text{Id}_{\text{meso}}) + (1|\text{Country}:\text{Month})$$

, where invT is the inverse-scaled water temperature, D and N are the treatment factors for depth and nutrient level, respectively, Country stands for the factor country, Id_{meso} uniquely identifies each mesocosm and Month stands for the factor month. An intercept and slope model for the random factor Id_{meso} nested in country and an intercept model for the random factor month nested in the country were considered. Model selection, validation and fit are assessed as described in the method part of the main text. Following the hypothesis that warm adaptation leads to lower temperature sensitivity than cold adaptation (Atkin, 2003), we would expect a systematic decrease in activation energy with increasing average country temperature and, possibly, a decrease in average absolute metabolic rate at the reference temperature. We tested for systematic increases or decreases in country-wise activation energies and average absolute metabolic rates using a Helmert contrast with the factor country following the same order as the country-wise average air temperature (Table 1) over the experimental period (SE, EE, CZ, GE, TR, GR). The results are summarised in S4 Table 1. In addition, Spearman correlations between average temperature of the countries and estimated country-wise absolute metabolic rates and activation energies were calculated (S4 Table 2).

Temperature sensitivity was highly variable between countries, yet we found no indication for a systematic change with average temperature in either temperature sensitivity or absolute metabolic rate at 15 °C. Thus, we have good justification for our main model (equation 6), where we test for one generic temperature sensitivity as suggested by the MTE and account for random variation around this temperature sensitivity with the help of random effects. The design of this experiment, however, does not allow a thorough investigation of the effects of temperature acclimation and adaptation on the temperature sensitivity of metabolic rates, due to the lack of replicates per average temperature and the limited amount of experimental sites.

S4 Table 1: Statistical results for models with country as fixed effect. The following abbreviations are used: Int = Intercept at 15 °C (Tc), invT = Inverted and scaled water temperature T in Kelvin ($k^{-1} T^{-1} - k^{-1} T_c^{-1}$), D = Depth, N = Nutrient, SE = Sweden, EE = Estonia, CZ = Czech Republic, GE = Germany, TR = Turkey, GR = Greece. Systematic differences between countries were tested using a Helmert contrast, for instance Country_SE_EE:CZ is the difference between average metabolic rates at 15 °C of SE and EE against the average rate in CZ, and invT x Country_SE_EE:CZ is the difference in average activation energy of SE and EE against the difference in average activation energy of CZ.

Response	Predictor	Estimate	Std. error	T-value	P-value	R ²
ln(GPP)	Int	11.40	0.07	160.69	< 0.01	0.65, 0.80
	invT	-0.78	0.07	-6.69	< 0.01	
	D	0.57	0.03	-9.88	< 0.01	
	N	-0.55	0.03	10.45	< 0.01	
	Country_SE:EE	-0.08	0.10	-2.10	0.04	
	Country_SE_EE:CZ	0.04	0.06	3.52	< 0.01	
	Country_SE_EE_CZ:GE	0.04	0.04	1.22	0.23	
	Country_SE_EE_CZ_GE:TR	0.02	0.03	1.91	0.07	
	Country_SE_EE_CZ_GE_TR:GR	0.09	0.05	2.31	0.03	
	invT x Country_SE:EE	-0.40	0.12	-2.08	0.05	
	invT x Country_SE_EE:CZ	0.50	0.08	4.17	< 0.01	
	invT x Country_SE_EE_CZ:GE	0.03	0.06	0.34	0.74	
	invT x Country_SE_EE_CZ_GE:TR	0.13	0.03	2.46	0.02	
	invT x Country_SE_EE_CZ_GE_TR:GR	0.06	0.03	1.04	0.31	
ln(ER)	Int	11.43	0.09	127.04	<0.01	0.64, 0.86
	invT	-0.94	0.09	-6.86	<0.01	
	D	-0.58	0.03	-9.40	<0.01	
	N	0.48	0.03	7.93	<0.01	
	Country_SE:EE	-0.24	0.13	-4.15	<0.01	
	Country_SE_EE:CZ	0.00	0.08	1.87	0.07	
	Country_SE_EE_CZ:GE	0.05	0.06	1.91	0.07	
	Country_SE_EE_CZ_GE:TR	0.08	0.04	3.18	<0.01	
	Country_SE_EE_CZ_GE_TR:GR	0.20	0.05	5.04	<0.01	
	invT x Country_SE:EE	-0.97	0.14	-4.25	<0.01	
	invT x Country_SE_EE:CZ	0.44	0.09	3.13	0.01	
	invT x Country_SE_EE_CZ:GE	0.19	0.07	1.73	0.10	
	invT x Country_SE_EE_CZ_GE:TR	0.16	0.04	2.53	0.02	
	invT x Country_SE_EE_CZ_GE_TR:GR	0.22	0.04	3.53	<0.01	
ln(GPP _{at})	Int	8.74	0.07	116.72	< 0.01	0.61, 0.78
	invT	-0.43	0.08	-3.47	< 0.01	
	D	-0.54	0.03	-9.71	< 0.01	
	N	0.58	0.03	10.43	< 0.01	
	Country_SE:EE	-0.04	0.11	-1.72	0.10	
	Country_SE_EE:CZ	0.06	0.06	3.67	< 0.01	
	Country_SE_EE_CZ:GE	0.06	0.05	1.69	0.10	
	Country_SE_EE_CZ_GE:TR	0.05	0.04	2.31	0.03	

	Country _SE_EE_CZ_GE_TR:GR	0.12	0.05	2.86	0.01	
	invT x Country _SE:EE	-0.43	0.13	-2.11	0.05	
	invT x Country _SE_EE:CZ	0.48	0.08	3.76	< 0.01	
	invT x Country _SE_EE_CZ:GE	0.04	0.06	0.41	0.68	
	invT x Country _SE_EE_CZ_GE:TR	0.09	0.04	1.59	0.13	
	invT x Country _SE_EE_CZ_GE_TR:GR	0.04	0.04	0.69	0.52	
ln(ER:GPP)	Int	0.01	0.06	-0.72	0.48	0.23, 0.58
	invT	-0.16	0.07	-1.47	0.15	
	D	-0.02	0.02	-0.33	0.74	
	N	-0.09	0.02	-2.01	0.05	
	Country _SE:EE	-0.14	0.10	-3.04	<0.01	
	Country _SE_EE:CZ	-0.05	0.05	-1.17	0.25	
	Country _SE_EE_CZ:GE	0.00	0.04	1.18	0.25	
	Country _SE_EE_CZ_GE:TR	0.06	0.03	2.19	0.04	
	Country _SE_EE_CZ_GE_TR:GR	0.08	0.04	3.02	0.01	
	invT x Country _SE:EE	-0.50	0.11	-2.72	0.01	
	invT x Country _SE_EE:CZ	-0.06	0.07	-0.51	0.62	
	invT x Country _SE_EE_CZ:GE	0.13	0.05	1.61	0.12	
	invT x Country _SE_EE_CZ_GE:TR	0.02	0.03	0.42	0.68	
	invT x Country _SE_EE_CZ_GE_TR:GR	0.11	0.03	2.30	0.03	

S4 Table 2: Table of country-wise activation energies and metabolic rates at 15 °C plus/minus standard error. In addition, Spearman correlation coefficients (r) are calculated between country-wise average water temperature and activation energies and metabolic rates at 15 °C.

		GPP	GPP _{at}	ER	ER/GPP
Slope [eV]	SE	-0.69 ± 0.15	-0.41 ± 0.16	-0.62 ± 0.18	0.08 ± 0.14
	EE	-1.19 ± 0.18	-0.95 ± 0.19	-1.82 ± 0.22	-0.54 ± 0.18
	CZ	0.00 ± 0.19	0.23 ± 0.21	-0.39 ± 0.22	-0.34 ± 0.18
	GE	-0.55 ± 0.21	-0.28 ± 0.22	-0.48 ± 0.24	0.07 ± 0.13
	TR	-0.20 ± 0.14	-0.07 ± 0.15	-0.33 ± 0.17	-0.12 ± 0.13
	GR	-0.31 ± 0.19	-0.15 ± 0.20	0.11 ± 0.22	0.26 ± 0.17
	Correlation coefficient with mean air temperature	r = 0.54 p = 0.30	r = 0.54 p = 0.30	r = 0.88 p = 0.3	r = 0.37 p = 0.50
Intercept at 15 °C (average of treatments)	SE	10.94 ± 0.13	8.27 ± 0.14	11.02 ± 0.17	0.08
	EE	10.52 ± 0.16	7.90 ± 0.17	9.92 ± 0.21	-0.52
	CZ	11.33 ± 0.14	8.74 ± 0.15	10.89 ± 0.19	-0.41
	GE	11.14 ± 0.16	8.61 ± 0.17	11.04 ± 0.20	-0.09
	TR	11.30 ± 0.15	8.79 ± 0.16	11.40 ± 0.20	0.10
	GR	11.67 ± 0.27	9.29 ± 0.28	12.48 ± 0.31	0.56
	Correlation coefficient with mean air temperature	r = 0.77, p = 0.10	r = 0.89, p = 0.03	r = 0.83, p = 0.06	r = 0.66 p = 0.18

Appendix S5: Details of the final random effect models

For all tested metabolic rates we started with the model given in equation (6). The “step” function of the package “lmerTest” (Kuznetsova et al., 2014) was then used for model selection. This function evaluates the significance of both fixed and random effects based on likelihood ratio tests (LRT), i.e. all terms which remain in the final model are significant based on a LRT (see S5 Table 1). Confidence intervals for the random and fixed effects were established using likelihood profiles as implemented in the function “confint.lmerMod” of the “lme4” package (Bates et al., 2014) (see S5 Table 2).

S5 Table 1: P-values of the random effects of the final metabolic rate models as estimated by likelihood ratio tests (“step” function of the package “lmerTest” (Kuznetsova et al., 2014)). ‘-’ indicates that this random term was not significant and thus not part of the final model.

Response	InvT Country	InvT Country: Mesocosm_Id	1 Country: Mesocosm_Id	1 Country:Month
GPP	0.00	-	0.00	0.00
GPP _{all}	0.02	-	0.00	0.00
ER	0.00	0.00	-	0.00
ER/GPP	0.04	0.00	-	0.00

S5 Table 2: Confidence intervals based on likelihood profiles (“confint.lmerMod” of the “lme4” package (Bates et al., 2014)).

	GPP		GPP _{all}		ER		ER/GPP	
	2.5%	97.5%	2.5%	97.5%	2.5%	97.5%	2.5%	97.5%
Sd Country:Id ($\epsilon_R^{c,m}$)	0.12	0.24	0.12	0.24	0.3	0.54	0.2	0.35
Sd InvT: Country::Id ($\epsilon_E^{c,m}$)	-	-	-	-	0.12	0.29	0.16	0.31
Sd Country:Month ($\epsilon_R^{c,s}$)	0.17	0.35	0.18	0.38	0.18	0.42	0.12	0.27
Sd Country (ϵ_R^c)	0.1	0.63	0.17	0.83	0.37	1.44	0.12	0.64
Sd InvT Country (ϵ_E^c)	0.15	0.72	0.09	0.66	0.25	1.07	0.04	0.44
Random error ($\epsilon_{c,(s,m),i}$)	0.33	0.39	0.33	0.39	0.33	0.4	0.31	0.37
Intercept	10.82	11.44	8.21	9.01	10.39	11.75	-0.41	0.21
InvT	-0.9	-0.2	-0.65	0.01	-1.14	-0.11	-0.36	0.08
Depth	0.44	0.66	0.43	0.65	0.45	0.7	-0.08	0.1
Nutrient	-0.68	-0.47	-0.69	-0.47	-0.6	-0.36	0	0.17

S5 References

- Bates D, Maechler M, Bolker B, Walker S (2014). *lme4*: Linear mixed-effects models using Eigen and S4. R package version 1.1-7, <URL:<http://CRAN.R-project.org/package=lme4>>.
- Kuznetsova A, Brockhoff PB and Christensen RHB (2014). *lmerTest*: Tests in Linear Mixed Effects Models. R package version 2.0-20. <https://CRAN.R-project.org/package=lmerTest>

Appendix S6: Evidence to support the assumptions of a predominately heterotrophic driven respiration and respiratory rates unconstrained by primary production

For a meaningful analysis of ER/GPP ratios and the derivation of MTE based predictions of the switch point temperature from net auto- to net heterotrophy (equation 5), we assume that respiration in the mesocosm is mainly driven by heterotrophic metabolism and is unconstrained by primary production, i.e. ER has in principle the potential to exhibit higher activation energies than GPP as predicted by MTE. To back up the made assumptions with data driven evidence we firstly established, if the difference in temperature dependence between ER and GPP is statistical significant and secondly estimated the background respiration as evidence for respiration independent from contemporaneous GPP.

S6.1: Difference between the temperature sensitivity of ER and GPP

Based on MTE we hypothesised that ER has a higher temperature sensitivity than GPP. Thus, if ER can increase with temperature unconstrained by GPP, we expect to find a higher average activation energy for ER than GPP. Ideally this difference is fortified by a statistical significant difference in the temperature sensitivity of the two metabolic types (ER, GPP). To test this we used ER and GPP as additional factors beside the treatments. The following basic linear mixed effect regression model (LMER) was tested (R notation):

$$\text{lmer}(\ln(\text{metabolic rate}) \sim \text{met}_{\text{type}} * \text{invT} * \text{N} * \text{D} + (\text{invT}|\text{Country}) + (\text{invT}|\text{Country}:\text{Id}_{\text{meso}}) + (1|\text{Country}:\text{Month})) \quad (\text{S6.1})$$

, where met_{type} is the metabolic type (GPP or ER); invT is the inverse scaled temperature ($\text{k}^{-1} (\text{T}_c^{-1} - \text{T}^{-1})$); N is the nutrient level (mesotrophic (L = low) or eutrophic (H = high)); D is the depth (1 m (S = shallow) or 2 m (D = deep)); Country is a factor with 6 factor levels, i.e. one for each country; Id_{meso} serves as factor to uniquely identify all mesocosms, and Month is a factor with 5 factor levels (July – November).

We used likelihood ratio tests (LRT) as implemented in the “step” function of the “lmerTest” package (Kuznetsova et al., 2014) for stepwise backward model selection (random and fixed effects). Factor covariate interaction was probed using two-tailed t tests for pairwise comparisons of least-square-means over the inverse scaled temperature gradient in 0.001 steps. The tests were conducted using the standard settings of the “lsmeans” package (Lenth, 2016), i.e. p-values were adjusted for multiple testing based on the Tukey method and the significance level was set to 0.05.

The result confirms that the interaction between temperature and metabolic rate type (i.e. GPP or ER) is significant and gives evidence that ER had the potential to change with temperature unconstrained by GPP. Significant differences between ER and GPP are given in the temperature range between $\sim 23.0^\circ \text{C} - 29.3^\circ \text{C}$ (significant higher ER) and $7.3^\circ \text{C} - 8.8^\circ \text{C}$ (significant higher GPP, see S6 Table 1 and Figure S6.1).

S6 Table 1: Results from linear mixed effect regression (equation S6.1) with metabolic type (i.e. ER or GPP) as additional factor. Int = Intercept, invT = inverse scaled temperature, Met_{type} = metabolic type, N = nutrient level, D = depth. In brackets the reference factor level is given: ER = ecosystem respiration, L = Low/ mesotrophic conditions, S = shallow depth (1m). Confidence intervals were established based on likelihood profiles (function “confint.merMod” of the “lme4” package (Bates et al.,2014)). The temperature range of significant difference between the metabolic types were established based on two-tailed t tests for pairwise comparisons of least-square-means.

Response	Predictor	Estimate	2.50 %	97.50 %	Std. Error	T-value	P-value	Temperature range of sig. difference
Metabolic rates	Int	11.13	10.61	11.67	0.25	44.88	< 0.01	
	invT	-0.52	-0.96	-0.09	0.21	4.9	0.05	
	Met _{type} (ER)	-0.03	-0.09	0.03	0.03	-0.91	0.36	
	N (L)	-0.52	-0.62	-0.41	0.05	-9.89	<0 .01	
	D (S)	0.54	0.43	0.65	0.05	10.31	< 0.01	
	Met _{type} (ER):invT	-0.09	-0.16	-0.02	0.03	-2.53	0.01	7.3 ° C – 8.8 ° C (GPP sig. higher) 23.0 ° C – 29.3 ° C (ER sig. higher)

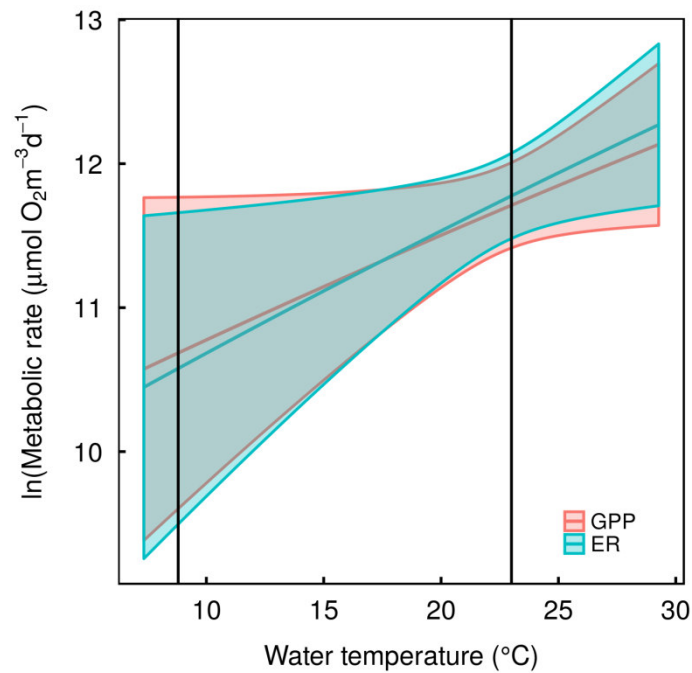


Figure S6.1: Least square means with 95% confidence intervals for gross primary production (GPP) and ecosystem respiration (ER). Vertical lines delimitate temperature ranges of significant difference between ER and GPP. GPP is significantly higher than ER in the temperature range between 7.3 ° C and 8.8 ° C. ER is significantly higher than GPP in the temperature range between 23.0 ° C and 29.3 ° C.

S6.2: Coupling of respiration to GPP

Coupling of respiration to GPP was analysed to identify background respiration and thus respiration unconstrained by GPP. We assessed background respiration following the approach presented in Solomon et al. (2013).

ER and GPP at 20 °C (ER₂₀, GPP₂₀) were estimated as follows:

$$ER_{20} = \frac{ER(T)}{\Phi_r^{(T-20)}} \quad (S6.2)$$

$$GPP_{20} = \frac{GPP(T)}{\Phi_p^{(T-20)}} \quad (S6.3)$$

,where $\Phi_r = 1.09$ and $\Phi_p = 1.04$ are the temperature forcing for respiration and primary production respectively. Φ is estimated based on the average of two point form of the Arrhenius equation over a temperature interval of 0 °C to 30 °C:

$$\Phi = \frac{1}{303.15 - 273.15} \int_{273.15}^{303.15} \exp(E/(kT_1T_2))^{-1} dT_2 \quad (S6.4)$$

,where $k = 8.6173324 \times 10^{-5}$ is the Boltzmann constant, E is the activation energy with either 0.6 eV (respiration) or 0.3 eV (primary production), $T_1 = 293.15$ K (20 °C) is the reference temperature and $T_2 = [273.15$ K, 303.15 K] ([0 °C, 30 °C]) is the considered temperature interval.

The relation between ER_{20} and GPP_{20} was analysed with linear mixed effects regression (“lme” function of the “nlme” package (Pinheiro et al., 2015)). Model selection was based on AICc (Akaike information criterion with correction for finite sample size). 95% confidence intervals at $GPP_{20} = 0$ were estimated using the R function “confint” of the “lsmeans” package (Lenth, 2016). The analysis was conducted in two ways. Firstly, background respiration was assessed for each treatment within country, using GPP at 20° C, country and treatments as fixed effects and individual mesocosms (slope and intercept) as random effect to account for repeated measurements. The following models with highest AICc were used (“lme” package notation):

$$\text{lme}(ER_{20} \sim \text{Country} + D + GPP_{20} + N + \text{Country:D} + \text{Country:GPP}_{20} + \text{Country:N} + D:GPP_{20} + \text{Country:D:GPP}_{20}, \text{random} = \sim 1 + GPP_{20} | Id_{\text{meso}}) \quad (S6.5)$$

,where ER_{20} and GPP_{20} are ecosystem respiration and gross primary production, respectively, standardised to 20 °C (see equations S6.2 and S6.3), D is depth (S = shallow, D = Deep), N is the nutrient level (H = high, L = low), Id_{meso} is a unique identifier for each mesocosm.

Secondly, country and individual mesocosms nested in country (slope and intercept) were regarded as random effect, to estimated average background respiration per treatment, which parallels the level of analysis presented in the main text. The following models with highest AICc were used (“lme” package notation):

$$\text{lme}(ER_{20} \sim GPP_{20} + N + D, \text{random} = \sim GPP_{20} | \text{Country} / Id_{\text{meso}}) \quad (S6.6)$$

,where ER_{20} and GPP_{20} are ecosystem respiration and gross primary production respectively, standardised to 20 °C (see equations S6.2 and S6.3), D is depth (S = shallow, D = Deep), N is the nutrient level (H = high, L = low), Id_{meso} is a unique identifier for each mesocosm.

Country-wise analysis showed that not all treatments within countries had positive background respiration or confidence intervals above zero (see S6 Table 2). Yet, no correlation between amount of background respiration and magnitude of the activation energy for ER could be confirmed.

Treatment-wise analysis showed that on average all treatments had significant positive background respiration (see S6 Table 3 and figure S6.2).

Based on these results the assumptions of dominance of heterotrophic respiration and an ER unconstrained by GPP is justifiable.

S6 Table 2: Estimated background respiration and 95% confidence intervals per treatment within country. Estimates are based on linear mixed effect regression models (see equation S6.5). 95% confidence intervals at $GPP_{20} = 0$ are based on least square means. D = deep (2 m), S = shallow (1m), H = high nutrient level (eutrophic), L = low nutrient level (mesotrophic), SE = Sweden, CZ = Czech Republic, GE = Germany, EE = Estonia, TR = Turkey and GR = Greece.

Country	Treatment	2.50%	Prediction	97.50%
SE	DH	26.30	51.60	76.89
	SH	102.64	152.87	203.09
	DL	6.27	28.65	51.03
	SL	82.95	129.92	176.89
CZ	DH	-6.79	34.58	75.96
	SH	41.91	83.53	125.14
	DL	-29.46	-5.39	18.68
	SL	15.71	43.56	71.40
GE	DH	56.11	89.69	123.28
	SH	45.91	90.85	135.80
	DL	27.84	50.65	73.47
	SL	12.25	51.81	91.38
EE	DH	-32.90	2.02	36.93
	SH	-38.53	-0.54	37.44
	DL	2.39	23.58	44.76
	SL	-4.62	21.02	46.65
TR	DH	21.31	53.27	85.24
	SH	-7.14	50.11	107.36
	DL	9.44	33.39	57.35
	SL	-21.86	30.23	82.32
GR	DH	-42.24	5.72	53.67
	SH	-218.74	-115.31	-11.88
	DL	-17.75	13.25	44.26
	SL	-210.94	-107.77	-4.61

S6 Table 3: Estimated background respiration and 95% confidence intervals per treatment. Estimates are based on linear mixed effect regression models (see equation S6.6). 95% confidence intervals at $GPP_{20} = 0$ are based on least square means. D = deep (2 m), S = shallow (1m), H = high nutrient level (eutrophic) and L = low nutrient level (mesotrophic).

Treatment	2.50%	Prediction	97.50%
DH	15.80	36.35	56.91
SH	24.43	48.42	72.42
DL	2.49	19.31	36.12
SL	11.63	31.38	51.12

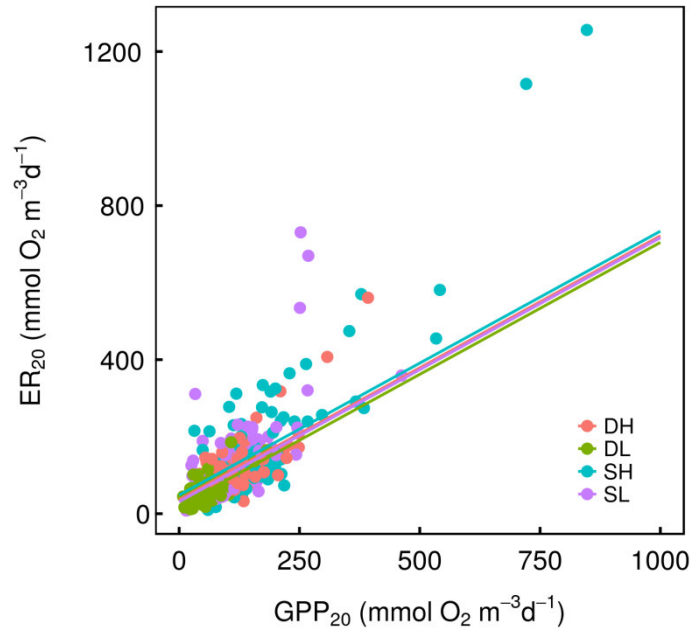


Figure S6.2: Treatment-wise coupling of ecosystem respiration (ER_{20}) to gross primary production (GPP_{20}) based on metabolic rates standardised to 20° C (see equation S6.2 and S6.3). Following Solomon et al. (2013) the slope of the relation quantifies coupling of respiration (respiration by autotrophs and respiration of autochthonous produced label organic matter by heterotrophs) to GPP, while the intercept quantifies the background respiration (respiration of recalcitrant autochthonous or surplus and allochthonous organic matter by heterotrophs; see also Solomon et al. (2013) Figure 1).

S6 References

- Bates D, Maechler M, Bolker B, Walker S (2014). *_lme4: Linear mixed-effects models using Eigen and S4_*. R package version 1.1-7, <URL:<http://CRAN.R-project.org/package=lme4>>.
- Kuznetsova A, Brockhoff PB and Christensen RHB (2014). *lmerTest: Tests in Linear Mixed Effects Models*. R package version 2.0-20. <https://CRAN.R-project.org/package=lmerTest>
- Lenth RV (2016). Least-Squares Means: The R Package lsmeans. *Journal of Statistical Software*, 69(1), 1-33. doi:10.18637/jss.v069.i01
- Pinheiro J, Bates D, DebRoy S, Sarkar D and R Core Team (2015). *_nlme: Linear and Nonlinear Mixed Effects Models_*. R package version 3.1-120, <URL: <http://CRAN.R-project.org/package=nlme>>.
- Solomon CT, Bruesewitz DA, Richardson DC et al. (2013) Ecosystem respiration: Drivers of daily variability and background respiration in lakes around the globe. *Limnology and Oceanography*, **58**, 849–866.

S7 Separation of the effects of the collinear variables temperature and daylight length on gross primary production (GPP)

In the experiment mean daylight length (DayL) is highly correlated with water temperature and thus with inverse scaled temperature (invT). Both variables in turn are correlated with GPP (see S7 Table 1). Under these circumstances it is problematic to use the two variables in the same regression model and the estimated coefficients could not be interpreted independently from each other. These problems can already arise at comparable low values of the variance inflation factor (VIF), which in our case is 1.64 (only defined and thus established for simple linear regression models) (Graham, 2003).

S7 Table 1: Person- and Spearman's rank correlation coefficient between inverse scaled water temperature (invT), daylight length (DayL) and logarithmised gross primary production (ln(GPP))

Variables	Pearson correlation coefficient	Spearman's rank correlation coefficient
InvT – mean DayL	-0.62	-0.55
ln(GPP) - invT	-0.57	-0.55
ln(GPP) - mean DayL	0.26	0.21

To consolidate the relevance and importance of temperature apart from daylight length as driver of GPP we used three different approaches: (1) semi-partial correlation (results presented in the main text), (2) two separate models with standardized variables and (3) residual regression (Graham 2003; Dormann et al., 2012). To estimate the activation energy without the potentially confounding influence of daylight length GPP per daylight hour was used (results presented in the main text).

The results from all the three different approaches coherently pinpoint both, daylight length and water temperature, as important variables (see Table 4 and S7 Table 2). Yet water temperature seems to have a slightly higher effect size and explanatory power compared to daylight length. This is also the case when the commonly explained variance is removed and only the partial explanatory power is compared, with the potential exception for deep high nutrient mesocosms (see Table 4). Daylight length is significantly more important in deep compared to shallow mesocosms (S7 Table 2),

S7 References

- Dormann CF, Elith J, Bacher S, Buchmann C, Carl G, Carré G, Marquéz JRG, Gruber B, Lafourcade B, Leitão PJ, Münkemüller T, McClean C, Osborne PE, Reineking B, Schröder B, Skidmore AK, Zurell D, Lautenbach S (2012) Collinearity: A review of methods to deal with it and a simulation study evaluating their performance. *Ecography* 35, no – no
- Graham MH (2003) Confronting multicollinearity in ecological multiple regression. *Ecology*, 84(11), 2809 – 2815.

S7 Table 2: Results from the two separate linear mixed effect and the residual regression models based on standardized variables to separating the relative importance of the two collinear predictors daylight length (DayL_{Std}) and inverse scaled water temperature (invT_{Std}) on gross primary production (GPP).

	Response	Predictor	Estimate	P-value	R ² conditional	R ² marginal
Separate mixed effect models with standardized variables	Models for GPP	$\ln(\text{GPP}) \sim \text{DayL}_{\text{Std}} + \text{Depth} + \text{Nutrient} + \text{DayL}_{\text{Std}}:\text{Depth} + (\text{DayL}_{\text{Std}} \text{Country}) + (\text{DayL}_{\text{Std}} \text{Country}:\text{Id}) + (1 \text{Country}:\text{Month})$ $\ln(\text{GPP}) \sim \text{invT}_{\text{Std}} + \text{Depth} + \text{Nutrient} + (\text{invT}_{\text{Std}} \text{Country}) + (1 \text{Country}:\text{Id}) + (1 \text{Country}:\text{Month})$				
	ln(GPP)	DayL _{Std}	0.34 (deep)	0.04	0.3	0.84
		DayL _{Std} : Depth	-0.13 (shallow)	0.00		
		invT _{Std}	-0.43	0.02	0.5	0.8
Residual regression	Models	$\text{invT}_{\text{Std}} \sim \text{DayL}_{\text{Std}} + (\text{DayL}_{\text{Std}} \text{Country}) \Rightarrow \text{invT}_{\text{Res}}$ $\ln(\text{GPP}) \sim \text{DayL}_{\text{Std}} + \text{invT}_{\text{Res}} + \text{Depth} + \text{Nutrient} + \text{DayL}_{\text{Std}}:\text{Depth} + (\text{DayL}_{\text{Std}} \text{Country}) + (\text{DayL}_{\text{Std}} \text{Country}:\text{Id}) + (1 \text{Country}:\text{Month})$				
	ln(GPP)	DayL _{Std}	0.34 (deep)	0.03	0.33	0.84
		DayL _{Std} : Depth	-0.14 (shallow)	0		
		invT _{Res}	-0.77	0		

Appendix S8: Simulation based assessment on the value of average vs. linear mixed effect regression approaches for the analysis of temperature sensitivity and absolute metabolic rate for the particular experimental design of a standardised pan-European mesocosm experiment

Abstract

We conducted a simulation to test the robustness of linear mixed effects regressions (LMER) to estimate average temperature sensitivity of metabolic rates and absolute metabolic rates in the special situation of our experimental set-up. For this purpose, we emulated the random structure of our experimental data, i.e. we simulated six countries with different temperature ranges and within those countries, different experimental units. We simulated 7 scenarios in regard to the behaviour of temperature sensitivity and absolute metabolic rate among countries. In scenario 1 we assume that all countries have the same generic temperatures sensitivity and absolute metabolic rate and random variation in these quantities only occurs on the level of the unit, in scenario 2 – 4 we consider random variation among countries for the absolute metabolic rate and or temperature sensitivity and in scenario 5 – 7 we assume systematic changes with average temperature in one or both of these quantities. An LMER model, comparable with the one used in the manuscript, was then applied to each of this scenarios to estimate one overall average temperature sensitivity and absolute metabolic rate. While the scenarios 1 – 4 concur with the LMER assumption of normally distributed random effects, this assumption is being violated in the scenarios 5 - 7. Moreover, because of overlapping but distinct temperature ranges for each country, country-wise average temperatures may correlate by chance or systematically with country-wise average metabolic rates or temperature sensitivity. Such a correlation could potentially confound the estimated overall averages for temperature sensitivity and absolute metabolic rate. We also compared the performance of the LMER against two potentially alternative approaches based on average temperatures and metabolic rates. We found that the LMER reliably and universally estimates the true average temperature sensitivities and absolute metabolic rates. This was even the case for scenarios 5-7, where we consistently violate LMER assumptions. On the other hand, the estimates of the tested average-based approaches were heavily confounded by chance or systematic correlation between country-wise average temperatures and absolute metabolic rates and to a lesser extent average temperature and temperature sensitivity. None of the 3 tested approaches were able to quantify or at least detect the simulated systematic changes in absolute metabolic rates and or temperature sensitivity. In summary, the simulation results demonstrate clearly that the chosen LMER approach is suitable for robustly and meaningfully estimating average temperature sensitivity and absolute metabolic rates for the data from our experiment, if we assume random variation of these quantities among countries around an average value. However, even though the LMER approach was robust against the violation of the assumption of normally distributed random effects, the estimated average values under the assumption of systematic change are of questionable informational value, and an evaluation of trends in country-wise established temperature sensitivities and absolute metabolic rates seems relevant in this situation. For our data, however, we did not find any evidence for systematic changes with average temperature neither for temperature sensitivity nor absolute metabolic rate (S4). However, the average-based approaches are contraindicated in connection with our data where the specific experimental set up can give rise to chance correlations between average temperatures and absolute metabolic rates and or temperature sensitivity.

Contents

1	The aim of the simulation	4
2	Method	5
2.1	Simulation set-up	5
2.2	Analysis of simulation results	6
2.2.1	Image: “Simulated metabolic rates and respective averages ”	6
2.2.2	Image: “Log transformed simulated metabolic rate, averages and model predictions”	6
2.2.3	Image: “Correlation of simulated parameters $A_{c,i}$ and $E_{c,i}$ with temperature”	7
2.2.4	Visual comparison between the parameters \hat{A} and \hat{E} estimated by the three different approaches and the simulated parameters $\overline{A_{c,i}}$ and $\overline{E_{c,i}}$	7
2.2.4.1	Comparison of the distribution of the differences between estimated and simulated values by the three approaches based on 1000 simulation runs.	7
2.2.4.2	Comparison of the distribution of the estimated and simulated values based on 1000 simulation runs	7
2.2.5	Analysis of the cause for the deviaten between estimated vs. simulated density distributions	7
3	Scenario one: All entities have the same generic activation energy E_c and intercept A_c	9
3.1	Description and assumptions of scenario one	9
3.2	Summary results scenario one:	11
3.3	Scenario one: Comparison between $\overline{E_{c,i}}$ and $\overline{\ln A_{c,i}}$ and \hat{E} and \hat{A} from the 3 different estimation approaches	11
3.4	Scenario one: Detailed results on the influnece of chance correlation of $\ln A_{c,i}$ $E_{c,i}$ with \bar{T}_c on the estimates of \hat{E} and \hat{A}	13
3.4.1	Log-first approach - Best model to explain \hat{E} and \hat{A} based on $\overline{E_{c,i}}$, $\overline{\ln A_{c,i}}$, $\beta_{E_{c,i}}$ and $\beta_{A_{c,i}}$	13
3.4.2	Average-first approach - Best model to explain \hat{E} and \hat{A} based on $\overline{E_{c,i}}$, $\overline{\ln A_{c,i}}$, $\beta_{E_{c,i}}$ and $\beta_{A_{c,i}}$	15
3.4.3	LMER approach - Best model to explain \hat{E} and \hat{A} based on $\overline{E_{c,i}}$, $\overline{\ln A_{c,i}}$, $\beta_{E_{c,i}}$ and $\beta_{A_{c,i}}$	17
4	Scenario two: All entities have the same generic activation energy E_c but have a variable intercept A_c	19
4.1	Description and assumptions of scenario two	19
4.2	Summary results scenario two:	21
4.3	Scenario two: Comparison between $\overline{E_{c,i}}$ and $\overline{\ln A_{c,i}}$ and \hat{E} and \hat{A} from the 3 different estimation approaches	21
4.4	Scenario two: Detailed results on the influnece of chance correlation of $\ln A_{c,i}$ $E_{c,i}$ with \bar{T}_c on the estimates of \hat{E} and \hat{A}	23
4.4.1	Log-first approach - Best model to explain \hat{E} and \hat{A} based on $\overline{E_{c,i}}$, $\overline{\ln A_{c,i}}$, $\beta_{E_{c,i}}$ and $\beta_{A_{c,i}}$	23
4.4.2	Average-first approach - Best model to explain \hat{E} and \hat{A} based on $\overline{E_{c,i}}$, $\overline{\ln A_{c,i}}$, $\beta_{E_{c,i}}$ and $\beta_{A_{c,i}}$	25
4.4.3	LMER approach - Best model to explain \hat{E} and \hat{A} based on $\overline{E_{c,i}}$, $\overline{\ln A_{c,i}}$, $\beta_{E_{c,i}}$ and $\beta_{A_{c,i}}$	27
5	Scenario three: All entities have the same generic absolute metabolic rate A_c but variable E_c	29
5.1	Description and assumptions of scenario three	29
5.2	Summary results scenario three:	31
5.3	Scenario three: Comparison between $\overline{E_{c,i}}$ and $\overline{\ln A_{c,i}}$ and \hat{E} and \hat{A} from the 3 different estimation approaches	31
5.4	Scenario three: Detailed results on the influnece of chance correlation of $\ln A_{c,i}$ $E_{c,i}$ with \bar{T}_c on the estimates of \hat{E} and \hat{A}	33
5.4.1	Log-first approach - Best model to explain \hat{E} and \hat{A} based on $\overline{E_{c,i}}$, $\overline{\ln A_{c,i}}$, $\beta_{E_{c,i}}$ and $\beta_{A_{c,i}}$	33

5.4.2	Average-first approach - Best model to explain \hat{E} and \hat{A} based on $\overline{E_{c,i}}$, $\overline{\ln A_{c,i}}$, $\beta_{E_{c,i}}$ and $\beta_{A_{c,i}}$	35
5.4.3	LMER approach - Best model to explain \hat{E} and \hat{A} based on $\overline{E_{c,i}}$, $\overline{\ln A_{c,i}}$, $\beta_{E_{c,i}}$ and $\beta_{A_{c,i}}$	37
6	Scenario four: All entities have variable absolute metabolic rates A_c and activation energies E_c	39
6.1	Description and assumptions of scenario four	39
6.2	Summary results scenario four:	41
6.3	Scenario four: Comparison between $\overline{E_{c,i}}$ and $\overline{\ln A_{c,i}}$ and \hat{E} and \hat{A} from the 3 different estimation approaches	41
6.4	Scenario four: Detailed results on the influence of chance correlation of $\ln A_{c,i}$ $E_{c,i}$ with \bar{T}_c on the estimates of \hat{E} and \hat{A}	43
6.4.1	Log-first approach - Best model to explain \hat{E} and \hat{A} based on $\overline{E_{c,i}}$, $\overline{\ln A_{c,i}}$, $\beta_{E_{c,i}}$ and $\beta_{A_{c,i}}$	43
6.4.2	Average-first approach - Best model to explain \hat{E} and \hat{A} based on $\overline{E_{c,i}}$, $\overline{\ln A_{c,i}}$, $\beta_{E_{c,i}}$ and $\beta_{A_{c,i}}$	45
6.4.3	LMER approach - Best model to explain \hat{E} and \hat{A} based on $\overline{E_{c,i}}$, $\overline{\ln A_{c,i}}$, $\beta_{E_{c,i}}$ and $\beta_{A_{c,i}}$	47
7	Scenario five: All entities are allowed to have variable E_c and A_c. Where E_c are negatively correlated with \bar{T}_c	49
7.1	Description and assumptions of scenario five	49
7.2	Summary results scenario five:	51
7.3	Scenario five: Comparison between $\overline{E_{c,i}}$ and $\overline{\ln A_{c,i}}$ and \hat{E} and \hat{A} from the 3 different estimation approaches	51
7.4	Scenario five: Detailed results on the influence of chance correlation of $\ln A_{c,i}$ $E_{c,i}$ with \bar{T}_c on the estimates of \hat{E} and \hat{A}	53
7.4.1	Log-first approach - Best model to explain \hat{E} and \hat{A} based on $\overline{E_{c,i}}$, $\overline{\ln A_{c,i}}$, $\beta_{E_{c,i}}$ and $\beta_{A_{c,i}}$	53
7.4.2	Average-first approach - Best model to explain \hat{E} and \hat{A} based on $\overline{E_{c,i}}$, $\overline{\ln A_{c,i}}$, $\beta_{E_{c,i}}$ and $\beta_{A_{c,i}}$	55
7.4.3	LMER approach - Best model to explain \hat{E} and \hat{A} based on $\overline{E_{c,i}}$, $\overline{\ln A_{c,i}}$, $\beta_{E_{c,i}}$ and $\beta_{A_{c,i}}$	57
8	Scenario six: All entities have variable A_c and E_c. A_c's systematically increase with increasing \bar{T}_c	59
8.1	Description and assumptions of scenario six	59
8.2	Summary results scenario six:	61
8.3	Scenario six: Comparison between $\overline{E_{c,i}}$ and $\overline{\ln A_{c,i}}$ and \hat{E} and \hat{A} from the 3 different estimation approaches	61
8.4	Scenario six: Detailed results on the influence of chance correlation of $\ln A_{c,i}$ $E_{c,i}$ with \bar{T}_c on the estimates of \hat{E} and \hat{A}	63
8.4.1	Log-first approach - Best model to explain \hat{E} and \hat{A} based on $\overline{E_{c,i}}$, $\overline{\ln A_{c,i}}$, $\beta_{E_{c,i}}$ and $\beta_{A_{c,i}}$	63
8.4.2	Average-first approach - Best model to explain \hat{E} and \hat{A} based on $\overline{E_{c,i}}$, $\overline{\ln A_{c,i}}$, $\beta_{E_{c,i}}$ and $\beta_{A_{c,i}}$	65
8.4.3	LMER approach - Best model to explain \hat{E} and \hat{A} based on $\overline{E_{c,i}}$, $\overline{\ln A_{c,i}}$, $\beta_{E_{c,i}}$ and $\beta_{A_{c,i}}$	67
9	Scenario seven: All entities are allowed to have variable A_c and E_c which systematically increase respectively decrease with \bar{T}	69
9.1	Description and assumptions of scenario seven	69
9.2	Summary results scenario seven:	71
9.3	Scenario seven: Comparison between $\overline{E_{c,i}}$ and $\overline{\ln A_{c,i}}$ and \hat{E} and \hat{A} from the 3 different estimation approaches	71
9.4	Scenario seven: Detailed results on the influence of chance correlation of $\ln A_{c,i}$ $E_{c,i}$ with \bar{T}_c on the estimates of \hat{E} and \hat{A}	73
9.4.1	Log-first approach - Best model to explain \hat{E} and \hat{A} based on $\overline{E_{c,i}}$, $\overline{\ln A_{c,i}}$, $\beta_{E_{c,i}}$ and $\beta_{A_{c,i}}$	73

9.4.2	Average-first approach - Best model to explain \hat{E} and \hat{A} based on $\overline{E_{c,i}}$, $\overline{\ln A_{c,i}}$, $\beta_{E_{c,i}}$ and $\beta_{A_{c,i}}$	75
9.4.3	LMER approach - Best model to explain \hat{E} and \hat{A} based on $\overline{E_{c,i}}$, $\overline{\ln A_{c,i}}$, $\beta_{E_{c,i}}$ and $\beta_{A_{c,i}}$	77

1 The aim of the simulation

A pan-European standardised mesocosm experiment was conducted to elucidate how metabolic rates change in response to increased temperatures. The experiment was conducted in parallel in six countries from Sweden to Greece and run from May to November, covering a temperature range from 7 - 29 °C. A monthly measurement scheme was applied.

Aim of this simulation was to emulate data from this experimental set-up with particular focus on the reproduction of the random structure of the data implied by the set-up. This data was used to evaluate how reliable a linear mixed effect regression approach (LMER) is able to retrieve biologically meaningful information about the activation energies and absolute metabolic rates realized by the experimental set-up. The performance of LMER was tested under different perceivable hypotheses regarding the temperature sensitivity of metabolic rates and absolute metabolic rates. Further, results from LMER were compared to results based on two different average approaches.

In all simulated scenarios a non-linear relation between water temperature and metabolic rates was assumed, which in a temperature range from approximately 0 to 30 °C can be reasonable described by the Arrhenius equation. Two general different behaviors of the temperature sensitivity are perceivable. Firstly, in accordance with the assumptions of the metabolic theory, there exist one generic temperature sensitivity, which in the single countries and mesocosms might vary randomly around this temperature sensitivity due to interactions or co variation of other drivers with temperature. Secondly, temperature sensitivity could be an adaptive property on individual, population or community level, thus that the temperature sensitivity systematically changes with the average temperature of the different experimental locations.

2 Method

Table 1: Glossary of terms.

Term	Description
$c = 1, \dots, 6$	Index of the simulated entities
$i = 1, \dots, 16$	Index of the simulated instances
T	Temperature
$T_c = [T_{c,min}, \dots, T_{c,max}]$	Temperature range of entity c with $T_{c,min}$ and $T_{c,max}$ as the minimal and maximal temperature of this range. $\forall c$ it holds that $T_{c,max} - T_{c,min} = 14$ °C. T_c is the same for all i belonging to entity c .
$\overline{T_c}$	Average temperature of entity c
$T_r = 15$ °C	Reference temperature
A	Generic absolute metabolic rate at T_r
E	Generic activation energy
$A_c \sim N(13, 4)$	Absolute metabolic rate at T_r of entity c
$E_c \sim N(0.6, 0.5)$	Activation energy of entity c . Values of E_c are limited to $E_c \geq 0$
$A_{c,i} \sim N(A_c, 0.4)$	Simulated absolute metabolic rate at T_r of instance i of entity c .
$E_{c,i} \sim N(E_c, 0.1)$	Simulated activation energy of instance i of entity c .
$\overline{\ln A_{c,i}}$	Average of the logarithmised $A_{c,i}$ over all simulated entities c and instances i
$\overline{E_{c,i}}$	Average $E_{c,i}$ over all simulated entities c and instances i
\hat{A}	Estimates of $\overline{\ln A_{c,i}}$ based on one of the three tested approaches
\hat{E}	Estimates of $\overline{E_{c,i}}$ based on one of the three tested approaches
$M_{c,i}(T)$	Metabolic rate of entity c and instance i at temperature T . $M_{c,i}(T) = A_{c,i} \cdot \exp\left(\frac{-E_{c,i}}{k} \cdot \left(\frac{1}{T} - \frac{1}{T_r}\right)\right) + \epsilon$ with $\epsilon \sim N(0, 1)$
$\epsilon \sim N(0, 1)$	Gaussian random noise
$\beta_{A_{c,i}}$	Regression coefficient quantifying the relation between the simulated absolute metabolic rates $A_{c,i}$ and $\overline{T_c}$
$\beta_{E_{c,i}}$	Regression coefficient quantifying the relation between the simulated activation energies $E_{c,i}$ and $\overline{T_c}$
$k = 8.62 \cdot 10^{-5} [eVK^{-1}]$	Boltzmann constant

2.1 Simulation set-up

Each simulation run considered six entities $c = 1, \dots, 6$, which were represented by sixteen instances $i = 1, \dots, 16$, comparable to the experimental set-up which comprised six countries each with sixteen mesocosms.

For each entity c a random temperature range of 14 °C was drawn in a potential temperature range between 0 and 35 °C.

In scenario 1 - 4 each of the entities c got assigned a randomly drawn activation energy $E_c \sim N(0.6, 0.5)$ and absolute metabolic rate $A_c \sim N(13, 4)$ at reference temperature T_r . The reference temperature T_r was set to 15 °C. Depending on the scenario each entity had the same or different A_c and E_c values (see details of scenarios 1-4 below). Different E_c and A_c for the entities c represented randomly distributed deviation from a generic absolute metabolic rate A and a generic activation energy E due to other factors which have an influence on metabolic rates and interact or correlated with temperature. However these factors were assumed to vary randomly between the entities. Based on the randomly drawn A_c and E_c , each instance i of entity c was assigned an absolute metabolic rate $A_{c,i} \sim N(A_c, 0.4)$ and an activation energy $E_{c,i} \sim N(E_c, 0.1)$.

In scenario 5 - 7 the effect of systematic changes in A_c and or E_c with increasing average temperature $\overline{T_c}$ were simulated. Without loss of generality E_c was assumed to decrease and A_c to increase with increasing $\overline{T_c}$. Increase of A_c and decrease of E_c with $\overline{T_c}$ was simulated by sorting the randomly drawn values of E_c and A_c decreasingly and increasingly respectively and thus assign them to the temperature ranges sorted by

increasing $\overline{T_c}$, i.e. the highest temperature range was associated with the smallest E_c and the highest A_c and the lowest temperature range with the highest E_c and smallest A_c , etc.. $E_{c,i}$ and $A_{c,i}$ values for the instances were than generated as described above.

The thus established T_c , $A_{c,i}$ and $E_{c,i}$ were used to simulate temperate dependent metabolic rates $M_{c,i}(T)$ for each instance i of entity c according to the Arrhenius equation:

$$M_{c,i}(T) = A_{c,i} \cdot \exp\left(\frac{-E_{c,i}}{k} \cdot \left(\frac{1}{T} - \frac{1}{T_c}\right)\right) + \epsilon \quad (1)$$

, where k is the Boltzmann constant and $\epsilon \sim N(0, 1)$ is added random noise.

The relation between $M_{c,i}$ and T as described above can be linearized by taking the logarithm of both side:

$$\ln M_{c,i}(T) = \ln A_{c,i} - \frac{E_{c,i}}{k} \cdot \left(\frac{1}{T} - \frac{1}{T_c}\right) \quad (2)$$

Linear regression can than be used to estimate an average metabolic rate at reference temperature $\overline{\ln A_{c,i}}$ (\hat{A}) and an average activation energy $\overline{E_{c,i}}$ (\hat{E}) based on $\ln M_{c,i}(T)$ from all entities c and instance i .

Estimation of \hat{E} and \hat{A} was conducted with three different approaches:

1. Linear mixed effect model (LMER) approach: The simulated $\ln M_{c,i}(T)$ values were used in a linear mixed effect model considering random effects for the slope and the intercept on the level of entity and instances. The random effects for instances were nested within entity. This approach is comparable to the one used in the manuscript to analyse the experiment data.
2. Average first approach: The simulated $\ln M_{c,i}(T)$ values were used first to estimate average absolute metabolic rates on the level of instances. The resulting averages were then log transformed. Similar, first the average temperature $\overline{T_c}$ was calculated. Based on those averages the average scaled inverse temperature was calculated. This average-first data was then used to estimate \hat{E} and \hat{A} based on a LMER, with random intercept on the level of entity.
3. Log first approach: The simulated $\ln M_{c,i}(T)$ values were first log transformed and then averaged. Similar, inverse scaled temperature was calculated based on T_c and then average inverse scaled temperatures estimated. This log-first data was then used to estimate \hat{E} and \hat{A} based on a LMER approach with random intercept on the level of entity.

For each scenario and each of the three approaches 1000 simulation runs were conducted.

2.2 Analysis of simulation results

2.2.1 Image: “Simulated metabolic rates and respective averages ”

In the first analysis plot, for each scenario the simulated metabolic rates $M_{c,i}(T)$ from one simulation run were shown exemplary (see for example figure 1). The lines represent the exponential relation between temperature and metabolic rates with out added noise. The dots show the final simulated data with noise. Added to the graph were the means calculated based on noiseless data (open square) and noisy data (closed triangle).

2.2.2 Image: “Log transformed simulated metabolic rate, averages and model predictions”

In the second analysis plot, a so called Arrhenius plot, the same exemplary noise free (line) and noisy (small dots) $\ln M_{c,i}(T)$ as in the previous image 2.2.1 were depicted (see for example figure 2). Added to the

Arrhenius plot were averages based on noiseless (closed symbols) and noisy (open symbols) data. Averages were calculated using either the Average-first (square) or in the Log-first (triangle) approach. In addition the resulting predicted metabolic rates based on the 3 different approaches to estimate \hat{E} and \hat{A} were depicted: LMER approach (continuous black line), Average-first approach (dotted line), Log-first approach (dashed line).

2.2.3 Image: “Correlation of simulated parameters $A_{c,i}$ and $E_{c,i}$ with temperature”

In the third analysis plot (see for example figure 3), the correlation between $E_{c,i}$ and $\overline{T_c}$ and $A_{c,i}$ and $\overline{T_c}$ was shown for each scenario and the same exemplary data as in the previous images, e.g. 2.2.1. For scenario 1 - 4 this correlation is based on chance alone. The strength of the relation was quantified by linear regression and expressed in the regression coefficients:

$$A_{c,i} = \alpha + \beta_{A_{c,i}} \cdot \overline{T_c} \quad (3)$$

$$E_{c,i} = \alpha + \beta_{E_{c,i}} \cdot \overline{T_c} \quad (4)$$

2.2.4 Visual comparison between the parameters \hat{A} and \hat{E} estimated by the three different approaches and the simulated parameters $\overline{A_{c,i}}$ and $\overline{E_{c,i}}$

2.2.4.1 Comparison of the distribution of the differences between estimated and simulated values by the three approaches based on 1000 simulation runs.

In the fourth analysis plot, for each of the three approaches and each simulation run the differences $\overline{A_{c,i}} - \hat{A}$ and $\overline{E_{c,i}} - \hat{E}$ were calculated. The distributions of the differences from the three approaches were compared with the help of histograms (see for example figure 4). Ideally, the difference distribution is centred at zero with a small standard variation.

2.2.4.2 Comparison of the distribution of the estimated and simulated values based on 1000 simulation runs

In the fifth analysis plot, the density distributions of the estimated (\hat{A} and \hat{E}) and simulated ($\overline{A_{c,i}}$ and $\overline{E_{c,i}}$) parameters were depicted. Comparison of the density distributions allows to assess how well the three different estimation procedures were able to reproduce the distribution of the simulated parameters (see for example figure 5). For scenarios where either $A_{c,i}$ or $E_{c,i}$ was variable between entities and thus their existed the possibility of chance correlation of this parameters with $\overline{T_c}$, also the density distribution of $\beta_{A_{c,i}}$ and $\beta_{E_{c,i}}$ were added (see next paragraph 2.2.5, as well as equation 5 and 6). Ideally the density distribution of a estimated parameter is congruent with the one from the simulated parameter.

2.2.5 Analysis of the cause for the deviation between estimated vs. simulated density distributions

In the sixth analysis plot, the potential causes for deviations between the density distribution of the estimated (\hat{A} and \hat{E}) and simulated ($\overline{A_{c,i}}$ and $\overline{E_{c,i}}$) parameters were assessed. To investigate the influence of $\overline{A_{c,i}}$, $\overline{E_{c,i}}$, $\beta_{A_{c,i}}$ and $\beta_{E_{c,i}}$ on the estimated parameter values the following two regression models for each of the three tested approach were evaluated:

$$\begin{aligned} \hat{A} = & \alpha + \beta_1 \overline{A_{c,i}} + \beta_2 \overline{E_{c,i}} + \beta_3 \beta_{A_{c,i}} + \beta_4 \beta_{E_{c,i}} + \beta_5 \overline{A_{c,i}} : \overline{E_{c,i}} + \beta_6 \overline{A_{c,i}} : \beta_{A_{c,i}} + \beta_7 \overline{A_{c,i}} : \beta_{E_{c,i}} + \\ & \beta_8 \overline{E_{c,i}} : \beta_{A_{c,i}} + \beta_9 \overline{E_{c,i}} : \beta_{E_{c,i}} + \beta_{10} \beta_{A_{c,i}} : \beta_{E_{c,i}} \end{aligned} \quad (5)$$

$$\begin{aligned} \hat{E} = & \alpha + \beta_1 \overline{A_{c,i}} + \beta_2 \overline{E_{c,i}} + \beta_3 \beta_{A_{c,i}} + \beta_4 \beta_{E_{c,i}} + \beta_5 \overline{A_{c,i}} : \overline{E_{c,i}} + \beta_6 \overline{A_{c,i}} : \beta_{A_{c,i}} + \beta_7 \overline{A_{c,i}} : \beta_{E_{c,i}} + \\ & \beta_8 \overline{E_{c,i}} : \beta_{A_{c,i}} + \beta_9 \overline{E_{c,i}} : \beta_{E_{c,i}} + \beta_{10} \beta_{A_{c,i}} : \beta_{E_{c,i}} \end{aligned} \quad (6)$$

Model selection was based on AIC with the help of the R package MuMIn. For the best model in terms of AIC relative importance of the retained parameters was established by hierarchical partitioning (Chevan and Sutherland (1991) Hierarchical partitioning. The American Statistician 45(2):90-96) as implemented in the relaimpo-package (lmg method).

For each scenario a summary on the results of the performance of the three approaches was given, followed by tables (see for example tables 2, 3, 4 and 5) and images (see for example figure 6) documenting the detailed results.

3 Scenario one: All entities have the same generic activation energy E_c and intercept A_c

3.1 Description and assumptions of scenario one

In this scenario it is assumed that there exists one generic temperature dependence $E_c = E \forall c$ and one generic absolute metabolic rate $A_c = A \forall c$. However, within the entities the $E_{c,i}$ and $A_{c,i}$ for each instance vary with Gaussian random noise ($A_{c,i} \sim N(A_c, 0.4)$ and $E_{c,i} \sim N(E_c, 0.1)$). While a generic activation energy is also assumed by MTE, the fixed A are rather artificial in this scenario. Note, due to the fact that E_c and A_c are the same for all entities and $A_{c,i}$ and $E_{c,i}$ only vary with $N(0,0.4)$ and $N(0,0.1)$ Gaussian random noise within each entity the probability of an chance increase of $\ln \overline{A_{c,i}}$ or $\overline{E_{c,i}}$ with $\overline{T_c}$ is very limited in this scenario (see figure 3).

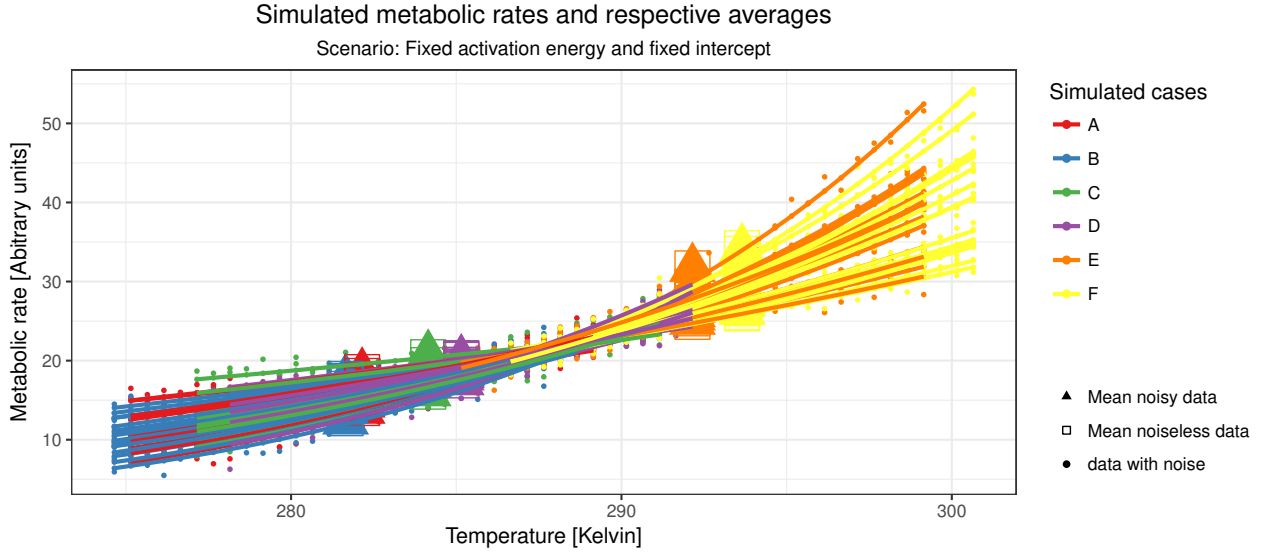


Figure 1: Exemplary simulated raw data for scenario one

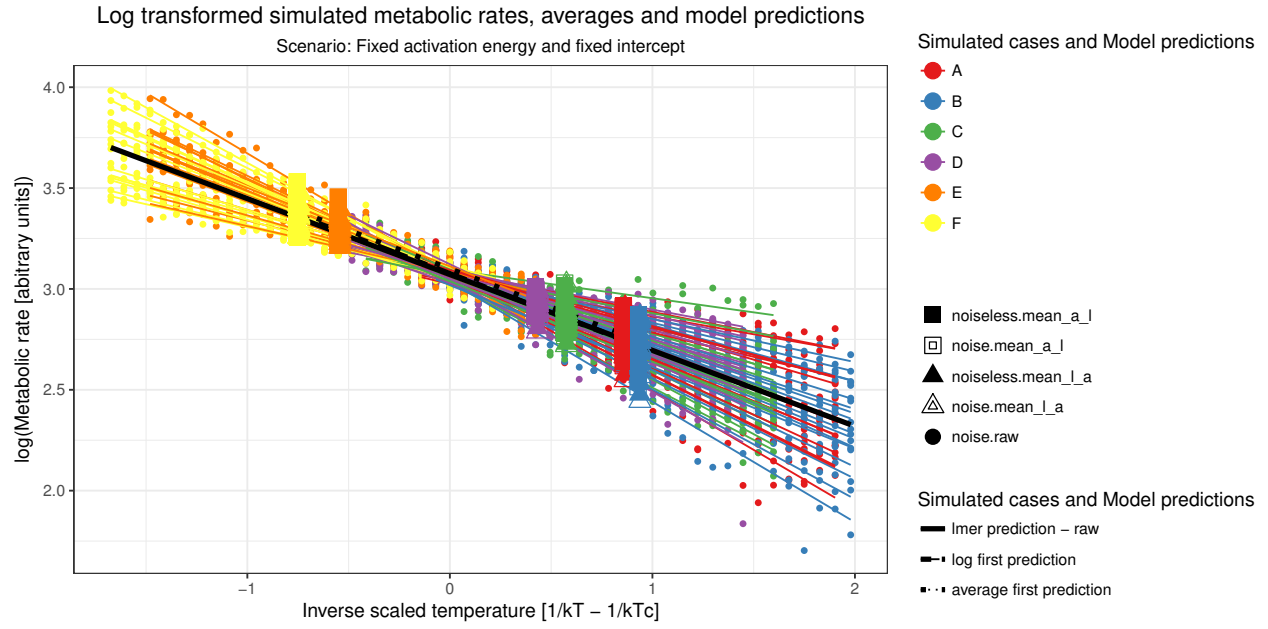


Figure 2: Exemplary Arrhenius plot for scenario one

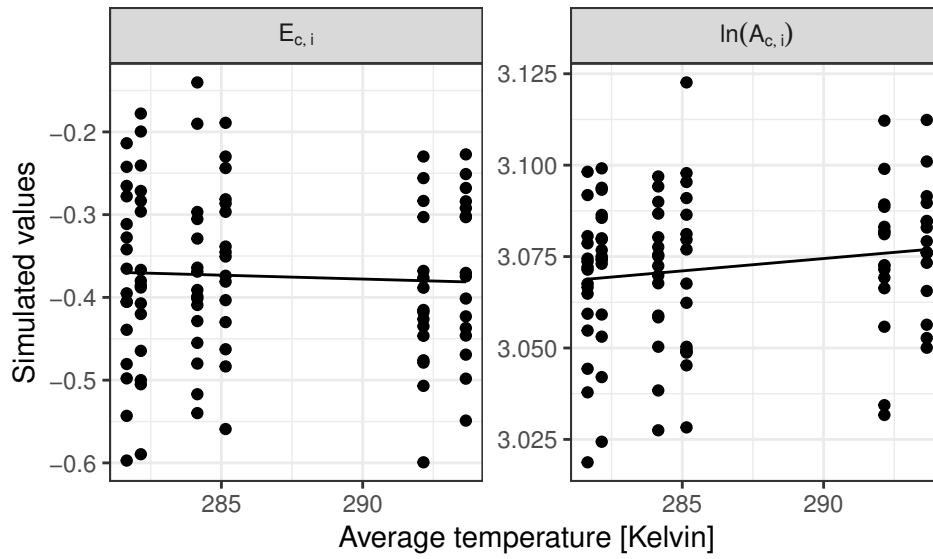


Figure 3: Scenario one: Exemplary regression of $\ln A_{c,i}$ and $E_{c,i}$ vs. \bar{T}_c

3.2 Summary results scenario one:

In this scenario all three approaches are able to estimate $\overline{\ln A_{c,i}}$ and $\overline{E_{c,i}}$ reasonable well (see figure 4 and 5). However, the variance in $\overline{\ln A_{c,i}} - \hat{A}$ is higher for the log-first and average-first approach compared to the LMER-approach. While the log-first approach seems to systematically underestimate $\overline{\ln A_{c,i}}$, the average-first approach seem to systematically overestimate $\overline{\ln A_{c,i}}$ (see figure 4).

The variance in the estimates of $\overline{E_{c,i}}$ is low for all approaches, yet estimates by the LMER-approach and the log-first approach show small systematic overestimation of $\overline{E_{c,i}}$. Overall, for both parameters the LMER-approach has the highest score in zero difference for $\overline{\ln A_{c,i}} - \hat{A}$ and $\overline{E_{c,i}} - \hat{E}$ (see figure 4).

This is inline with very similar density distributions of estimated parameters for all 3 approaches (see figure 5) and the fact that \hat{A} and \hat{E} are almost exclusively determined by $\overline{\ln A_{c,i}}$ and $\overline{E_{c,i}}$ respectively (see tables 3, 5, 7, 9, 11 and 13, as well as figures 6, 7 and 8).

3.3 Scenario one: Comparison between $\overline{E_{c,i}}$ and $\overline{\ln A_{c,i}}$ and \hat{E} and \hat{A} from the 3 different estimation approaches

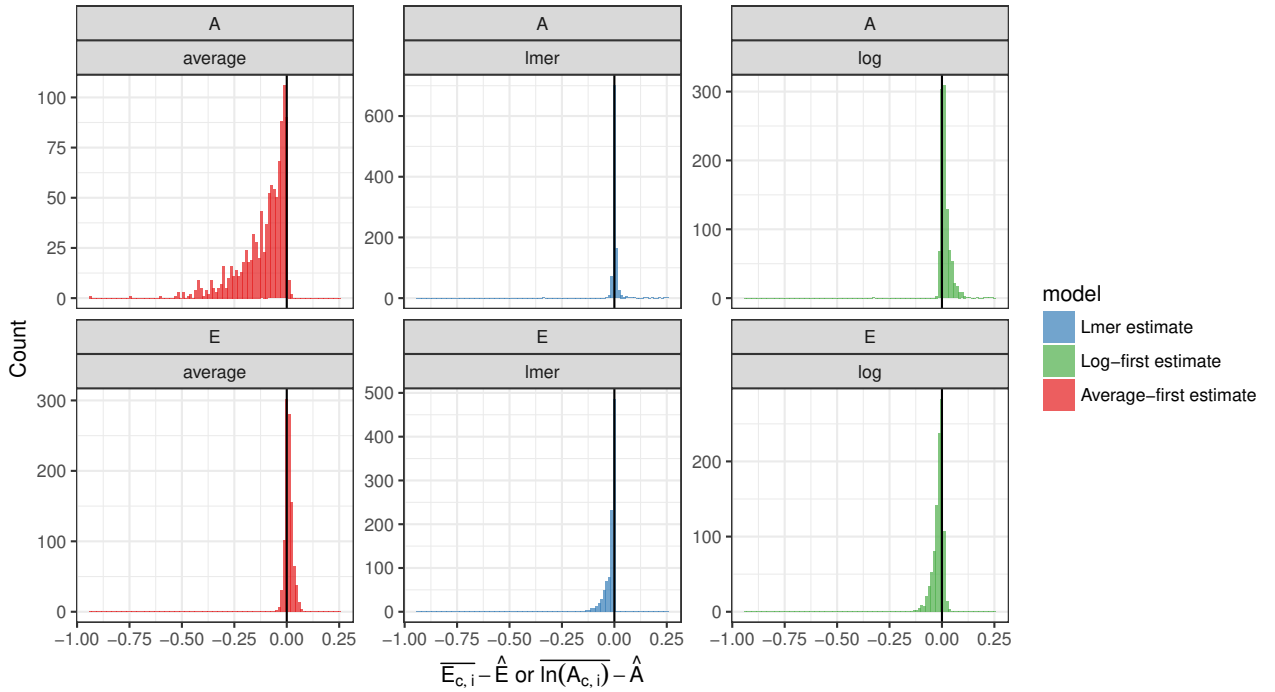


Figure 4: Scenario one: Comparison of $\overline{E_{c,i}} - \hat{E}$ and $\overline{\ln A_{c,i}} - \hat{A}$ for the 3 tested estimation approaches

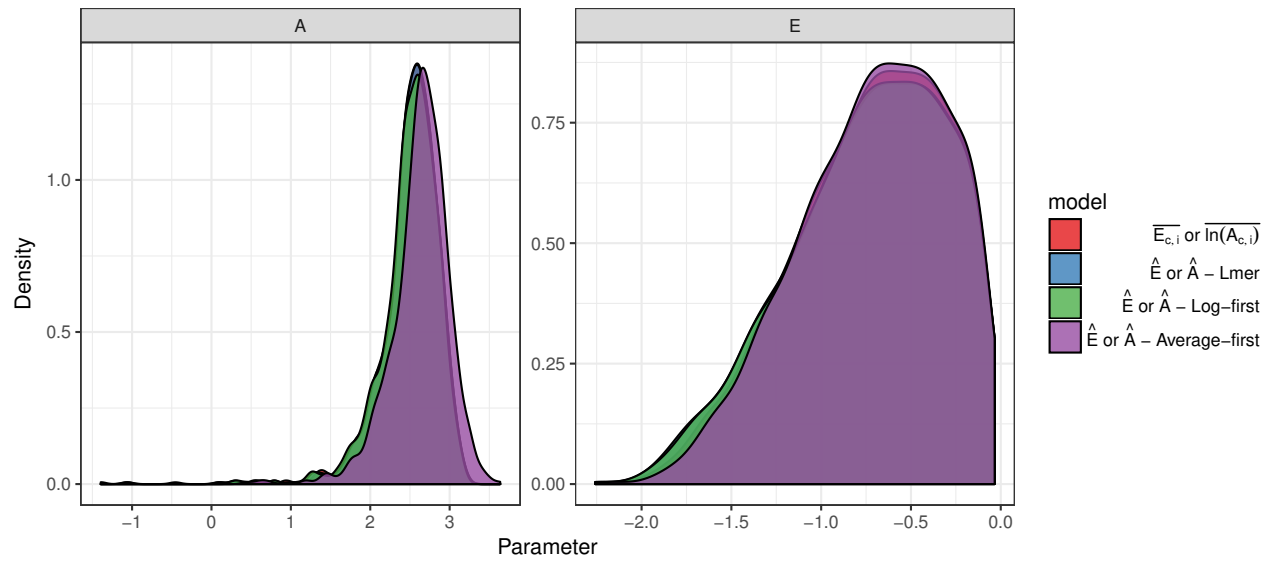


Figure 5: Scenario one: Comparison between simulated and estimated parameter

3.4 Scenario one: Detailed results on the influence of chance correlation of $\ln A_{c,i}$ $E_{c,i}$ with \bar{T}_c on the estimates of \hat{E} and \hat{A}

3.4.1 Log-first approach - Best model to explain \hat{E} and \hat{A} based on $\overline{E_{c,i}}$, $\overline{\ln A_{c,i}}$, $\beta_{E_{c,i}}$ and $\beta_{A_{c,i}}$

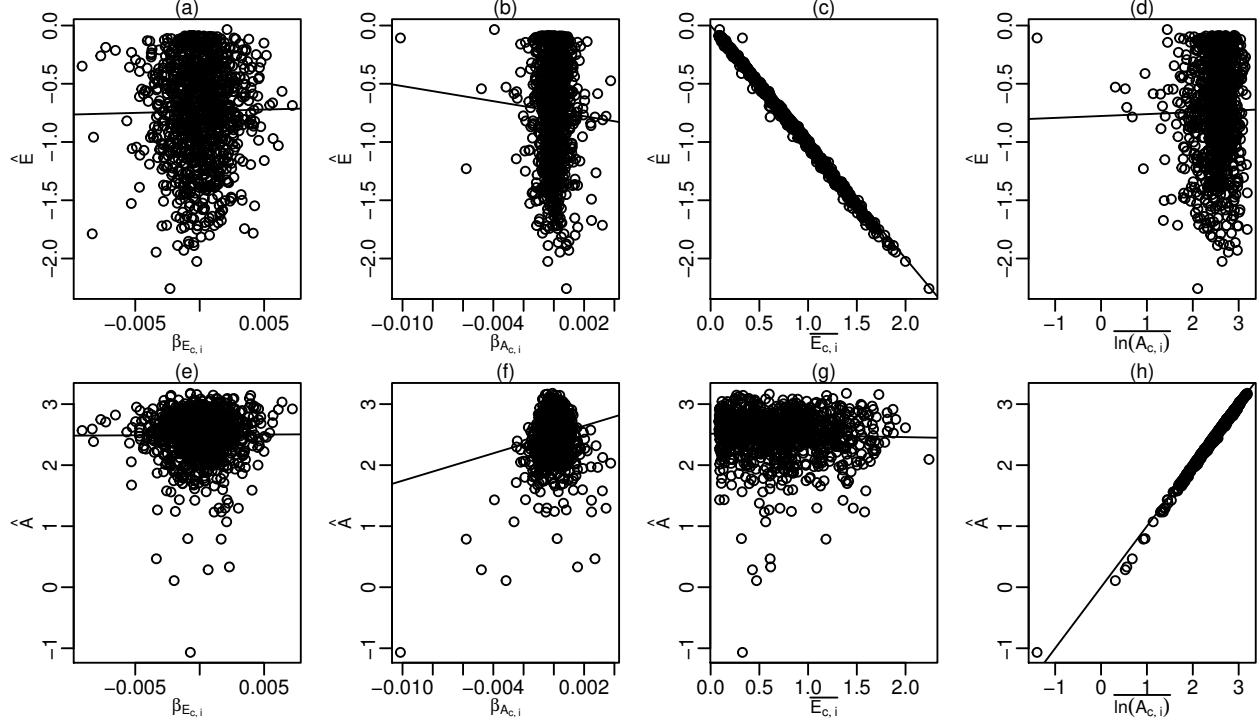


Figure 6: Scenario one - Log-first approach: Influence of $\beta_{E_{c,i}}$, $\beta_{A_{c,i}}$, $\overline{E_{c,i}}$, and $\overline{\ln A_{c,i}}$ on \hat{E} and \hat{A} . Solid lines depict linear regression relations for all plot except (c) and (h) where a bisection line is plotted since identity relations are expected.

Table 2: Scenario one - Log-first approach: Best model for \hat{E}

	Estimate	Std. Error	t.value	Pr(> t)
(Intercept)	0.028	0.008	3.408	0.001
$\overline{\ln A_{c,i}}$	-0.008	0.003	-2.451	0.014
$\overline{E_{c,i}}$	-1.125	0.011	-106.382	0.000
$\overline{\ln A_{c,i}} : \overline{E_{c,i}}$	0.037	0.004	8.826	0.000

Table 3: Scenario one - Log-first approach: Relative importance of best model parameters to explain \hat{E}

	Rel. Importance
$\overline{\ln A_{c,i}}$	0
$\overline{E_{c,i}}$	1
$\overline{\ln A_{c,i}} : \overline{E_{c,i}}$	0

Table 4: Scenario one - Log-first approach: Best model for \hat{A}

	Estimate	Std. Error	t.value	Pr(> t)
(Intercept)	0.000	0.009	-0.034	0.973
$\overline{\ln A_{c,i}}$	1.002	0.004	278.490	0.000
$\overline{E_{c,i}}$	-0.124	0.012	-10.633	0.000
$\overline{\ln A_{c,i} : E_{c,i}}$	0.038	0.005	8.266	0.000

Table 5: Scenario one - Log-first approach: Relative importance of best model parameters to explain \hat{A}

	Rel. Importance
$\overline{\ln A_{c,i}}$	0.999
$\overline{E_{c,i}}$	0.001
$\overline{\ln A_{c,i} : E_{c,i}}$	0.000

3.4.2 Average-first approach - Best model to explain \hat{E} and \hat{A} based on $\overline{E_{c,i}}$, $\overline{\ln A_{c,i}}$, $\beta_{E_{c,i}}$ and $\beta_{A_{c,i}}$

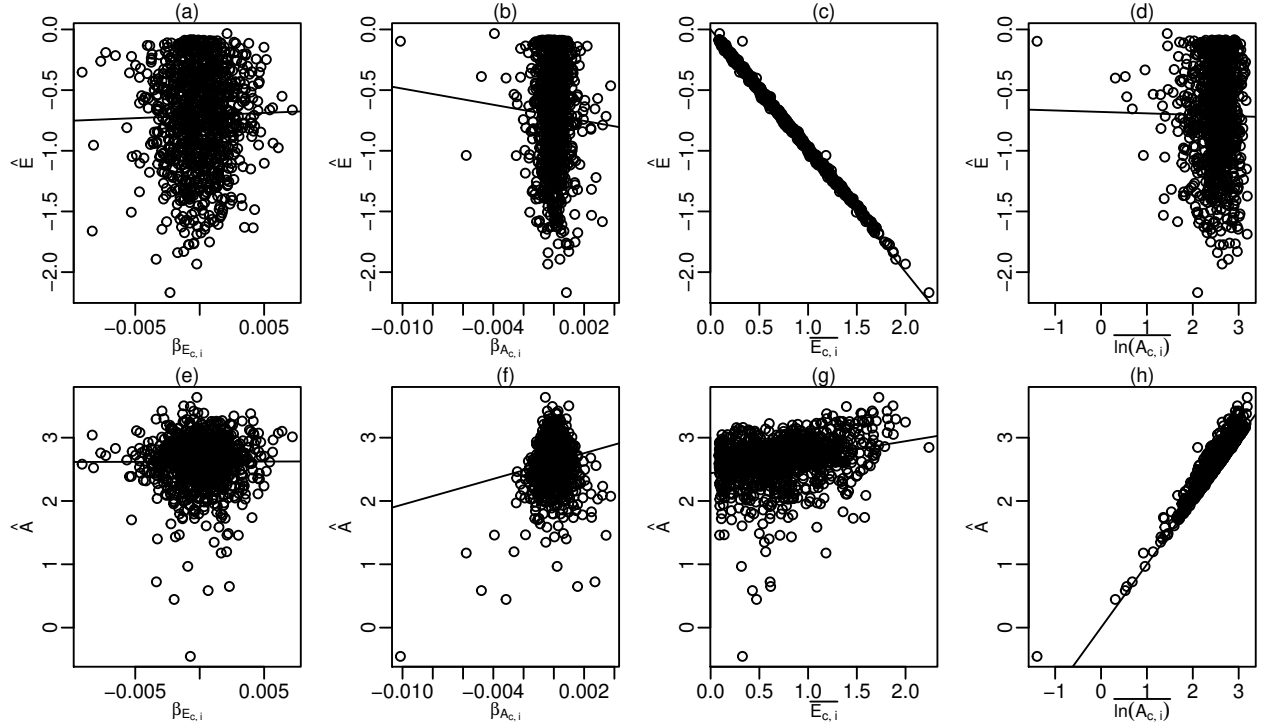


Figure 7: Scenario one - Average-first approach: Influence of $\beta_{E_{c,i}}$, $\beta_{A_{c,i}}$, $\overline{E_{c,i}}$, and $\overline{\ln A_{c,i}}$ on \hat{E} and \hat{A} . Solid lines depict linear regression relations for all plot except (c) and (h) where a bisection line is plotted since identity relations are expected.

Table 6: Scenario one - average-first approach: Best model for \hat{E}

	Estimate	Std. Error	t.value	Pr(> t)
(Intercept)	0.033	0.007	4.893	0.000
$\overline{\ln A_{c,i}}$	-0.016	0.003	-6.105	0.000
$\overline{E_{c,i}}$	-0.991	0.008	-116.844	0.000
$\overline{\ln A_{c,i}} : \overline{E_{c,i}}$	0.006	0.003	1.927	0.054

Table 7: Scenario one - average-first approach: Relative importance of best model parameters to explain \hat{E}

	Rel. Importance
$\overline{\ln A_{c,i}}$	0
$\overline{E_{c,i}}$	1
$\overline{\ln A_{c,i}} : \overline{E_{c,i}}$	0

Table 8: Scenario one - average-first approach: Best model for \hat{A}

	Estimate	Std. Error	t.value	Pr(> t)
(Intercept)	0.077	0.017	4.500	0
$\overline{\ln A_{c,i}}$	0.940	0.007	139.700	0
$\overline{E_{c,i}}$	0.134	0.022	6.118	0
$\overline{\ln A_{c,i} : E_{c,i}}$	0.047	0.009	5.482	0

Table 9: Scenario one - average-first approach: Relative importance of best model parameters to explain \hat{A}

	Rel. Importance
$\overline{\ln A_{c,i}}$	0.921
$\overline{E_{c,i}}$	0.079
$\overline{\ln A_{c,i} : E_{c,i}}$	0.000

3.4.3 LMER approach - Best model to explain \hat{E} and \hat{A} based on $\overline{E_{c,i}}$, $\overline{\ln A_{c,i}}$, $\beta_{E_{c,i}}$ and $\beta_{A_{c,i}}$

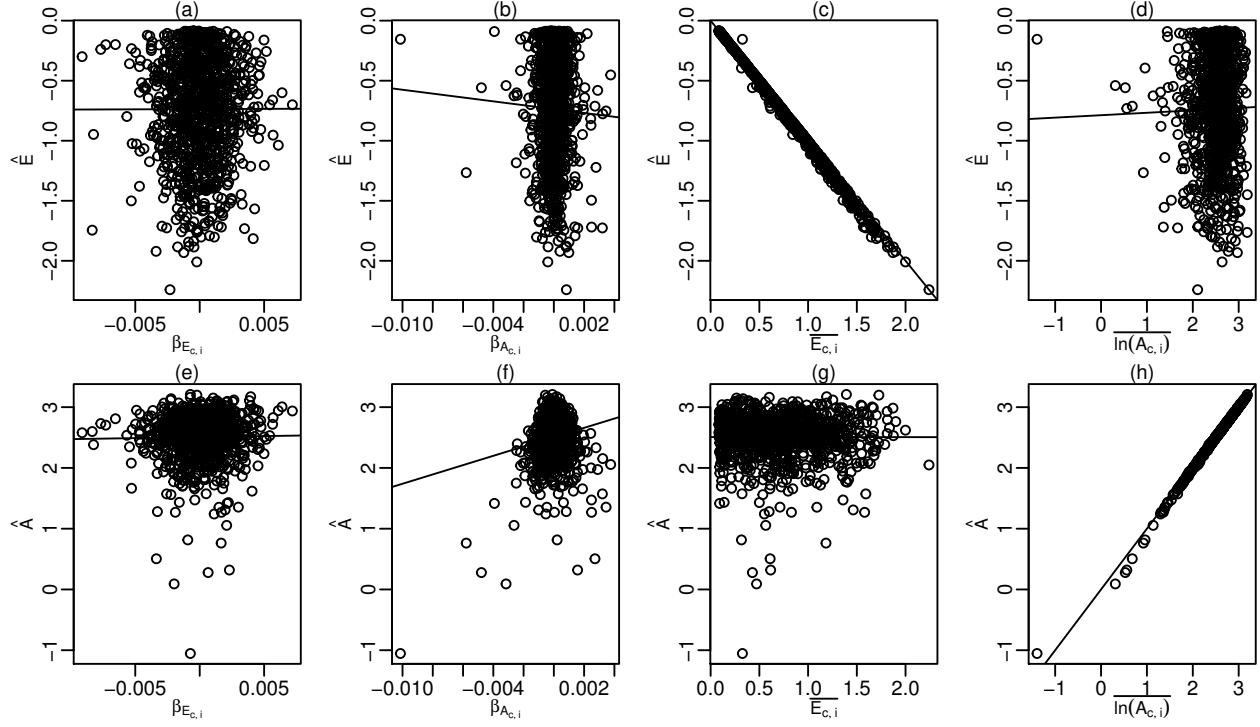


Figure 8: Scenario one - LMER approach: Influence of $\beta_{E_{c,i}}$, $\beta_{A_{c,i}}$, $\overline{E_{c,i}}$, and $\overline{\ln A_{c,i}}$ on \hat{E} and \hat{A} . Solid lines depict linear regression relations for all plot except (c) and (h) where a bisection line is plotted since identity relations are expected.

Table 10: Scenario one - lmer approach: Best model for \hat{E}

	Estimate	Std. Error	t.value	Pr(> t)
(Intercept)	0.023	0.007	3.116	0.002
$\overline{\ln A_{c,i}}$	-0.005	0.003	-1.759	0.079
$\overline{E_{c,i}}$	-1.133	0.009	-122.179	0.000
$\overline{\ln A_{c,i}} : \overline{E_{c,i}}$	0.038	0.004	10.474	0.000

Table 11: Scenario one - lmer approach: Relative importance of best model parameters to explain \hat{E}

	Rel. Importance
$\overline{\ln A_{c,i}}$	0
$\overline{E_{c,i}}$	1
$\overline{\ln A_{c,i}} : \overline{E_{c,i}}$	0

Table 12: Scenario one - lmer approach: Best model for \hat{A}

	Estimate	Std. Error	t.value	Pr(> t)
(Intercept)	0.005	0.008	0.669	0.504
$\overline{\ln A_{c,i}}$	0.996	0.003	314.838	0.000
$\overline{E_{c,i}}$	-0.090	0.010	-8.776	0.000
$\overline{\ln A_{c,i} : E_{c,i}}$	0.036	0.004	8.812	0.000

Table 13: Scenario one - lmer approach: Relative importance of best model parameters to explain \hat{A}

	Rel. Importance
$\overline{\ln A_{c,i}}$	1
$\overline{E_{c,i}}$	0
$\overline{\ln A_{c,i} : E_{c,i}}$	0

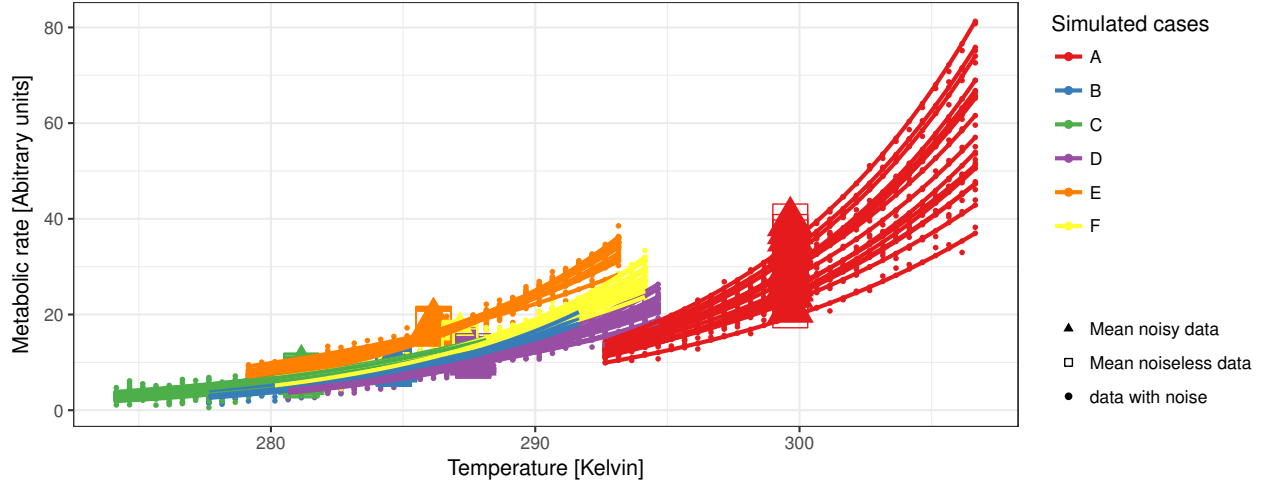
4 Scenario two: All entities have the same generic activation energy E_c but have a variable intercept A_c

4.1 Description and assumptions of scenario two

In this scenario it is assumed that there exists one generic temperature dependence $E_c = E \forall c$, however A_c is assumed to be different between entities. This makes scenario two more realistic and at the same time accords to MTE. Since A_c differ between entities, $\overline{\ln A_{c,i}}$ might exhibit chance correlation with \bar{T}_c (see figure 9).

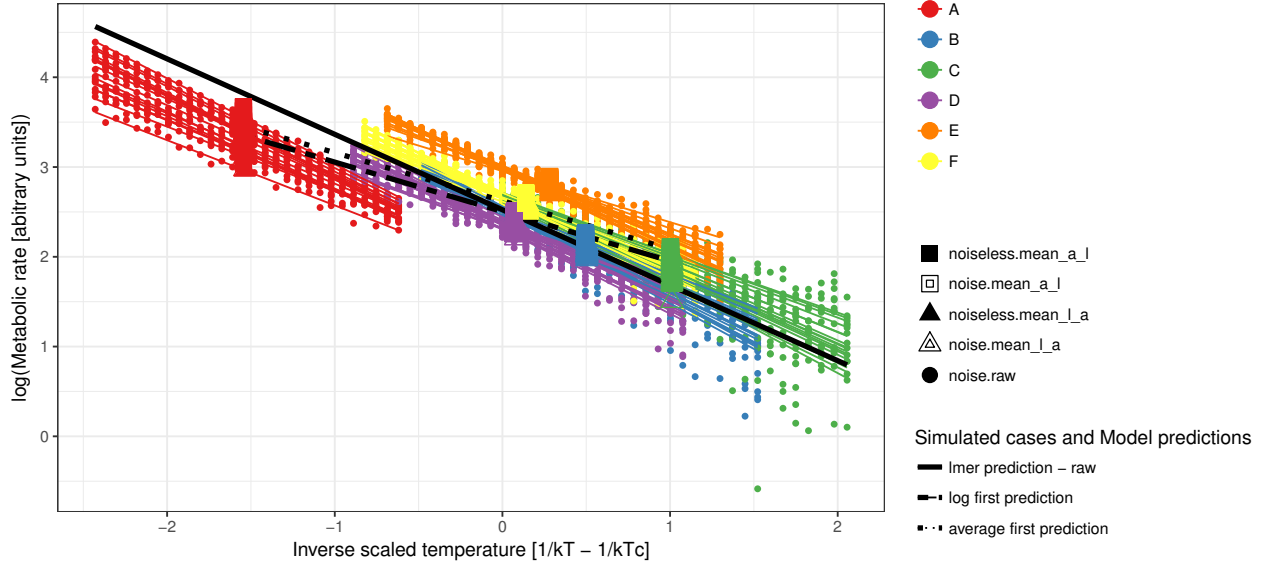
Simulated metabolic rates and respective averages

Scenario: Fixed activation energy and variable intercept



Log transformed simulated metabolic rates, averages and model predictions

Scenario: Fixed activation energy and variable intercept



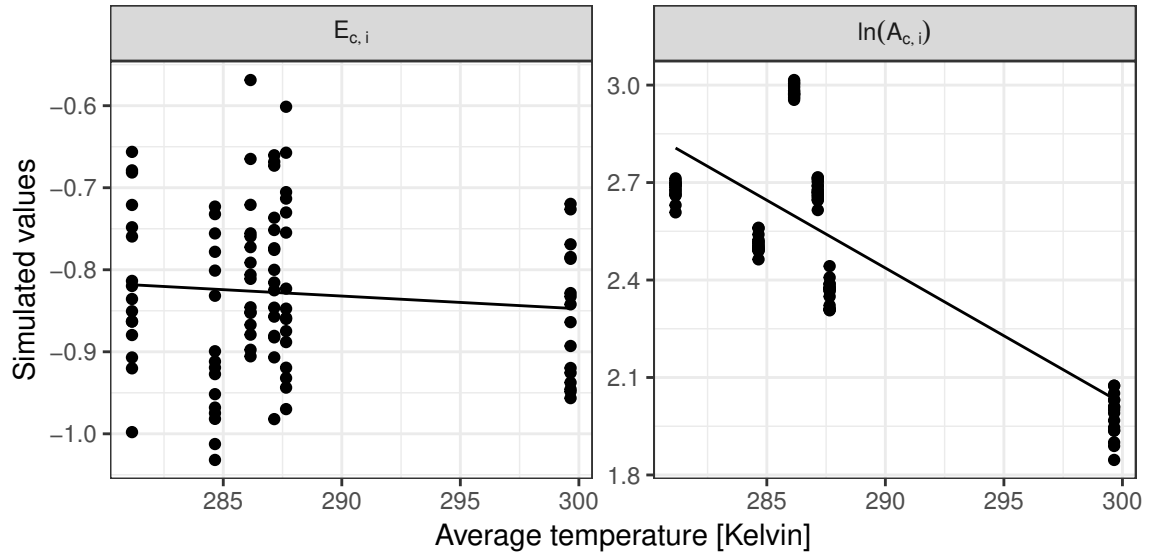


Figure 9: Scenario two: Regression of $\ln A_{c,i}$ and $E_{c,i}$ vs. $\overline{T_c}$

4.2 Summary results scenario two:

\hat{E} for both the average-first and log-first approaches is mainly determined by $\overline{E_{c,i}}$ but also to a considerable amount by $\beta_{A_{c,i}}$, the chance co variation of simulated $\ln A_{c,i}$ values with \bar{T}_c (see tables 15, 19 and figures 12, 13). This is not the case for the LMER approach (see table 23 and figure 14).

Similar, \hat{A} is not only determined by $\ln A_{c,i}$ but also to a considerable degree by $\beta_{A_{c,i}}$ and partly also $\overline{E_{c,i}}$ for the average-first and log-first approach (see tables 17, 21 and figures 12, 13). Again, this is not the case for the LMER approach where estimated \hat{A} are only driven by $\ln A_{c,i}$ (see table 25 and figure 14).

This is consistent with the fact that both average based approaches are marked by a large spread in $\ln A_{c,i} - \hat{A}$ and $\overline{E_{c,i}} - \hat{E}$ (see figure 10), indicating that while \hat{A} and \hat{E} might be close to \bar{E} and \bar{A} also large deviations are possible likely driven by $\beta_{A_{c,i}}$. In contrast difference between estimated and simulated values have a much smaller spread for the LMER approach. Similar, the density distributions of the estimated parameters from the LMER approach are much closer to the density distributions of the simulated parameters, as is the case for the ones from the average based approaches (see figure 11).

4.3 Scenario two: Comparison between $\overline{E_{c,i}}$ and $\ln A_{c,i}$ and \hat{E} and \hat{A} from the 3 different estimation approaches

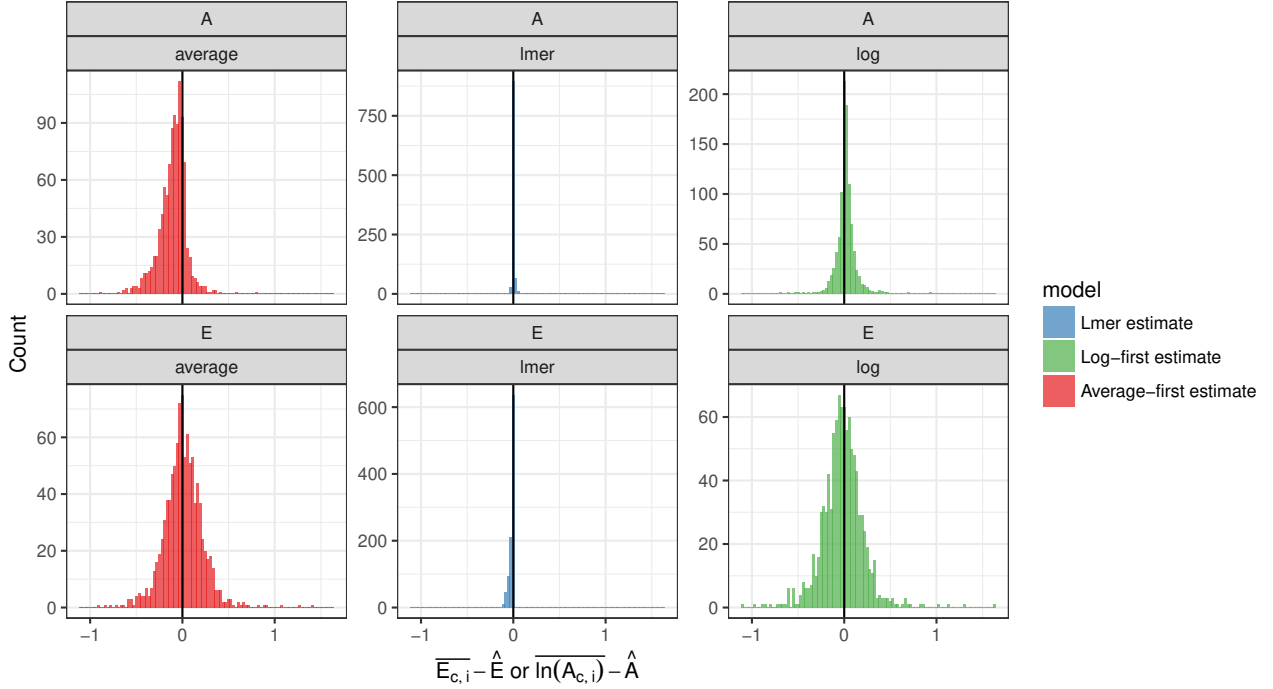


Figure 10: Scenario two: Comparison of $\overline{E_{c,i}} - \hat{E}$ and $\ln A_{c,i} - \hat{A}$ for the 3 tested estimation approaches

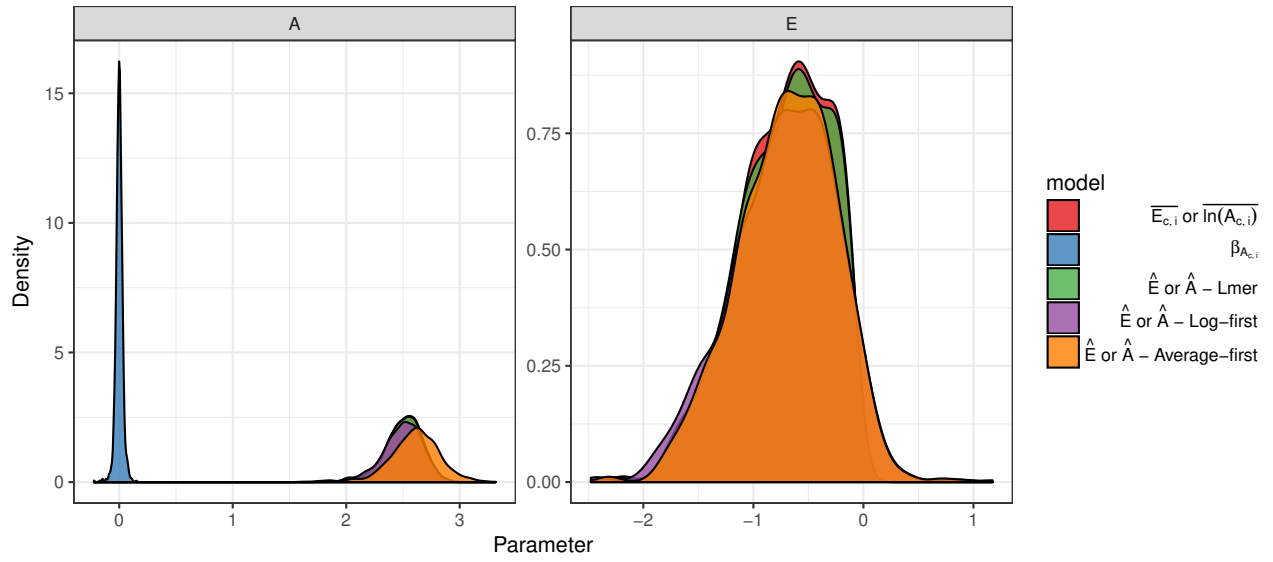


Figure 11: Scenario two: Comparison between simulated and estimated parameter

4.4 Scenario two: Detailed results on the influence of chance correlation of $\ln A_{c,i}$, $E_{c,i}$ with \bar{T}_c on the estimates of \hat{E} and \hat{A}

4.4.1 Log-first approach - Best model to explain \hat{E} and \hat{A} based on $\overline{E_{c,i}}$, $\overline{\ln A_{c,i}}$, $\beta_{E_{c,i}}$ and $\beta_{A_{c,i}}$

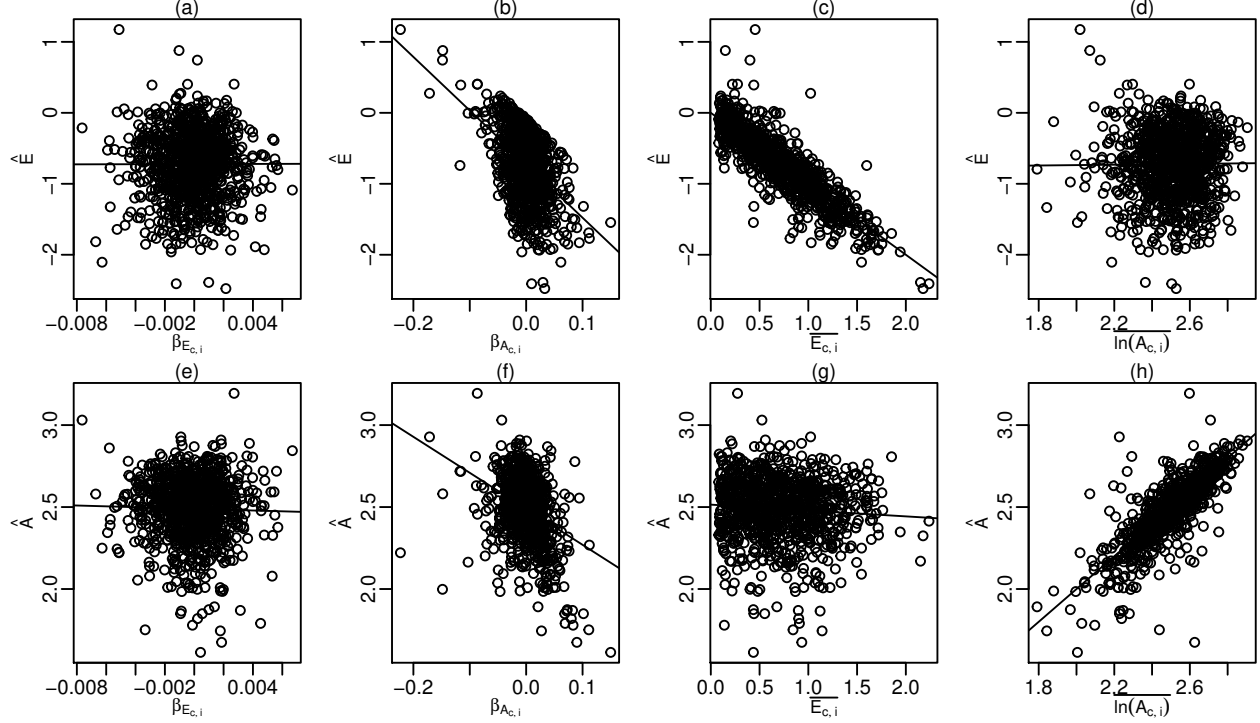


Figure 12: Scenario two - Log-first approach: Influence of $\beta_{E_{c,i}}$, $\beta_{A_{c,i}}$, $\overline{E_{c,i}}$, and $\overline{\ln A_{c,i}}$ on \hat{E} and \hat{A} . Solid lines depict linear regression relations for all plot except (c) and (h) where a bisection line is plotted since identity relations are expected.

Table 14: Scenario two - Log-first approach: Best model for \hat{E}

	Estimate	Std. Error	t.value	Pr(> t)
(Intercept)	0.011	0.019	0.571	0.568
$\overline{\ln A_{c,i}}$	-0.001	0.008	-0.065	0.948
$\beta_{A_{c,i}}$	-7.705	0.229	-33.684	0.000
$\overline{E_{c,i}}$	-1.117	0.025	-44.764	0.000
$\overline{\ln A_{c,i}} : \beta_{A_{c,i}}$	0.171	0.097	1.767	0.078
$\overline{\ln A_{c,i}} : \overline{E_{c,i}}$	0.032	0.010	3.213	0.001
$\beta_{A_{c,i}} : \overline{E_{c,i}}$	-0.300	0.053	-5.712	0.000

Table 15: Scenario two - Log-first approach: Relative importance of best model parameters to explain \hat{E}

	Rel. Importance
$\overline{\ln A_{c,i}}$	0.000
$\beta_{A_{c,i}}$	0.233
$\overline{E_{c,i}}$	0.767

	Rel. Importance
$\overline{\ln A_{c,i}} : \overline{\beta_{A_{c,i}}}$	0.000
$\overline{\ln A_{c,i}} : \overline{E_{c,i}}$	0.000
$\overline{\beta_{A_{c,i}}} : \overline{E_{c,i}}$	0.000

Table 16: Scenario two - Log-first approach: Best model for \hat{A}

	Estimate	Std. Error	t.value	Pr(> t)
(Intercept)	0.013	0.043	0.309	0.758
$\overline{\ln A_{c,i}}$	0.996	0.017	59.315	0.000
$\overline{\beta_{A_{c,i}}}$	-2.317	0.087	-26.739	0.000
$\overline{E_{c,i}}$	-0.029	0.007	-4.422	0.000

Table 17: Scenario two - Log-first approach: Relative importance of best model parameters to explain \hat{A}

	Rel. Importance
$\overline{\ln A_{c,i}}$	0.832
$\overline{\beta_{A_{c,i}}}$	0.162
$\overline{E_{c,i}}$	0.006

4.4.2 Average-first approach - Best model to explain \hat{E} and \hat{A} based on $\overline{E_{c,i}}$, $\overline{\ln A_{c,i}}$, $\beta_{E_{c,i}}$ and $\beta_{A_{c,i}}$

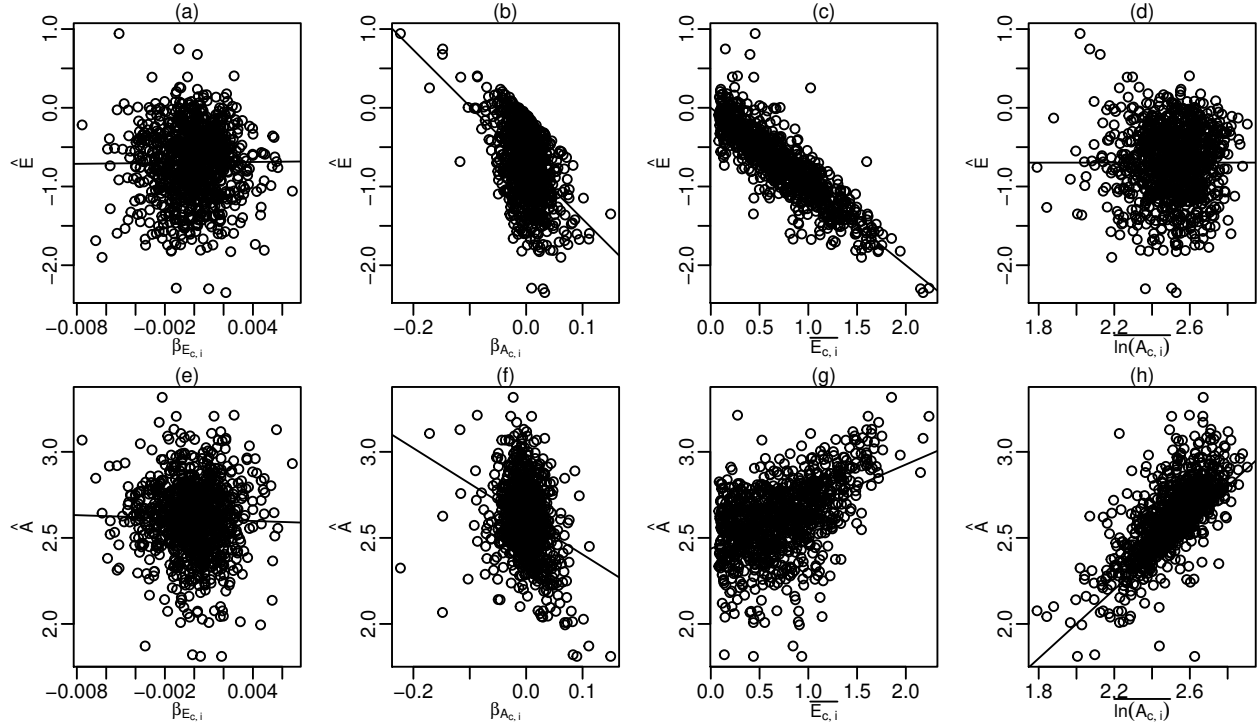


Figure 13: Scenario two - Average-first approach: Influence of $\beta_{E_{c,i}}$, $\beta_{A_{c,i}}$, $\overline{E_{c,i}}$, and $\overline{\ln A_{c,i}}$ on \hat{E} and \hat{A} . Solid lines depict linear regression relations for all plot except (c) and (h) where a bisection line is plotted since identity relations are expected.

Table 18: Scenario two - average-first approach: Best model for \hat{E}

	Estimate	Std. Error	t.value	Pr(> t)
(Intercept)	-0.033	0.015	-2.191	0.029
$\overline{\ln A_{c,i}}$	0.010	0.006	1.709	0.088
$\beta_{A_{c,i}}$	-4.430	0.177	-25.016	0.000
$\overline{E_{c,i}}$	-0.918	0.019	-47.517	0.000
$\overline{\ln A_{c,i}} : \beta_{A_{c,i}}$	-1.074	0.075	-14.319	0.000
$\overline{\ln A_{c,i}} : \overline{E_{c,i}}$	-0.023	0.008	-3.045	0.002
$\beta_{A_{c,i}} : \overline{E_{c,i}}$	-0.178	0.041	-4.382	0.000

Table 19: Scenario two - average-first approach: Relative importance of best model parameters to explain \hat{E}

	Rel. Importance
$\overline{\ln A_{c,i}}$	0.000
$\beta_{A_{c,i}}$	0.235
$\overline{E_{c,i}}$	0.765
$\overline{\ln A_{c,i}} : \beta_{A_{c,i}}$	0.000
$\overline{\ln A_{c,i}} : \overline{E_{c,i}}$	0.000

	Rel. Importance
$\beta_{A_{c,i}} : \overline{E_{c,i}}$	0.000

Table 20: Scenario two - average-first approach: Best model for \hat{A}

	Estimate	Std. Error	t.value	Pr(> t)
(Intercept)	0.028	0.044	0.647	0.518
$\overline{\ln A_{c,i}}$	0.959	0.017	55.244	0.000
$\beta_{A_{c,i}}$	-0.558	1.043	-0.535	0.593
$\overline{E_{c,i}}$	0.251	0.007	36.915	0.000
$\overline{\ln A_{c,i}} : \beta_{A_{c,i}}$	-0.685	0.436	-1.570	0.117

Table 21: Scenario two - average-first approach: Relative importance of best model parameters to explain \hat{A}

	Rel. Importance
$\overline{\ln A_{c,i}}$	0.610
$\beta_{A_{c,i}}$	0.115
$\overline{E_{c,i}}$	0.274
$\overline{\ln A_{c,i}} : \beta_{A_{c,i}}$	0.001

4.4.3 LMER approach - Best model to explain \hat{E} and \hat{A} based on $\overline{E_{c,i}}$, $\overline{\ln A_{c,i}}$, $\beta_{E_{c,i}}$ and $\beta_{A_{c,i}}$

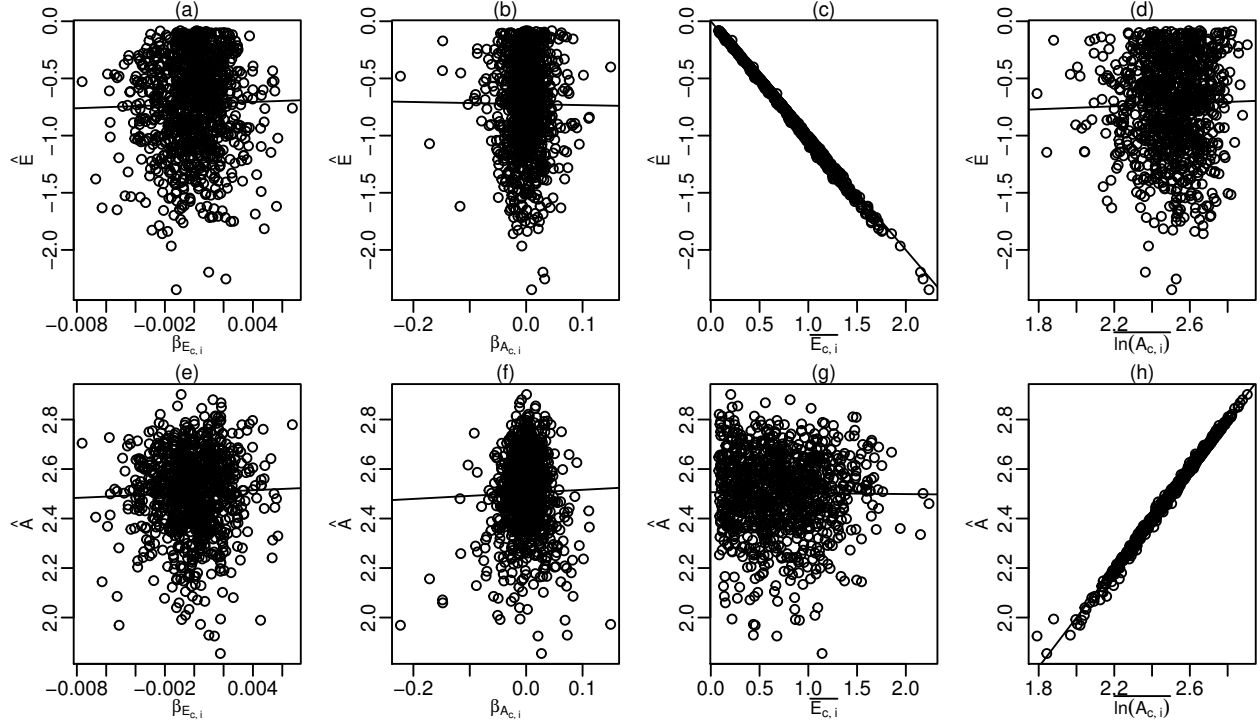


Figure 14: Scenario two - LMER approach: Influence of $\beta_{E_{c,i}}$, $\beta_{A_{c,i}}$, $\overline{E_{c,i}}$, and $\overline{\ln A_{c,i}}$ on \hat{E} and \hat{A} . Solid lines depict linear regression relations for all plot except (c) and (h) where a bisection line is plotted since identity relations are expected.

Table 22: Scenario two - lmer approach: Best model for \hat{E}

	Estimate	Std. Error	t.value	Pr(> t)
(Intercept)	0.019	0.016	1.180	0.238
$\overline{\ln A_{c,i}}$	-0.003	0.006	-0.475	0.635
$\beta_{A_{c,i}}$	0.747	0.193	3.881	0.000
$\overline{E_{c,i}}$	-1.135	0.021	-54.084	0.000
$\overline{\ln A_{c,i}} : \beta_{A_{c,i}}$	-0.304	0.082	-3.722	0.000
$\overline{\ln A_{c,i}} : \overline{E_{c,i}}$	0.037	0.008	4.501	0.000
$\beta_{A_{c,i}} : \overline{E_{c,i}}$	-0.090	0.044	-2.034	0.042

Table 23: Scenario two - lmer approach: Relative importance of best model parameters to explain \hat{E}

	Rel. Importance
$\overline{\ln A_{c,i}}$	0
$\beta_{A_{c,i}}$	0
$\overline{E_{c,i}}$	1
$\overline{\ln A_{c,i}} : \beta_{A_{c,i}}$	0
$\overline{\ln A_{c,i}} : \overline{E_{c,i}}$	0
$\beta_{A_{c,i}} : \overline{E_{c,i}}$	0

Rel. Importance

Table 24: Scenario two - lmer approach: Best model for \hat{A}

	Estimate	Std. Error	t.value	Pr(> t)
(Intercept)	-0.009	0.011	-0.850	0.395
$\ln A_{c,i}$	1.002	0.004	230.270	0.000
$\beta_{A_{c,i}}$	0.341	0.129	2.646	0.008
$\overline{E_{c,i}}$	-0.051	0.014	-3.615	0.000
$\ln A_{c,i} : \beta_{A_{c,i}}$	-0.110	0.055	-2.006	0.045
$\ln A_{c,i} : \overline{E_{c,i}}$	0.021	0.006	3.782	0.000
$\beta_{A_{c,i}} : \overline{E_{c,i}}$	-0.119	0.030	-4.007	0.000

Table 25: Scenario two - lmer approach: Relative importance of best model parameters to explain \hat{A}

	Rel. Importance
$\overline{\ln A_{c,i}}$	0.999
$\overline{\beta_{A_{c,i}}}$	0.000
$\overline{E_{c,i}}$	0.000
$\overline{\ln A_{c,i} : \beta_{A_{c,i}}}$	0.000
$\overline{\ln A_{c,i} : E_{c,i}}$	0.000
$\overline{\beta_{A_{c,i}} : E_{c,i}}$	0.000

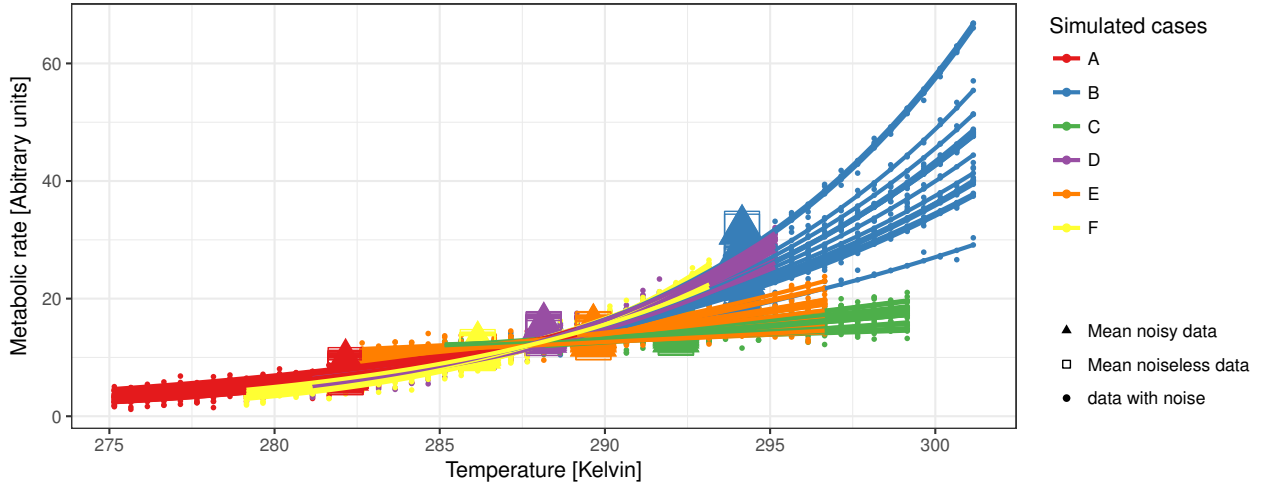
5 Scenario three: All entities have the same generic absolute metabolic rate A_c but variable E_c

5.1 Description and assumptions of scenario three

In this scenario it is assumed that E_c can vary with entity, but independent of \bar{T}_c . For the absolute metabolic rates it is assumed that $A_c = A \forall c$, i.e. similar production levels for all entities are simulated. This scenario no longer assumes an unchangeable generic activation energy as proposed by MTE but allows random variation of E_c . Chance correlation of E_c with \bar{T}_c can occur, particular since, like in the experiment, temperature ranges are represented by one entity only (see figure 15).

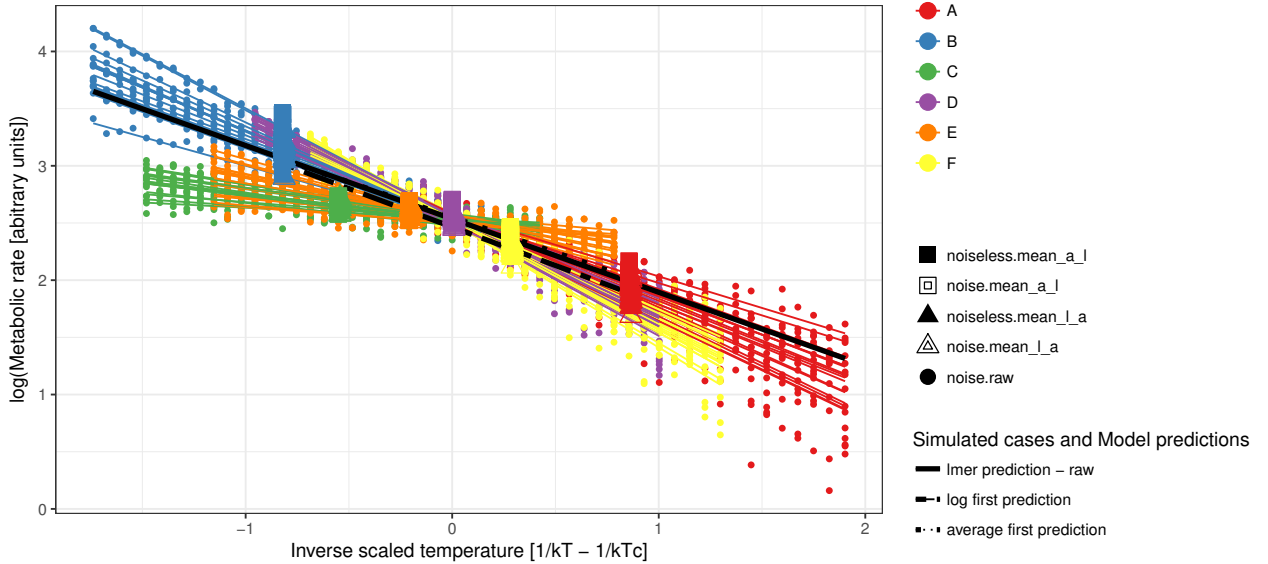
Simulated metabolic rates and respective averages

Scenario: Variable activation energy and fixed intercept



Log transformed simulated metabolic rates, averages and model predictions

Scenario: Variable activation energy and fixed intercept



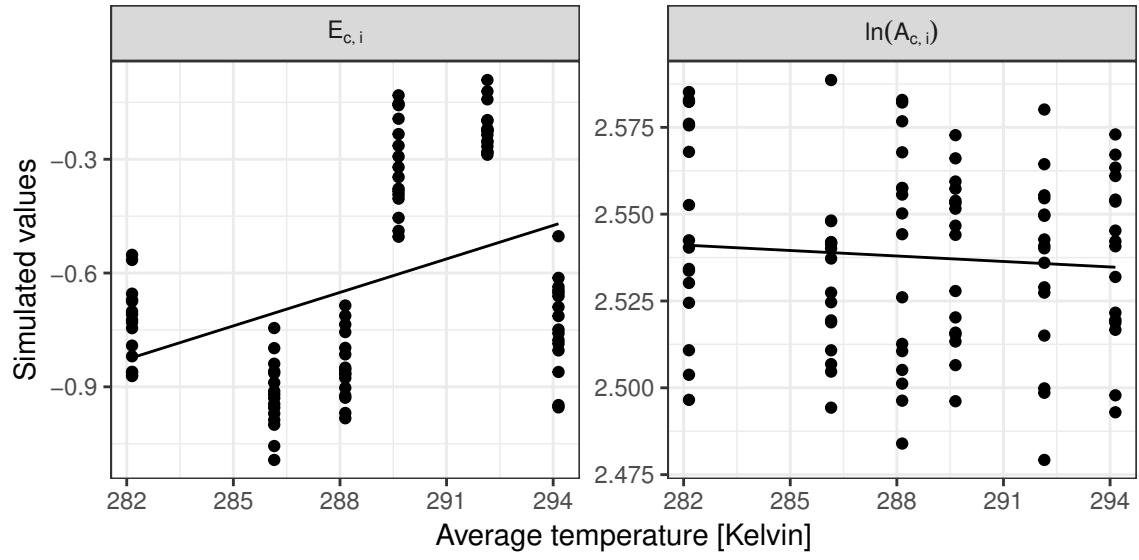


Figure 15: Scenario three: Regression of $\ln A_{c,i}$ and $E_{c,i}$ vs. $\overline{T_c}$

5.2 Summary results scenario three:

Estimated \hat{E} by the log-first approaches are mainly determined by $\overline{E_{c,i}}$, however, also $\beta_{E_{c,i}}$ is important (see table 27 and figure 18). This influential role of $\beta_{E_{c,i}}$ gets even greater for the average-first approach (see table 31 and figure 19). Contrary \hat{E} estimated by the LMER-approach is almost exclusively determined by $\overline{E_{c,i}}$ (see table 35 and figure 20).

Estimated \hat{A} from all three approaches are almost solely determined by $\overline{\ln A_{c,i}}$ (see tables 29, 33, 37 and figures 18, 19, 20).

This results are consistent with a good representation of the distribution of $\overline{\ln A_{c,i}}$ by the distributions of \hat{A} of all 3 methods (see figure 17). Still, the spread of the difference $\overline{\ln A_{c,i}} - \hat{A}$ is much higher for the average based approaches (see figure 16).

On the other hand the distributions of the \hat{E} estimated by the average based approaches do not reproduce the distribution $\overline{E_{c,i}}$, while the one from the LMER approach does (see figure 17). In addition, the differences between $\overline{E_{c,i}} - \hat{E}$ have much smaller spread for the LMER approach (see figure 16).

5.3 Scenario three: Comparison between $\overline{E_{c,i}}$ and $\overline{\ln A_{c,i}}$ and \hat{E} and \hat{A} from the 3 different estimation approaches

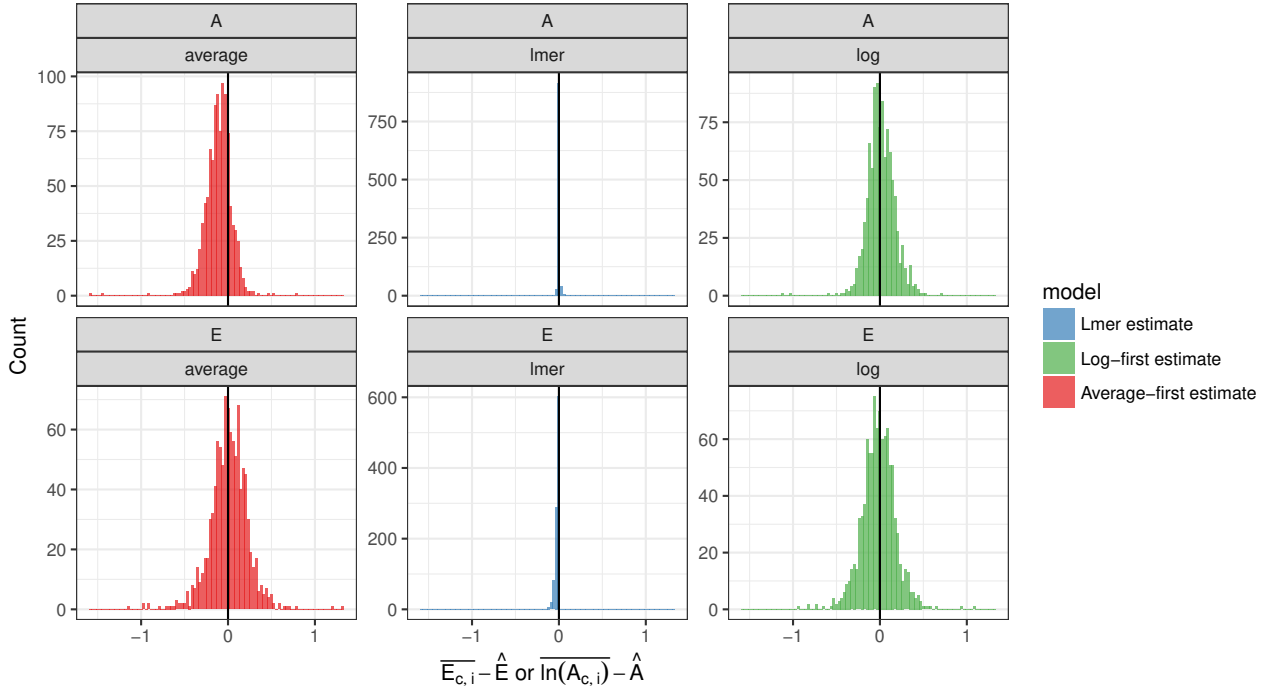


Figure 16: Scenario three: Comparison of $\overline{E_{c,i}} - \hat{E}$ and $\overline{\ln A_{c,i}} - \hat{A}$ for the 3 tested estimation approaches

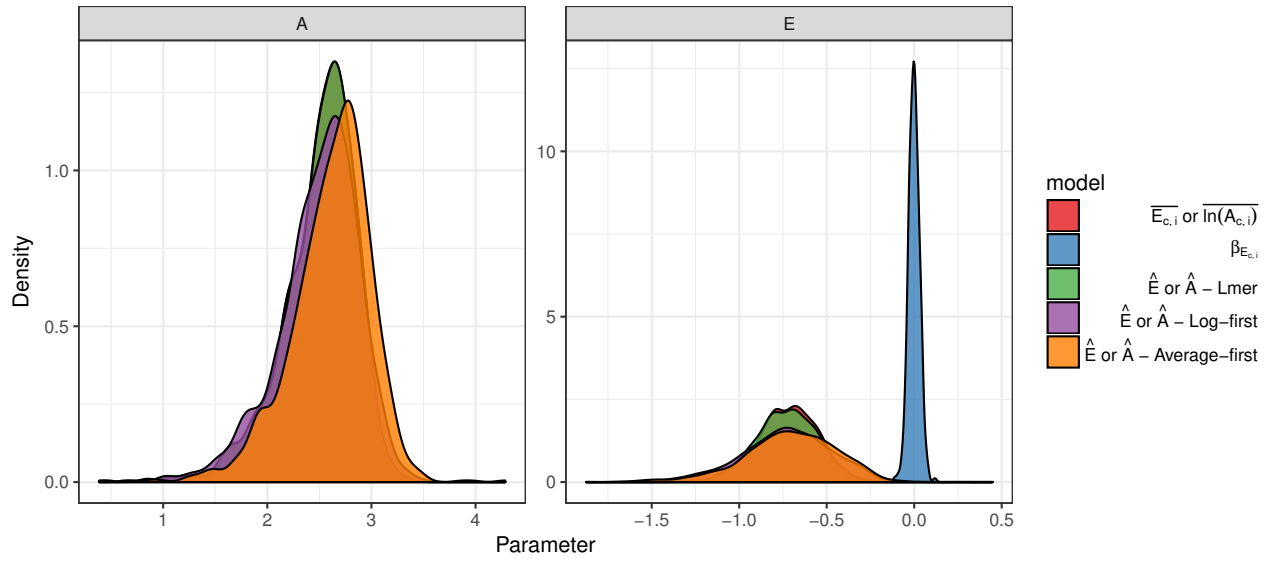


Figure 17: Scenario three: Comparison between simulated and estimated parameter

5.4 Scenario three: Detailed results on the influence of chance correlation of $\ln A_{c,i}$ $E_{c,i}$ with \bar{T}_c on the estimates of \hat{E} and \hat{A}

5.4.1 Log-first approach - Best model to explain \hat{E} and \hat{A} based on $\overline{E_{c,i}}$, $\overline{\ln A_{c,i}}$, $\beta_{E_{c,i}}$ and $\beta_{A_{c,i}}$

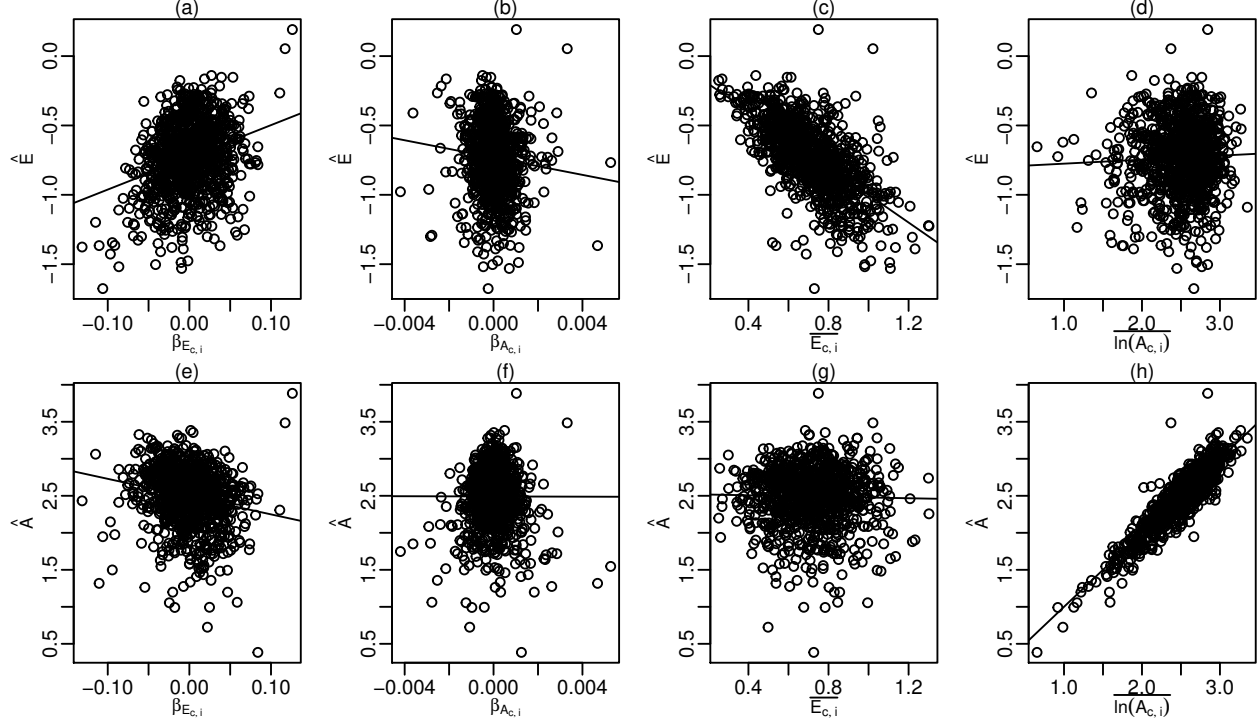


Figure 18: Scenario three - Log-first approach: Influence of $\beta_{E_{c,i}}$, $\beta_{A_{c,i}}$, $\overline{E_{c,i}}$, and $\overline{\ln A_{c,i}}$ on \hat{E} and \hat{A} . Solid lines depict linear regression relations for all plot except (c) and (h) where a bisection line is plotted since identity relations are expected.

Table 26: Scenario three - Log-first approach: Best model for \hat{E}

	Estimate	Std. Error	t.value	Pr(> t)
(Intercept)	-0.075	0.047	-1.592	0.112
$\overline{\ln A_{c,i}}$	0.025	0.016	1.540	0.124
$\beta_{E_{c,i}}$	2.480	0.177	13.986	0.000
$\overline{E_{c,i}}$	-1.001	0.034	-29.743	0.000

Table 27: Scenario three - Log-first approach: Relative importance of best model parameters to explain \hat{E}

	Rel. Importance
$\overline{\ln A_{c,i}}$	0.003
$\beta_{E_{c,i}}$	0.173
$\overline{E_{c,i}}$	0.824

Table 28: Scenario three - Log-first approach: Best model for \hat{A}

	Estimate	Std. Error	t.value	Pr(> t)
(Intercept)	-0.100	0.031	-3.166	0.002
$\ln A_{c,i}$	1.033	0.012	83.173	0.000
$\beta_{E_{c,i}}$	-2.377	0.137	-17.292	0.000

Table 29: Scenario three - Log-first approach: Relative importance of best model parameters to explain \hat{A}

	Rel. Importance
$\ln A_{c,i}$	0.958
$\beta_{E_{c,i}}$	0.042

5.4.2 Average-first approach - Best model to explain \hat{E} and \hat{A} based on $\overline{E_{c,i}}$, $\overline{\ln A_{c,i}}$, $\beta_{E_{c,i}}$ and $\beta_{A_{c,i}}$

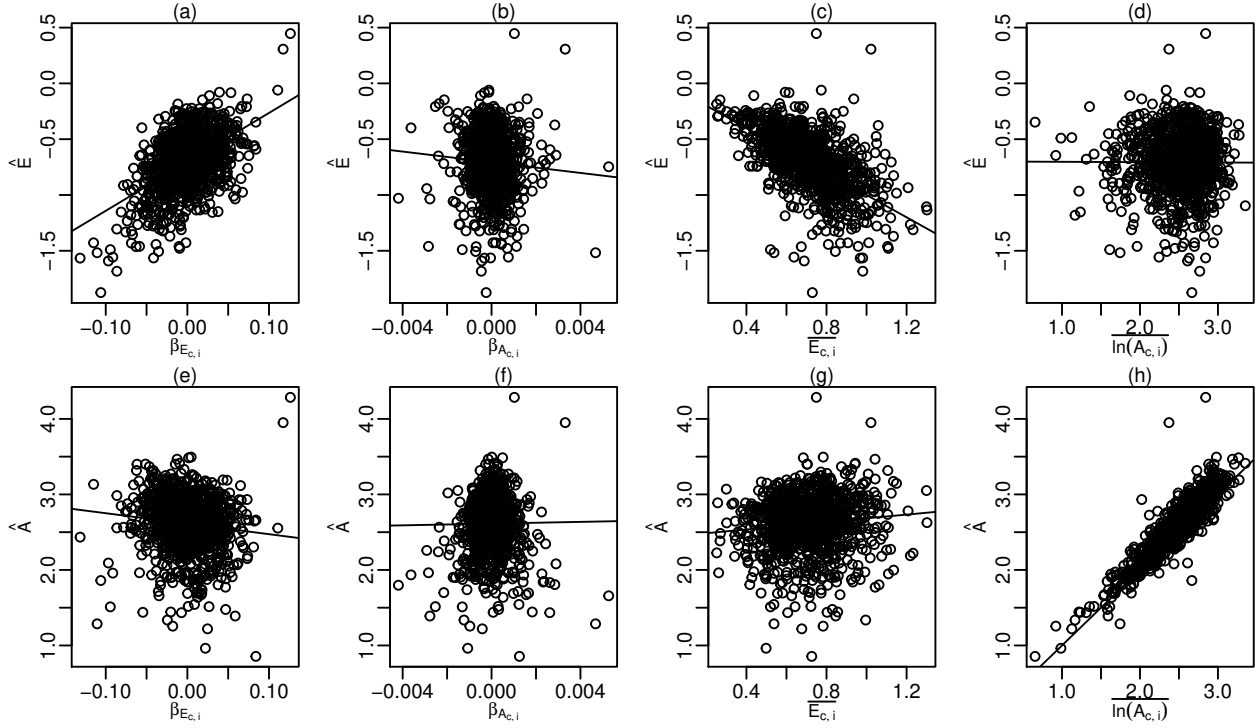


Figure 19: Scenario three - Average-first approach: Influence of $\beta_{E_{c,i}}$, $\beta_{A_{c,i}}$, $\overline{E_{c,i}}$, and $\overline{\ln A_{c,i}}$ on \hat{E} and \hat{A} . Solid lines depict linear regression relations for all plot except (c) and (h) where a bisection line is plotted since identity relations are expected.

Table 30: Scenario three - average-first approach: Best model for \hat{E}

	Estimate	Std. Error	t.value	Pr(> t)
(Intercept)	-0.031	0.023	-1.319	0.187
$\beta_{E_{c,i}}$	2.794	0.801	3.487	0.001
$\overline{E_{c,i}}$	-0.940	0.032	-29.698	0.000
$\beta_{E_{c,i}} : \overline{E_{c,i}}$	2.331	1.051	2.219	0.027

Table 31: Scenario three - average-first approach: Relative importance of best model parameters to explain \hat{E}

	Rel. Importance
$\beta_{E_{c,i}}$	0.452
$\overline{E_{c,i}}$	0.544
$\beta_{E_{c,i}} : \overline{E_{c,i}}$	0.003

Table 32: Scenario three - average-first approach: Best model for \hat{A}

	Estimate	Std. Error	t.value	Pr(> t)
(Intercept)	-0.072	0.038	-1.888	0.059
$\overline{\ln A_{c,i}}$	0.993	0.013	77.129	0.000
$\overline{\beta_{E_{c,i}}}$	0.212	0.977	0.217	0.828
$\overline{E_{c,i}}$	0.273	0.027	10.113	0.000
$\overline{\ln A_{c,i} : \beta_{E_{c,i}}}$	-0.649	0.388	-1.675	0.094

Table 33: Scenario three - average-first approach: Relative importance of best model parameters to explain \hat{A}

	Rel. Importance
$\overline{\ln A_{c,i}}$	0.968
$\overline{\beta_{E_{c,i}}}$	0.016
$\overline{E_{c,i}}$	0.016
$\overline{\ln A_{c,i} : \beta_{E_{c,i}}}$	0.000

5.4.3 LMER approach - Best model to explain \hat{E} and \hat{A} based on $\overline{E_{c,i}}$, $\overline{\ln A_{c,i}}$, $\beta_{E_{c,i}}$ and $\beta_{A_{c,i}}$

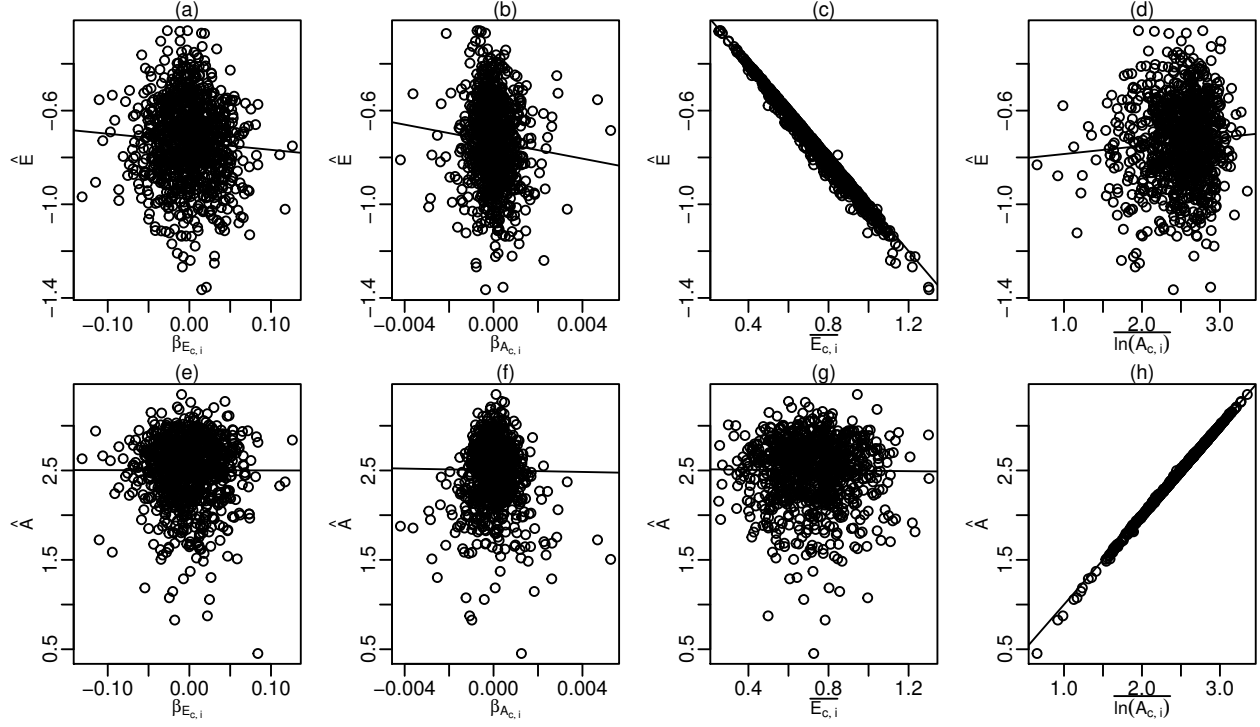


Figure 20: Scenario three - LMER approach: Influence of $\beta_{E_{c,i}}$, $\beta_{A_{c,i}}$, $\overline{E_{c,i}}$, and $\overline{\ln A_{c,i}}$ on \hat{E} and \hat{A} . Solid lines depict linear regression relations for all plot except (c) and (h) where a bisection line is plotted since identity relations are expected.

Table 34: Scenario three - lmer approach: Best model for \hat{E}

	Estimate	Std. Error	t.value	Pr(> t)
(Intercept)	-0.018	0.015	-1.169	0.243
$\overline{\ln A_{c,i}}$	0.011	0.006	1.872	0.062
$\beta_{E_{c,i}}$	-0.180	0.015	-12.081	0.000
$\overline{E_{c,i}}$	-1.104	0.020	-54.495	0.000
$\overline{\ln A_{c,i}} : \overline{E_{c,i}}$	0.026	0.008	3.213	0.001

Table 35: Scenario three - lmer approach: Relative importance of best model parameters to explain \hat{E}

	Rel. Importance
$\overline{\ln A_{c,i}}$	0.004
$\beta_{E_{c,i}}$	0.002
$\overline{E_{c,i}}$	0.993
$\overline{\ln A_{c,i}} : \overline{E_{c,i}}$	0.000

Table 36: Scenario three - lmer approach: Best model for \hat{A}

	Estimate	Std. Error	t.value	Pr(> t)
(Intercept)	-0.014	0.011	-1.283	0.2
$\overline{\ln A_{c,i}}$	1.004	0.004	237.478	0.0
$\overline{\beta_{E_{c,i}}}$	-0.524	0.072	-7.280	0.0
$\overline{E_{c,i}}$	-0.054	0.014	-3.801	0.0
$\overline{\ln A_{c,i} : \beta_{E_{c,i}}}$	0.214	0.029	7.484	0.0
$\overline{\ln A_{c,i} : E_{c,i}}$	0.022	0.006	3.889	0.0

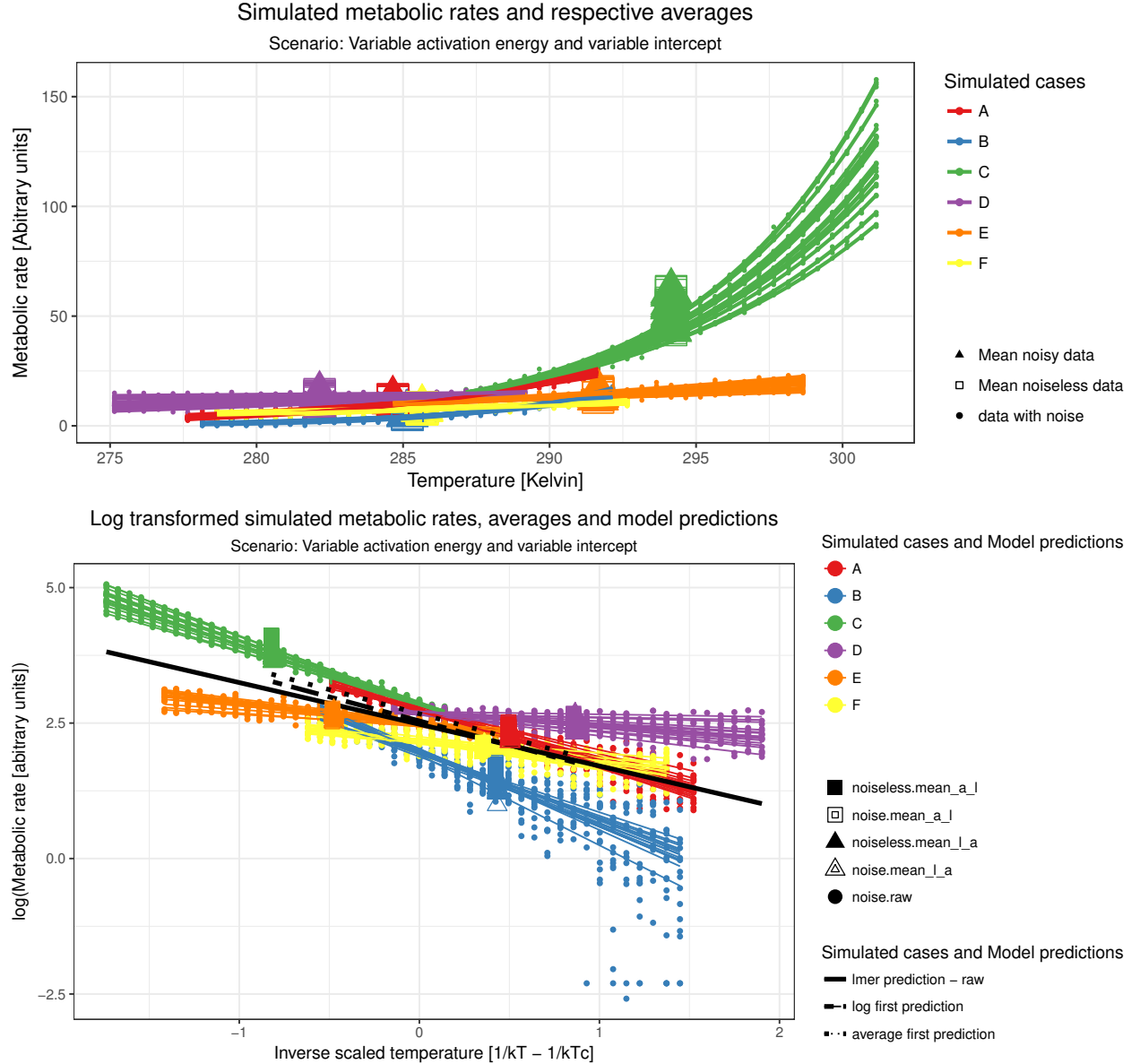
Table 37: Scenario three - lmer approach: Relative importance of best model parameters to explain \hat{A}

	Rel. Importance
$\overline{\ln A_{c,i}}$	1
$\overline{\beta_{E_{c,i}}}$	0
$\overline{E_{c,i}}$	0
$\overline{\ln A_{c,i} : \beta_{E_{c,i}}}$	0
$\overline{\ln A_{c,i} : E_{c,i}}$	0

6 Scenario four: All entities have variable absolute metabolic rates A_c and activation energies E_c

6.1 Description and assumptions of scenario four

In this scenario both A_c and E_c are assumed to vary randomly between the entities. Thus, both $\ln A_{c,i}$ and $E_{c,i}$ can by chance exhibit a correlation with \bar{T}_c (see figure 21). This scenario is likely the most realistic one. Since random variation is assumed for both parameters it is justified that in a regression approach we are interested in an average effect for both parameters. The assumptions in this scenario are identical to the ones made to analyse the mesocosm data.



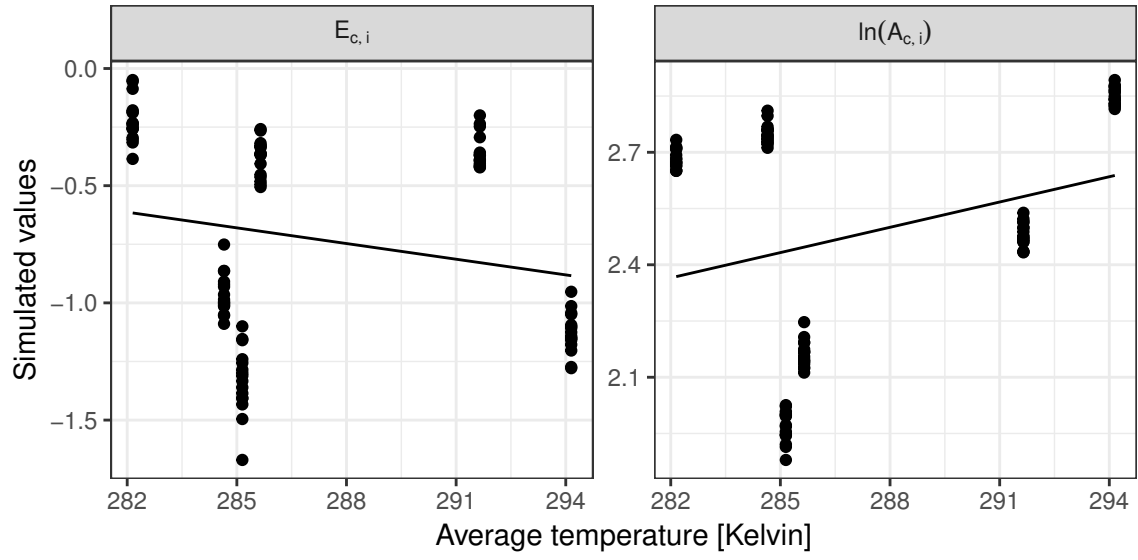


Figure 21: Scenario four: Regression of $\ln A_{c,i}$ and $E_{c,i}$ vs. $\overline{T_c}$

6.2 Summary results scenario four:

For both average based approaches \hat{E} are heavily influenced by $\beta_{A_{c,i}}$, which seems to be even more important than the value of $\overline{E_{c,i}}$ itself (see tables 39, 43 and figures 24, 25). In addition, \hat{E} by the average first approach is also influenced by $\beta_{E_{c,i}}$ (see table 43 and figure 25). Contrary \hat{E} estimated by the LMER approach is determined by $\overline{E_{c,i}}$ only (see table 47 and figure 26).

The estimates of \hat{A} based the two average based methods are mainly driven by $\overline{\ln A_{c,i}}$, but also by $\beta_{A_{c,i}}$ and for the log-first approach also by $\beta_{E_{c,i}}$ (see tables 41, 45 and figures 24, 25). \hat{A} estimated by LMER is almost exclusively determined by $\overline{\ln A_{c,i}}$ (see table 49 and figure 26). This results coincide with a by far smallest spread of $\ln A_{c,i} - \hat{A}$ and $\overline{E_{c,i}} - \hat{E}$ for the LMER approach (see figure 22). Also, only estimates of the LMER approach capture the density distributions of $\ln A_{c,i}$ and $\overline{E_{c,i}}$ (see figure 23). It is important to note that the average based approaches do not convey any “new” or “extra” information, which LMER does not capture but only seem to estimate $\overline{E_{c,i}}$ and $\overline{\ln A_{c,i}}$ very badly, most likely due to the heavy influence of $\beta_{A_{c,i}}$ and $\beta_{E_{c,i}}$.

6.3 Scenario four: Comparison between $\overline{E_{c,i}}$ and $\overline{\ln A_{c,i}}$ and \hat{E} and \hat{A} from the 3 different estimation approaches

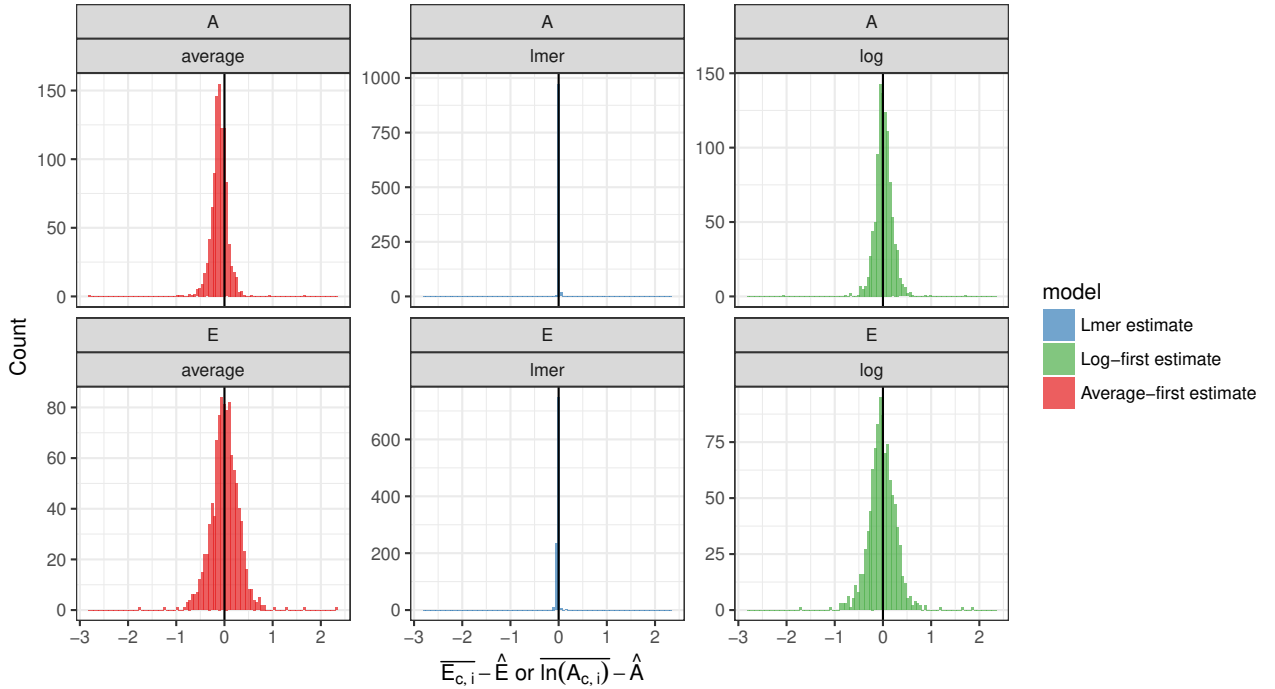


Figure 22: Scenario three: Comparison of $\overline{E_{c,i}} - \hat{E}$ and $\overline{\ln A_{c,i}} - \hat{A}$ for the 3 tested estimation approaches

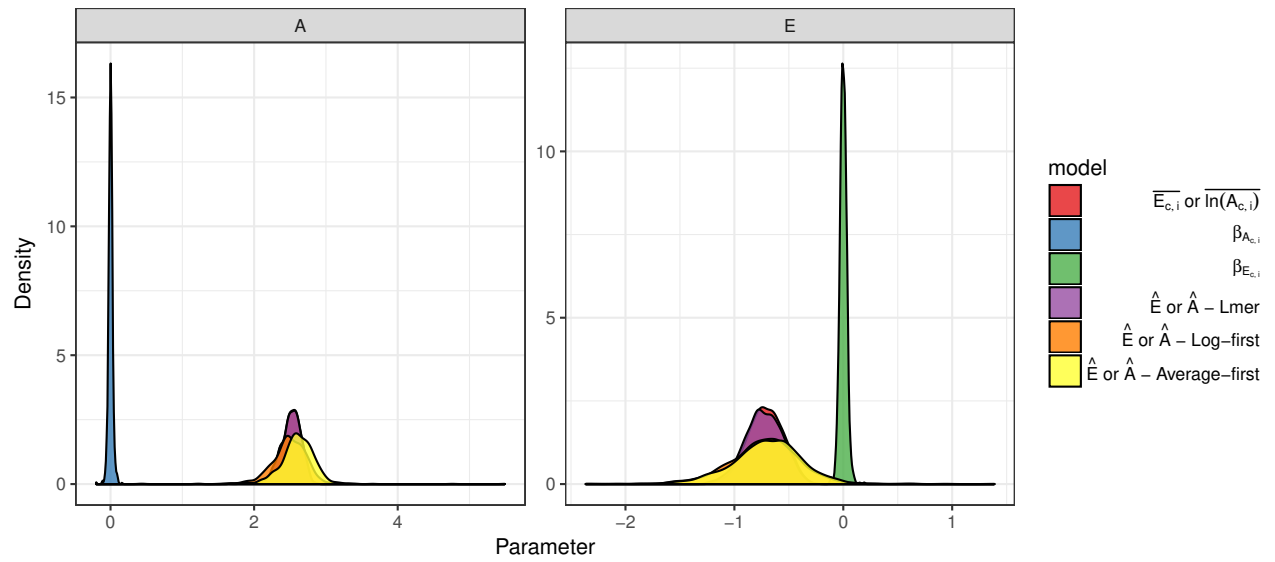


Figure 23: Scenario four: Comparison between simulated and estimated parameter

6.4 Scenario four: Detailed results on the influence of chance correlation of $\ln A_{c,i}$ $E_{c,i}$ with \bar{T}_c on the estimates of \hat{E} and \hat{A}

6.4.1 Log-first approach - Best model to explain \hat{E} and \hat{A} based on $\overline{E_{c,i}}$, $\overline{\ln A_{c,i}}$, $\beta_{E_{c,i}}$ and $\beta_{A_{c,i}}$

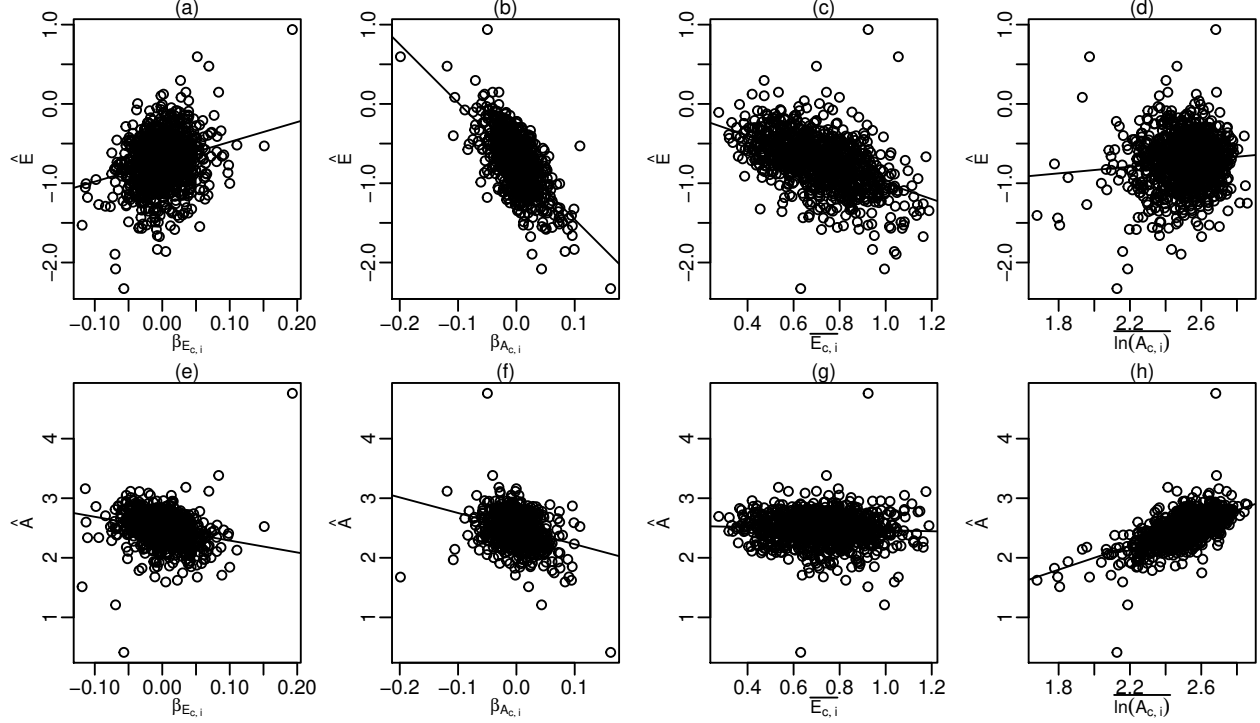


Figure 24: Scenario four - Log-first approach: Influence of $\beta_{E_{c,i}}$, $\beta_{A_{c,i}}$, $\overline{E_{c,i}}$, and $\overline{\ln A_{c,i}}$ on \hat{E} and \hat{A} . Solid lines depict linear regression relations for all plot except (c) and (h) where a bisection line is plotted since identity relations are expected.

Table 38: Scenario four - Log-first approach: Best model for \hat{E}

	Estimate	Std. Error	t.value	Pr(> t)
(Intercept)	0.841	0.435	1.933	0.054
$\overline{\ln A_{c,i}}$	-0.333	0.173	-1.930	0.054
$\beta_{A_{c,i}}$	-7.336	0.191	-38.460	0.000
$\beta_{E_{c,i}}$	-5.407	2.629	-2.057	0.040
$\overline{E_{c,i}}$	-2.320	0.582	-3.983	0.000
$\overline{\ln A_{c,i}} : \beta_{E_{c,i}}$	1.784	0.990	1.803	0.072
$\overline{\ln A_{c,i}} : \overline{E_{c,i}}$	0.517	0.231	2.237	0.026
$\beta_{E_{c,i}} : \overline{E_{c,i}}$	4.247	1.118	3.799	0.000

Table 39: Scenario four - Log-first approach: Relative importance of best model parameters to explain \hat{E}

	Rel. Importance
$\overline{\ln A_{c,i}}$	0.008
$\beta_{A_{c,i}}$	0.567

	Rel. Importance
$\frac{\beta_{E_{c,i}}}{E_{c,i}}$	0.079
$\frac{\overline{E_{c,i}}}{E_{c,i}}$	0.339
$\frac{\ln A_{c,i}}{\overline{E_{c,i}}} : \frac{\beta_{E_{c,i}}}{E_{c,i}}$	0.001
$\frac{\ln A_{c,i}}{\overline{E_{c,i}}} : \frac{\overline{E_{c,i}}}{E_{c,i}}$	0.001
$\frac{\beta_{E_{c,i}}}{E_{c,i}} : \frac{\overline{E_{c,i}}}{E_{c,i}}$	0.006

Table 40: Scenario four - Log-first approach: Best model for \hat{A}

	Estimate	Std. Error	t.value	Pr(> t)
(Intercept)	1.159	0.427	2.713	0.007
$\ln A_{c,i}$	0.548	0.170	3.230	0.001
$\beta_{A_{c,i}}$	-3.863	0.847	-4.560	0.000
$\frac{\beta_{E_{c,i}}}{E_{c,i}}$	-5.273	0.840	-6.279	0.000
$\frac{\overline{E_{c,i}}}{E_{c,i}}$	-1.920	0.572	-3.357	0.001
$\frac{\ln A_{c,i}}{\overline{E_{c,i}}} : \frac{\overline{E_{c,i}}}{E_{c,i}}$	0.743	0.227	3.271	0.001
$\beta_{A_{c,i}} : \frac{\overline{E_{c,i}}}{E_{c,i}}$	2.083	1.109	1.878	0.061
$\beta_{E_{c,i}} : \frac{\overline{E_{c,i}}}{E_{c,i}}$	4.049	1.101	3.677	0.000

Table 41: Scenario four - Log-first approach: Relative importance of best model parameters to explain \hat{A}

	Rel. Importance
$\ln A_{c,i}$	0.722
$\beta_{A_{c,i}}$	0.132
$\frac{\beta_{E_{c,i}}}{E_{c,i}}$	0.122
$\frac{\overline{E_{c,i}}}{E_{c,i}}$	0.004
$\frac{\ln A_{c,i}}{\overline{E_{c,i}}} : \frac{\overline{E_{c,i}}}{E_{c,i}}$	0.007
$\beta_{A_{c,i}} : \frac{\overline{E_{c,i}}}{E_{c,i}}$	0.003
$\beta_{E_{c,i}} : \frac{\overline{E_{c,i}}}{E_{c,i}}$	0.010

6.4.2 Average-first approach - Best model to explain \hat{E} and \hat{A} based on $\overline{E_{c,i}}$, $\overline{\ln A_{c,i}}$, $\beta_{E_{c,i}}$ and $\beta_{A_{c,i}}$

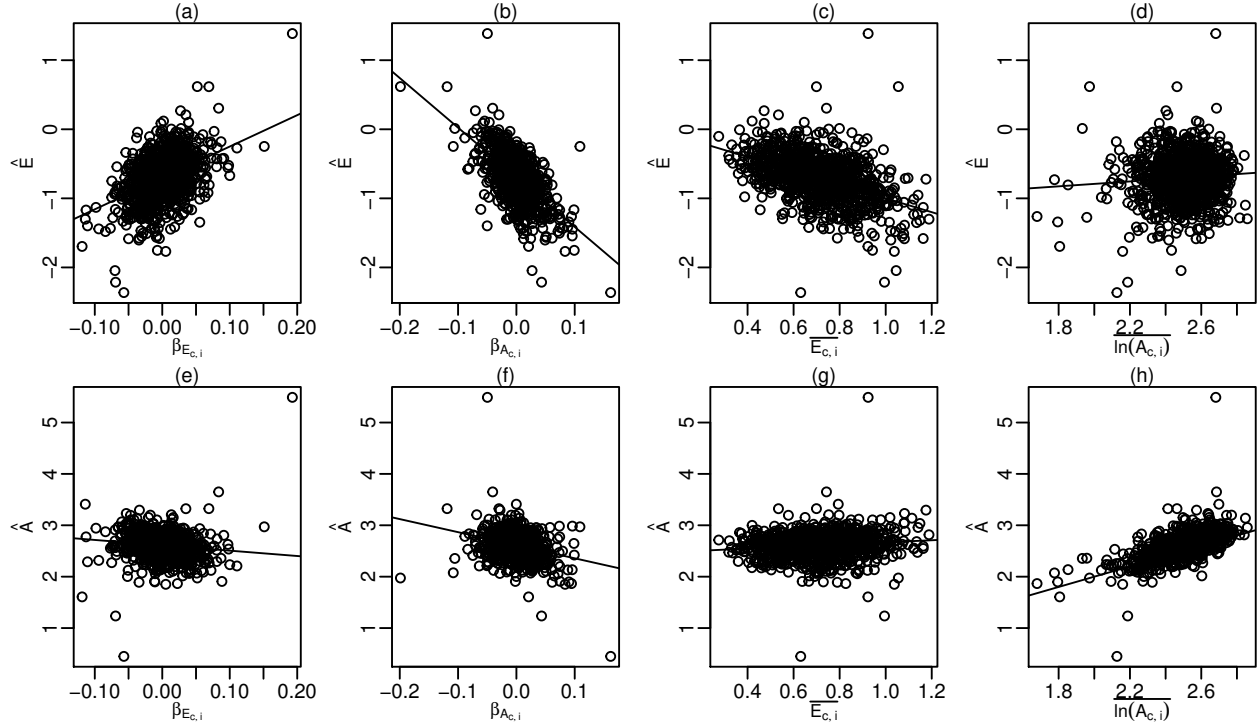


Figure 25: Scenario four - Average-first approach: Influence of $\beta_{E_{c,i}}$, $\beta_{A_{c,i}}$, $\overline{E_{c,i}}$, and $\overline{\ln A_{c,i}}$ on \hat{E} and \hat{A} . Solid lines depict linear regression relations for all plot except (c) and (h) where a bisection line is plotted since identity relations are expected.

Table 42: Scenario four - average-first approach: Best model for \hat{E}

	Estimate	Std. Error	t.value	Pr(> t)
(Intercept)	0.904	0.408	2.216	0.027
$\overline{\ln A_{c,i}}$	-0.364	0.162	-2.248	0.025
$\beta_{A_{c,i}}$	-7.033	0.179	-39.317	0.000
$\beta_{E_{c,i}}$	-4.712	2.466	-1.911	0.056
$\overline{E_{c,i}}$	-2.247	0.546	-4.113	0.000
$\overline{\ln A_{c,i}} : \beta_{E_{c,i}}$	1.922	0.928	2.070	0.039
$\overline{\ln A_{c,i}} : \overline{E_{c,i}}$	0.510	0.217	2.350	0.019
$\beta_{E_{c,i}} : \overline{E_{c,i}}$	5.608	1.048	5.348	0.000

Table 43: Scenario four - average-first approach: Relative importance of best model parameters to explain \hat{E}

	Rel. Importance
$\overline{\ln A_{c,i}}$	0.004
$\beta_{A_{c,i}}$	0.474
$\beta_{E_{c,i}}$	0.240
$\overline{E_{c,i}}$	0.271

	Rel. Importance
$\overline{\ln A_{c,i}} : \overline{\beta_{E_{c,i}}}$	0.001
$\overline{\ln A_{c,i}} : \overline{E_{c,i}}$	0.001
$\overline{\beta_{E_{c,i}}} : \overline{E_{c,i}}$	0.009

Table 44: Scenario four - average-first approach: Best model for \hat{A}

	Estimate	Std. Error	t.value	Pr(> t)
(Intercept)	1.158	0.449	2.581	0.010
$\overline{\ln A_{c,i}}$	0.516	0.178	2.896	0.004
$\beta_{A_{c,i}}$	-3.842	0.890	-4.318	0.000
$\overline{\beta_{E_{c,i}}}$	-5.259	0.882	-5.962	0.000
$\overline{E_{c,i}}$	-1.596	0.601	-2.656	0.008
$\overline{\ln A_{c,i}} : \overline{E_{c,i}}$	0.727	0.239	3.048	0.002
$\beta_{A_{c,i}} : \overline{E_{c,i}}$	2.262	1.165	1.942	0.052
$\overline{\beta_{E_{c,i}}} : \overline{E_{c,i}}$	5.285	1.157	4.570	0.000

Table 45: Scenario four - average-first approach: Relative importance of best model parameters to explain \hat{A}

	Rel. Importance
$\overline{\ln A_{c,i}}$	0.754
$\beta_{A_{c,i}}$	0.136
$\overline{\beta_{E_{c,i}}}$	0.043
$\overline{E_{c,i}}$	0.037
$\overline{\ln A_{c,i}} : \overline{E_{c,i}}$	0.008
$\beta_{A_{c,i}} : \overline{E_{c,i}}$	0.004
$\overline{\beta_{E_{c,i}}} : \overline{E_{c,i}}$	0.019

6.4.3 LMER approach - Best model to explain \hat{E} and \hat{A} based on $\overline{E_{c,i}}$, $\overline{\ln A_{c,i}}$, $\beta_{E_{c,i}}$ and $\beta_{A_{c,i}}$

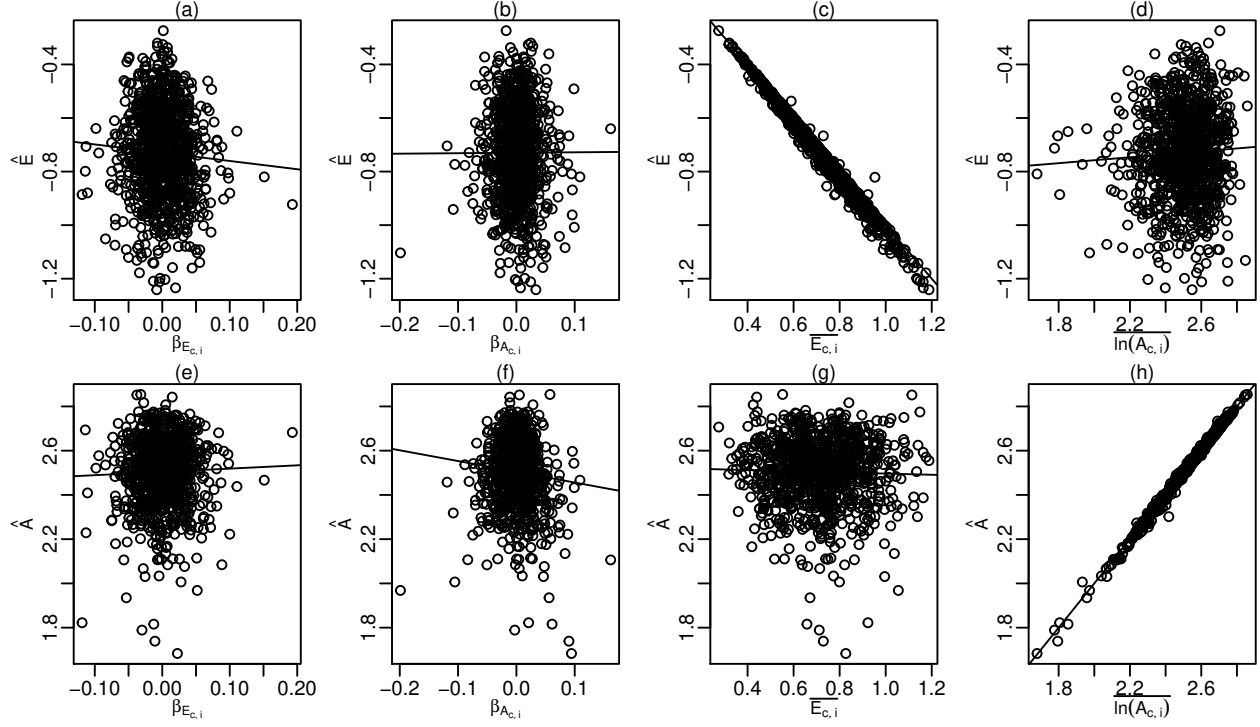


Figure 26: Scenario four - LMER approach: Influence of $\beta_{E_{c,i}}$, $\beta_{A_{c,i}}$, $\overline{E_{c,i}}$, and $\overline{\ln A_{c,i}}$ on \hat{E} and \hat{A} . Solid lines depict linear regression relations for all plot except (c) and (h) where a bisection line is plotted since identity relations are expected.

Table 46: Scenario four - lmer approach: Best model for \hat{E}

	Estimate	Std. Error	t.value	Pr(> t)
(Intercept)	-0.038	0.010	-3.933	0.000
$\overline{\ln A_{c,i}}$	0.020	0.004	5.360	0.000
$\beta_{A_{c,i}}$	1.211	0.261	4.641	0.000
$\beta_{E_{c,i}}$	-0.761	0.249	-3.055	0.002
$\overline{E_{c,i}}$	-1.041	0.003	-311.565	0.000
$\overline{\ln A_{c,i}} : \beta_{A_{c,i}}$	-0.464	0.093	-5.004	0.000
$\overline{\ln A_{c,i}} : \beta_{E_{c,i}}$	0.224	0.100	2.249	0.025
$\beta_{A_{c,i}} : \overline{E_{c,i}}$	-0.265	0.116	-2.279	0.023

Table 47: Scenario four - lmer approach: Relative importance of best model parameters to explain \hat{E}

	Rel. Importance
$\overline{\ln A_{c,i}}$	0.001
$\beta_{A_{c,i}}$	0.000
$\beta_{E_{c,i}}$	0.002
$\overline{E_{c,i}}$	0.996
$\overline{\ln A_{c,i}} : \beta_{A_{c,i}}$	0.000

	Rel. Importance
$\overline{\ln A_{c,i}} : \beta_{E_{c,i}}$	0.000
$\beta_{A_{c,i}} : \overline{E_{c,i}}$	0.000

Table 48: Scenario four - lmer approach: Best model for \hat{A}

	Estimate	Std. Error	t.value	Pr(> t)
(Intercept)	-0.042	0.005	-8.072	0.000
$\overline{\ln A_{c,i}}$	1.015	0.002	509.080	0.000
$\beta_{A_{c,i}}$	-0.735	0.118	-6.231	0.000
$\beta_{E_{c,i}}$	-0.355	0.136	-2.599	0.009
$\overline{E_{c,i}}$	0.005	0.002	2.510	0.012
$\overline{\ln A_{c,i}} : \beta_{A_{c,i}}$	0.288	0.049	5.880	0.000
$\overline{\ln A_{c,i}} : \beta_{E_{c,i}}$	0.154	0.055	2.815	0.005

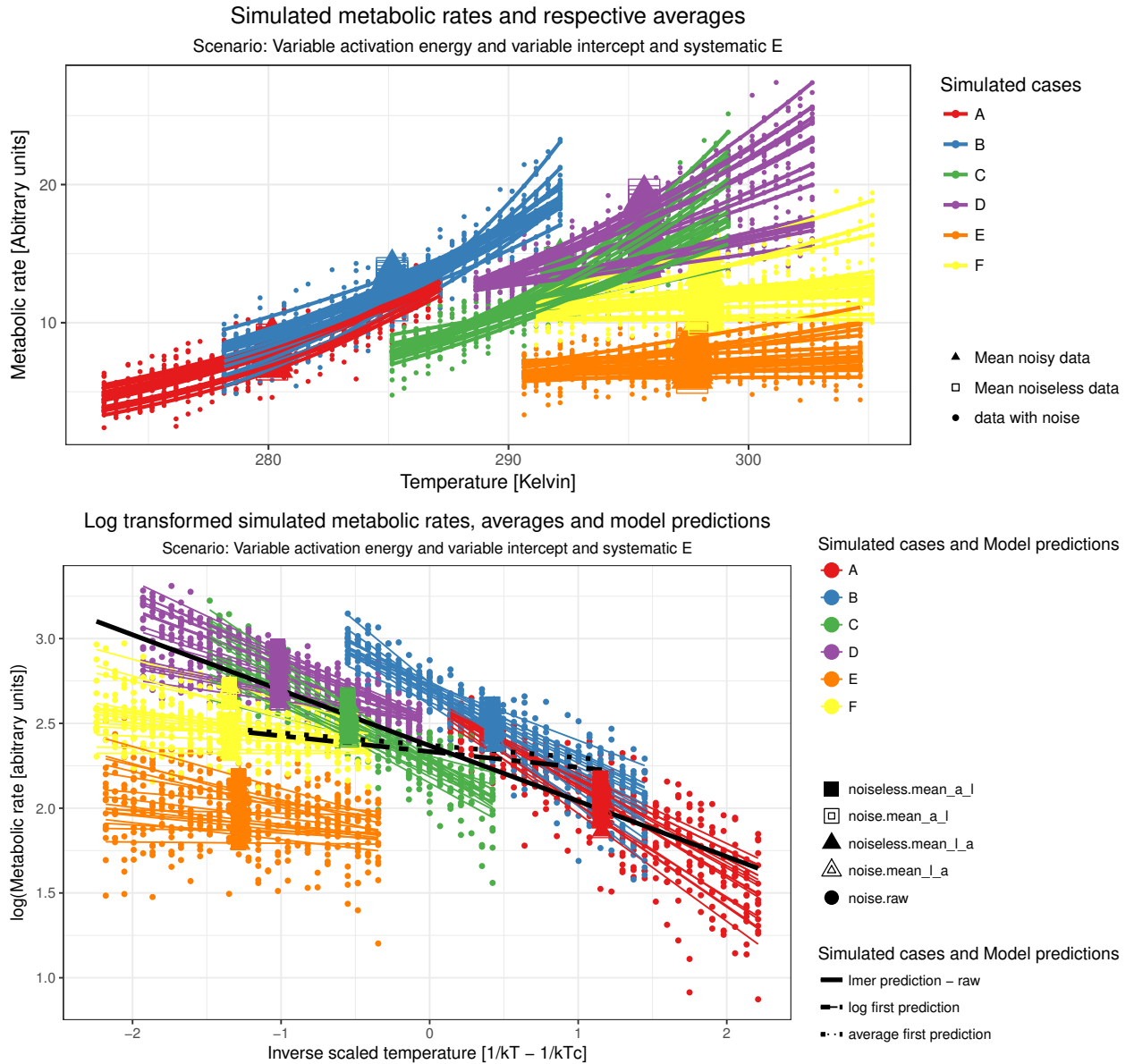
Table 49: Scenario four - lmer approach: Relative importance of best model parameters to explain \hat{A}

	Rel. Importance
$\overline{\ln A_{c,i}}$	0.995
$\beta_{A_{c,i}}$	0.004
$\beta_{E_{c,i}}$	0.000
$\overline{E_{c,i}}$	0.000
$\overline{\ln A_{c,i}} : \beta_{A_{c,i}}$	0.000
$\overline{\ln A_{c,i}} : \beta_{E_{c,i}}$	0.000

7 Scenario five: All entities are allowed to have variable E_c and A_c . Where E_c are negatively correlated with \bar{T}_c

7.1 Description and assumptions of scenario five

In this scenario entities have random variation in A_c , while E_c , even so first randomly drawn, are sorted such that they decrease with increasing \bar{T}_c (see figure 27). Since random variation is only assumed for parameter A , but E changes systematical, it seems questionable if a average response of \hat{E} over the temperature gradient is of any core interest. Rather, if such a systematic decrease of E_c with \bar{T}_c is hypothesized entities of the higher temperature ranges stand for future systems, while the ones from colder temperature ranges stand for contemporary ones. Thus, the focus of interest would be to qualify and quantify the systematic change, i.e. $\hat{E}_c \sim \bar{T}_c$. Still, the question is if either LMER or average based approaches are able to capture meaning full information about such a systematic change and if the average based approaches can capture any of the dynamics which the LMER approach could not?



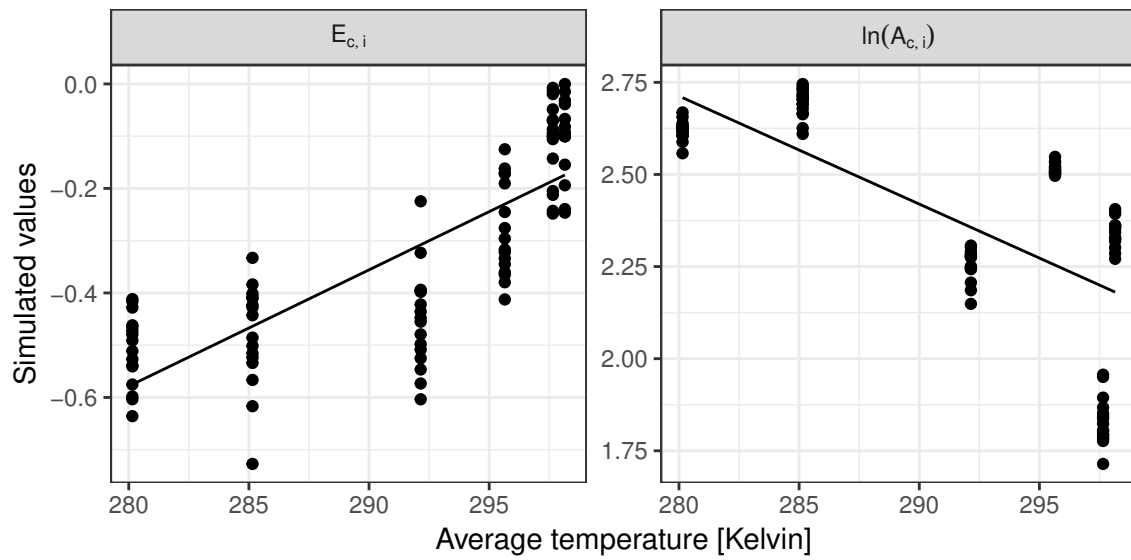


Figure 27: Scenario five: Regression of $\ln A_{c,i}$ and $E_{c,i}$ vs. $\overline{T_c}$

7.2 Summary results scenario five:

The estimates of \hat{A} based on the LMER approach are almost exclusively determined by $\overline{\ln A_{c,i}}$ (see table 61 and figure 32). The estimates of \hat{E} are solely determined by $\overline{E_{c,i}}$ (see table 59 and figure 32).

On the other hand, \hat{E} estimated by the average approaches is largely influenced by $\beta_{A_{c,i}}$, i.e. the chance increases of $\ln A_{c,i}$ with \bar{T}_c and to a much smaller extent by $\overline{E_{c,i}}$ or $\beta_{E_{c,i}}$ the systematic increase of $\overline{E_{c,i}}$ with \bar{T}_c (see tables 51 55 and figures 30, 31). \hat{A} estimated by the average approaches is dominantly determined by $\overline{\ln A_{c,i}}$, still also the influence of $\beta_{A_{c,i}}$ is considerable (see tables 53 57 and figures 30, 31). These difference between the 3 approaches are reflected in a much larger spread in $\overline{E_{c,i}} - \hat{E}$ and $\overline{\ln A_{c,i}} - \hat{A}$ for the average based approaches compared to the LMER approach (see figure 28) and the inability of the average based approaches to reproduce the distribution of $\overline{\ln A_{c,i}}$ or $\overline{E_{c,i}}$ (see figure 29). It seems clear that the LMER approach reproduces $\overline{E_{c,i}}$ faithfully, however the estimated average does not reveal that there is a systematic decrease of E_c with increasing \bar{T}_c . It is arguable if $\overline{E_{c,i}}$ is of any interest, given that to understand changes in future temperature sensitivity of metabolic rates one would need to quantify the decrease in $\overline{E_{c,i}}$ with increasing \bar{T}_c . However, it is also clear that the average based approach are no alternative at all. The estimate \hat{E} mainly seem to mirror chance correlation of $\overline{\ln A_{c,i}}$ with \bar{T}_c and only to a very small extent $\overline{E_{c,i}}$ or even $\beta_{E_{c,i}}$.

7.3 Scenario five: Comparison between $\overline{E_{c,i}}$ and $\overline{\ln A_{c,i}}$ and \hat{E} and \hat{A} from the 3 different estimation approaches

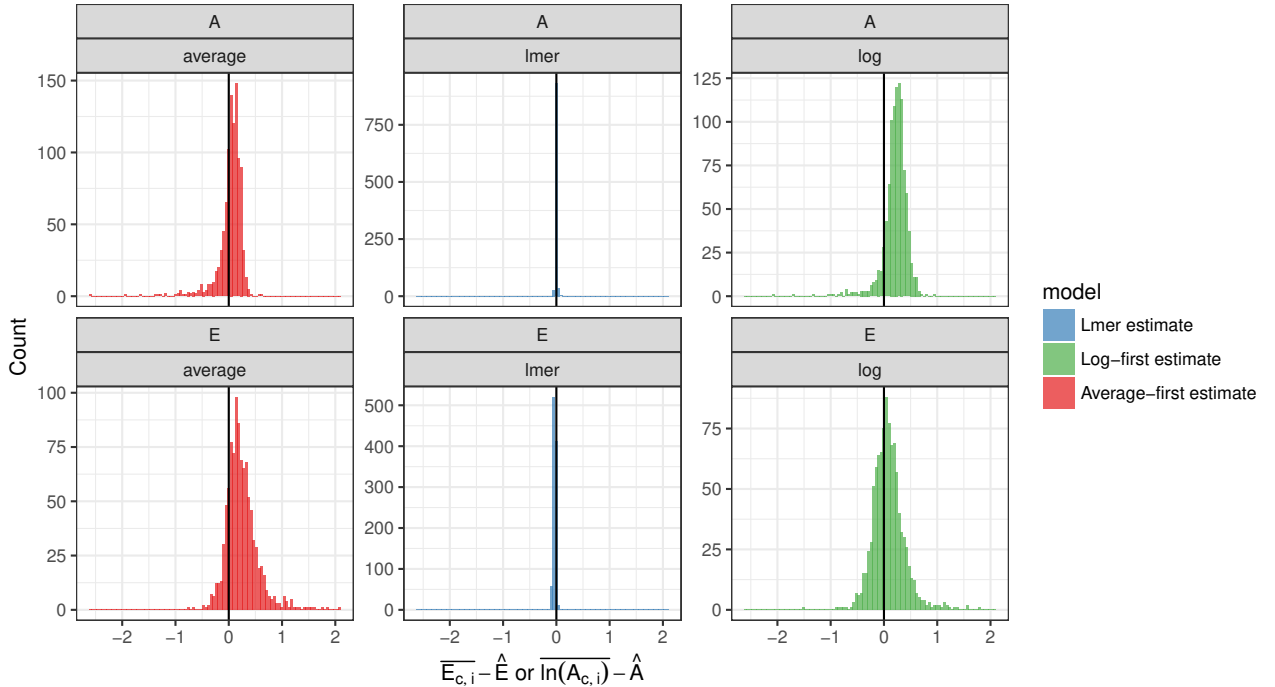


Figure 28: Scenario five: Comparison of $\overline{E_{c,i}} - \hat{E}$ and $\overline{\ln A_{c,i}} - \hat{A}$ for the 3 tested estimation approaches

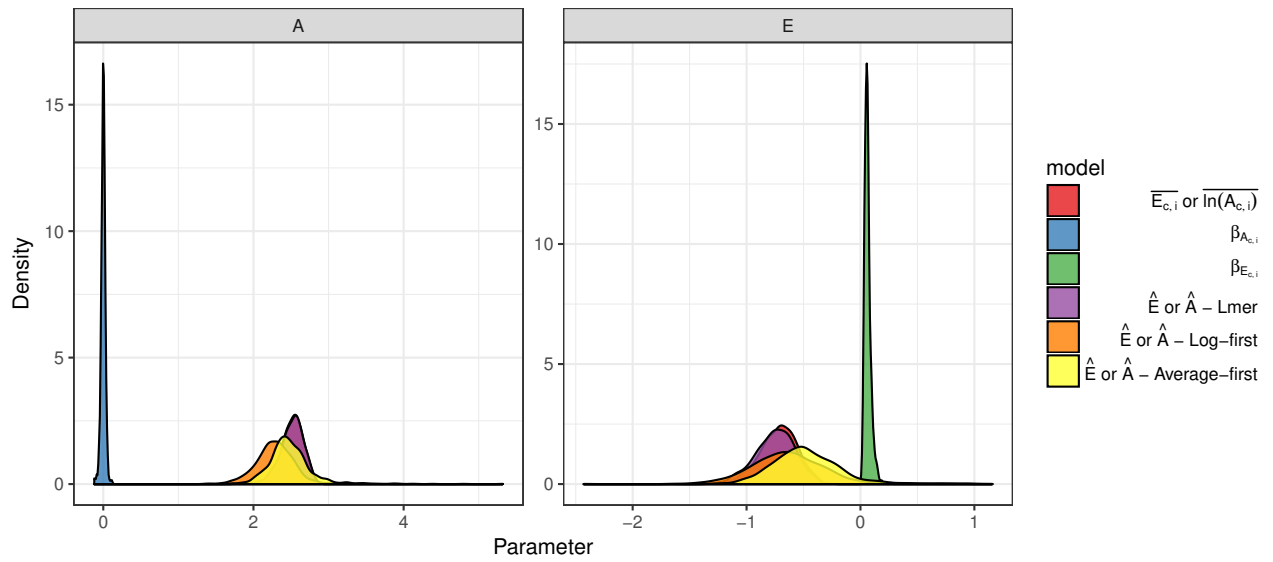


Figure 29: Scenario five: Comparison between simulated and estimated parameter

7.4 Scenario five: Detailed results on the influence of chance correlation of $\ln A_{c,i}$ $E_{c,i}$ with \bar{T}_c on the estimates of \hat{E} and \hat{A}

7.4.1 Log-first approach - Best model to explain \hat{E} and \hat{A} based on $\overline{E_{c,i}}$, $\overline{\ln A_{c,i}}$, $\beta_{E_{c,i}}$ and $\beta_{A_{c,i}}$

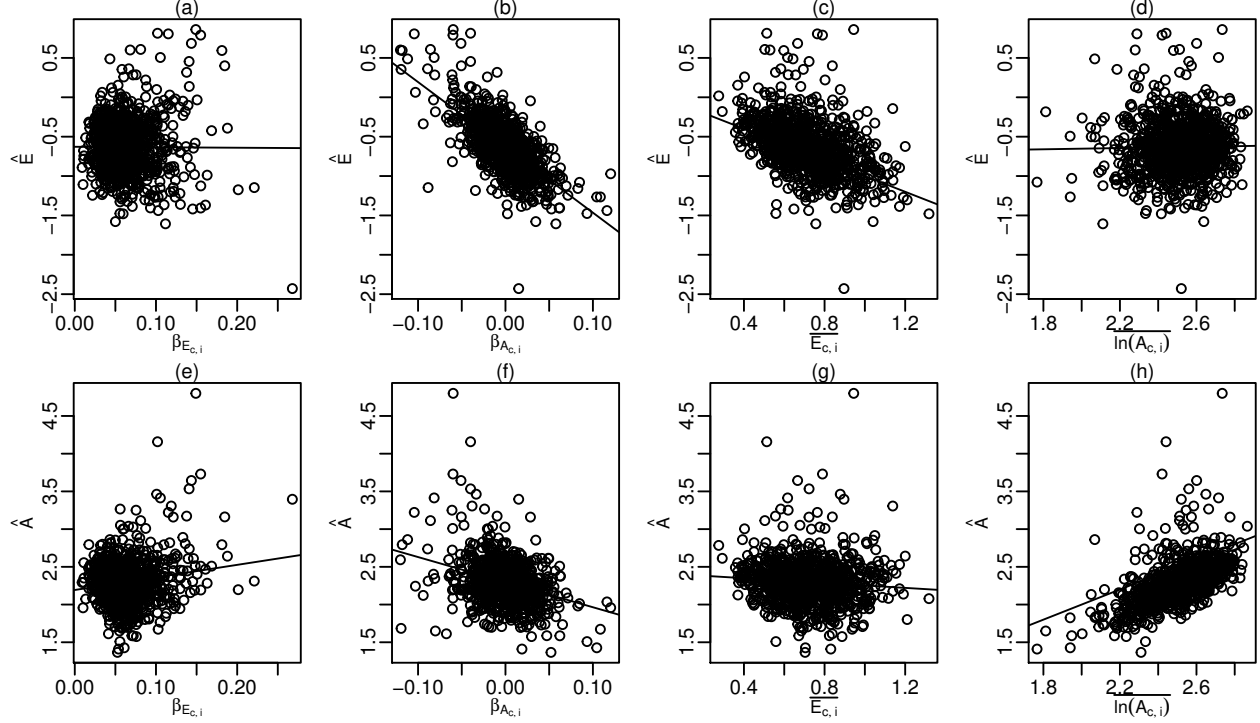


Figure 30: Scenario five - Log-first approach: Influence of $\beta_{E_{c,i}}$, $\beta_{A_{c,i}}$, $\overline{E_{c,i}}$, and $\overline{\ln A_{c,i}}$ on \hat{E} and \hat{A} . Solid lines depict linear regression relations for all plot except (c) and (h) where a bisection line is plotted since identity relations are expected.

Table 50: Scenario five - Log-first approach: Best model for \hat{E}

	Estimate	Std. Error	t.value	Pr(> t)
(Intercept)	0.537	0.272	1.971	0.049
$\overline{\ln A_{c,i}}$	-0.171	0.106	-1.619	0.106
$\beta_{A_{c,i}}$	-1.363	2.999	-0.454	0.650
$\beta_{E_{c,i}}$	-10.731	4.103	-2.615	0.009
$\overline{E_{c,i}}$	-1.088	0.092	-11.887	0.000
$\overline{\ln A_{c,i}} : \beta_{A_{c,i}}$	-2.329	1.246	-1.870	0.062
$\overline{\ln A_{c,i}} : \beta_{E_{c,i}}$	3.781	1.582	2.390	0.017
$\beta_{A_{c,i}} : \beta_{E_{c,i}}$	-15.593	6.241	-2.498	0.013
$\beta_{E_{c,i}} : \overline{E_{c,i}}$	2.469	1.356	1.820	0.069

Table 51: Scenario five - Log-first approach: Relative importance of best model parameters to explain \hat{E}

	Rel. Importance
$\overline{\ln A_{c,i}}$	0.001

	Rel. Importance
$\beta_{A_{c,i}}$	0.688
$\beta_{E_{c,i}}$	0.005
$\overline{E_{c,i}}$	0.297
$\ln A_{c,i} : \beta_{A_{c,i}}$	0.002
$\ln A_{c,i} : \beta_{E_{c,i}}$	0.002
$\beta_{A_{c,i}} : \overline{E_{c,i}}$	0.003
$\beta_{E_{c,i}} : \overline{E_{c,i}}$	0.001

Table 52: Scenario five - Log-first approach: Best model for \hat{A}

	Estimate	Std. Error	t.value	Pr(> t)
(Intercept)	1.350	0.544	2.483	0.013
$\ln A_{c,i}$	0.464	0.214	2.163	0.031
$\beta_{A_{c,i}}$	3.486	3.243	1.075	0.283
$\beta_{E_{c,i}}$	-1.207	1.143	-1.056	0.291
$\overline{E_{c,i}}$	-2.561	0.738	-3.470	0.001
$\ln A_{c,i} : \beta_{A_{c,i}}$	-2.057	1.349	-1.525	0.127
$\ln A_{c,i} : \overline{E_{c,i}}$	0.853	0.291	2.933	0.003
$\beta_{A_{c,i}} : \beta_{E_{c,i}}$	-25.528	6.661	-3.833	0.000
$\beta_{E_{c,i}} : \overline{E_{c,i}}$	3.403	1.467	2.319	0.021

Table 53: Scenario five - Log-first approach: Relative importance of best model parameters to explain \hat{A}

	Rel. Importance
$\ln A_{c,i}$	0.677
$\beta_{A_{c,i}}$	0.215
$\beta_{E_{c,i}}$	0.051
$\overline{E_{c,i}}$	0.022
$\ln A_{c,i} : \beta_{A_{c,i}}$	0.003
$\ln A_{c,i} : \overline{E_{c,i}}$	0.010
$\beta_{A_{c,i}} : \beta_{E_{c,i}}$	0.016
$\beta_{E_{c,i}} : \overline{E_{c,i}}$	0.005

7.4.2 Average-first approach - Best model to explain \hat{E} and \hat{A} based on $\overline{E_{c,i}}$, $\overline{\ln A_{c,i}}$, $\beta_{E_{c,i}}$ and $\beta_{A_{c,i}}$

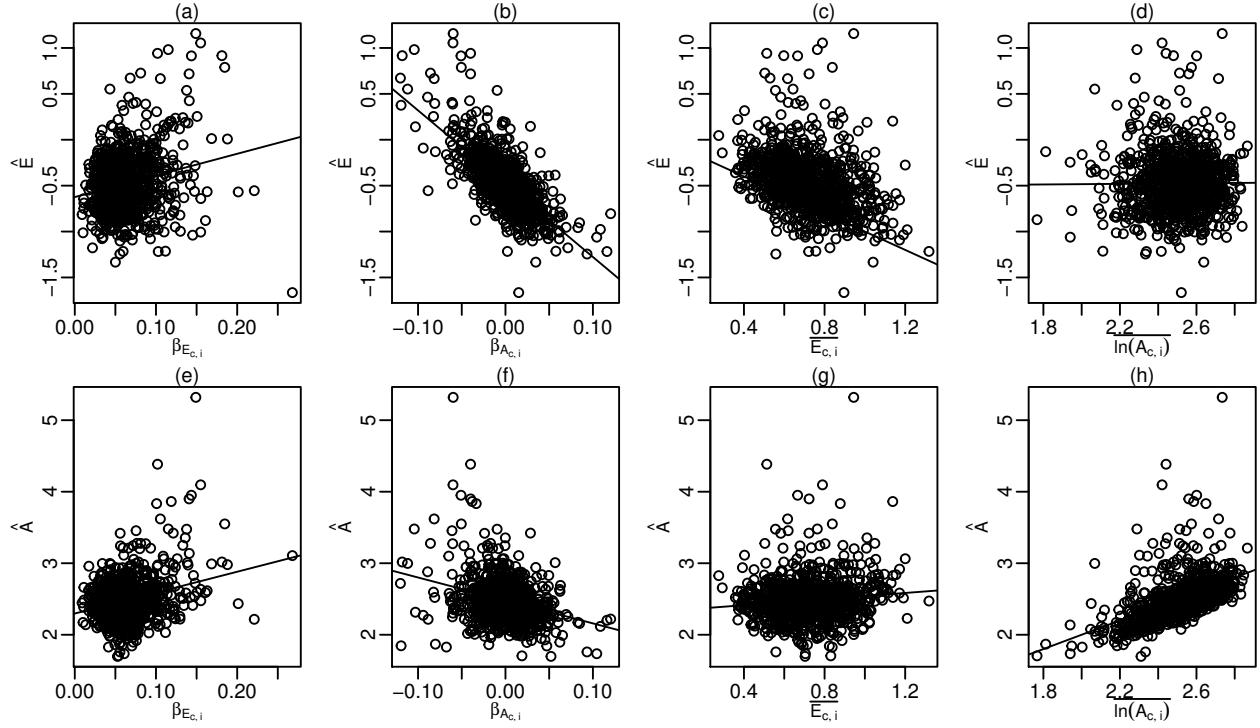


Figure 31: Scenario five - Average-first approach: Influence of $\beta_{E_{c,i}}$, $\beta_{A_{c,i}}$, $\overline{E_{c,i}}$, and $\overline{\ln A_{c,i}}$ on \hat{E} and \hat{A} . Solid lines depict linear regression relations for all plot except (c) and (h) where a bisection line is plotted since identity relations are expected.

Table 54: Scenario five - average-first approach: Best model for \hat{E}

	Estimate	Std. Error	t.value	Pr(> t)
(Intercept)	0.529	0.242	2.184	0.029
$\overline{\ln A_{c,i}}$	-0.190	0.094	-2.025	0.043
$\beta_{A_{c,i}}$	-0.036	2.668	-0.013	0.989
$\beta_{E_{c,i}}$	-8.534	3.650	-2.338	0.020
$\overline{E_{c,i}}$	-0.983	0.081	-12.080	0.000
$\overline{\ln A_{c,i}} : \beta_{A_{c,i}}$	-2.728	1.108	-2.462	0.014
$\overline{\ln A_{c,i}} : \beta_{E_{c,i}}$	3.427	1.408	2.435	0.015
$\beta_{A_{c,i}} : \beta_{E_{c,i}}$	-14.758	5.552	-2.658	0.008
$\beta_{E_{c,i}} : \overline{E_{c,i}}$	3.660	1.207	3.033	0.002

Table 55: Scenario five - average-first approach: Relative importance of best model parameters to explain \hat{E}

	Rel. Importance
$\overline{\ln A_{c,i}}$	0.000
$\beta_{A_{c,i}}$	0.707
$\beta_{E_{c,i}}$	0.081

	Rel. Importance
$\overline{E_{c,i}}$	0.201
$\overline{\ln A_{c,i}} : \beta_{A_{c,i}}$	0.003
$\overline{\ln A_{c,i}} : \beta_{E_{c,i}}$	0.002
$\beta_{A_{c,i}} : \overline{\beta_{E_{c,i}}}$	0.003
$\beta_{E_{c,i}} : \overline{E_{c,i}}$	0.004

Table 56: Scenario five - average-first approach: Best model for \hat{A}

	Estimate	Std. Error	t.value	Pr(> t)
(Intercept)	1.470	0.577	2.550	0.011
$\overline{\ln A_{c,i}}$	0.372	0.228	1.633	0.103
$\beta_{A_{c,i}}$	6.485	3.314	1.956	0.051
$\beta_{E_{c,i}}$	-10.350	4.647	-2.227	0.026
$\overline{E_{c,i}}$	-1.530	0.773	-1.980	0.048
$\overline{\ln A_{c,i}} : \beta_{A_{c,i}}$	-3.190	1.377	-2.316	0.021
$\overline{\ln A_{c,i}} : \beta_{E_{c,i}}$	3.917	1.789	2.189	0.029
$\overline{\ln A_{c,i}} : \overline{E_{c,i}}$	0.579	0.304	1.902	0.057
$\beta_{A_{c,i}} : \beta_{E_{c,i}}$	-27.692	6.902	-4.012	0.000
$\beta_{E_{c,i}} : \overline{E_{c,i}}$	3.461	1.499	2.309	0.021

Table 57: Scenario five - average-first approach: Relative importance of best model parameters to explain \hat{A}

	Rel. Importance
$\overline{\ln A_{c,i}}$	0.608
$\beta_{A_{c,i}}$	0.196
$\beta_{E_{c,i}}$	0.137
$\overline{E_{c,i}}$	0.019
$\overline{\ln A_{c,i}} : \beta_{A_{c,i}}$	0.007
$\overline{\ln A_{c,i}} : \beta_{E_{c,i}}$	0.005
$\overline{\ln A_{c,i}} : \overline{E_{c,i}}$	0.005
$\beta_{A_{c,i}} : \beta_{E_{c,i}}$	0.017
$\beta_{E_{c,i}} : \overline{E_{c,i}}$	0.005

7.4.3 LMER approach - Best model to explain \hat{E} and \hat{A} based on $\overline{E_{c,i}}$, $\overline{\ln A_{c,i}}$, $\beta_{E_{c,i}}$ and $\beta_{A_{c,i}}$

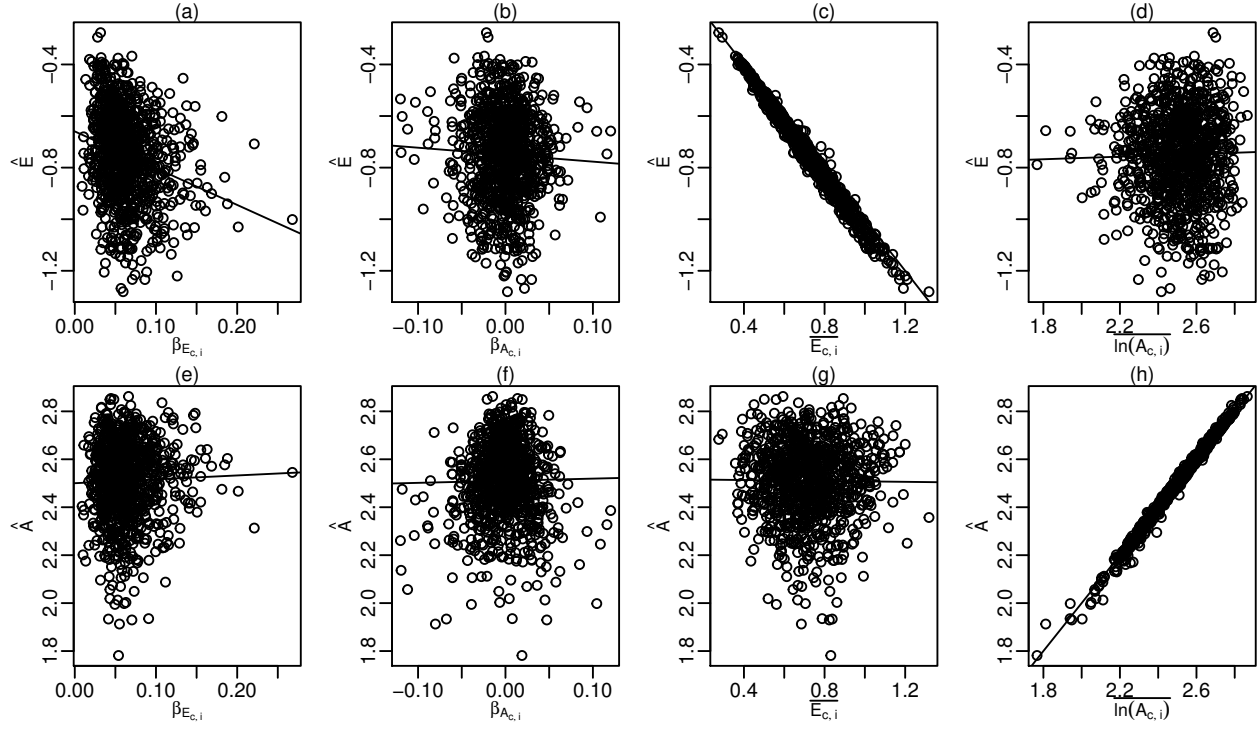


Figure 32: Scenario five - LMER approach: Influence of $\beta_{E_{c,i}}$, $\beta_{A_{c,i}}$, $\overline{E_{c,i}}$, and $\overline{\ln A_{c,i}}$ on \hat{E} and \hat{A} . Solid lines depict linear regression relations for all plot except (c) and (h) where a bisection line is plotted since identity relations are expected.

Table 58: Scenario five - lmer approach: Best model for \hat{E}

	Estimate	Std. Error	t.value	Pr(> t)
(Intercept)	-0.030	0.012	-2.564	0.010
$\overline{\ln A_{c,i}}$	0.013	0.004	2.996	0.003
$\beta_{A_{c,i}}$	1.660	0.350	4.735	0.000
$\beta_{E_{c,i}}$	0.041	0.025	1.663	0.097
$\overline{E_{c,i}}$	-1.053	0.004	-239.409	0.000
$\overline{\ln A_{c,i}} : \beta_{A_{c,i}}$	-0.811	0.138	-5.879	0.000
$\beta_{A_{c,i}} : \overline{E_{c,i}}$	0.274	0.169	1.625	0.104

Table 59: Scenario five - lmer approach: Relative importance of best model parameters to explain \hat{E}

	Rel. Importance
$\overline{\ln A_{c,i}}$	0.000
$\beta_{A_{c,i}}$	0.001
$\beta_{E_{c,i}}$	0.021
$\overline{E_{c,i}}$	0.976
$\overline{\ln A_{c,i}} : \beta_{A_{c,i}}$	0.001
$\beta_{A_{c,i}} : \overline{E_{c,i}}$	0.000

Table 60: Scenario five - lmer approach: Best model for \hat{A}

	Estimate	Std. Error	t.value	Pr(> t)
(Intercept)	-0.085	0.008	-10.261	0.000
$\overline{\ln A_{c,i}}$	1.030	0.003	376.800	0.000
$\beta_{A_{c,i}}$	-0.458	0.215	-2.132	0.033
$\beta_{\overline{E_{c,i}}}$	0.101	0.072	1.415	0.157
$\overline{E_{c,i}}$	0.018	0.006	2.909	0.004
$\overline{\ln A_{c,i} : \beta_{A_{c,i}}}$	0.236	0.084	2.788	0.005
$\beta_{A_{c,i} : \overline{E_{c,i}}}$	-0.250	0.103	-2.419	0.016
$\beta_{\overline{E_{c,i}} : \overline{E_{c,i}}}$	-0.240	0.092	-2.595	0.010

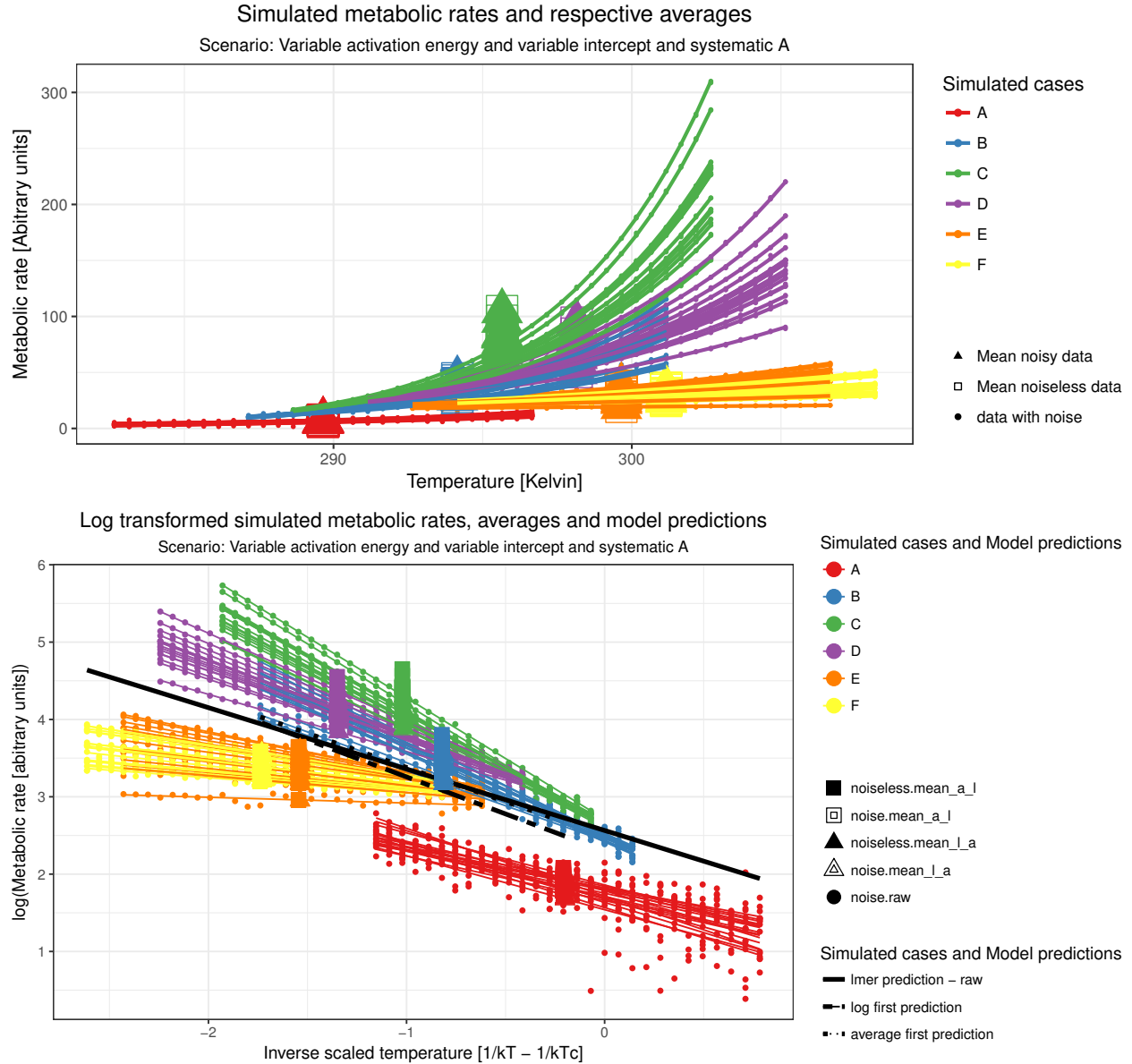
Table 61: Scenario five - lmer approach: Relative importance of best model parameters to explain \hat{A}

	Rel. Importance
$\overline{\ln A_{c,i}}$	0.999
$\beta_{A_{c,i}}$	0.000
$\beta_{\overline{E_{c,i}}}$	0.001
$\overline{E_{c,i}}$	0.000
$\overline{\ln A_{c,i} : \beta_{A_{c,i}}}$	0.000
$\beta_{A_{c,i} : \overline{E_{c,i}}}$	0.000
$\beta_{\overline{E_{c,i}} : \overline{E_{c,i}}}$	0.000

8 Scenario six: All entities have variable A_c and E_c . A_c 's systematically increase with increasing \bar{T}_c

8.1 Description and assumptions of scenario six

In this scenario A_c and E_c are both randomly drawn and thus are different for all entities. It is, however, assumed that the A_c systematically increases with \bar{T}_c , while E_c can only exhibit chance correlation with \bar{T}_c (see figure 33). Thus, while under this assumption the estimation of $\overline{E_{c,i}}$ is of interest, this is not necessarily the case for $\ln \overline{A_{c,i}}$. Rather in the light of a systematic temperature dependence of the absolute metabolic rates the qualification and quantification of $\beta_{A_{c,i}}$ would be of core interest.



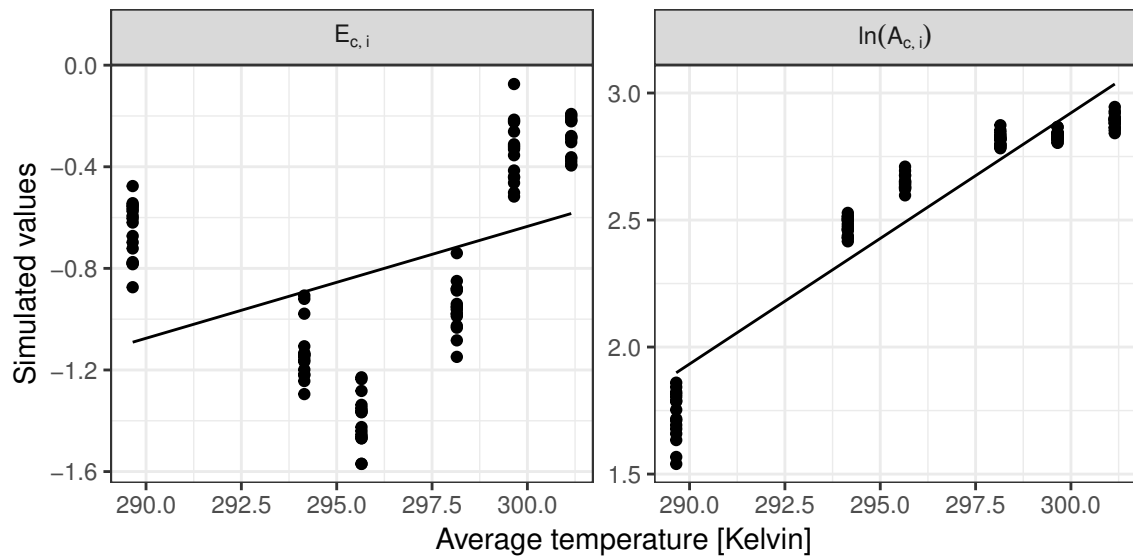


Figure 33: Scenario six: Regression of $\ln A_{c,i}$ and $E_{c,i}$ vs. $\overline{T_c}$

8.2 Summary results scenario six:

\hat{E} estimated by the LMER approach are almost exclusively determined by $\overline{E_{c,i}}$ (see table 71 and figure 38) and \hat{A} by $\overline{\ln A_{c,i}}$, yet to a smaller amount also by $\beta_{A_{c,i}}$ (see table 73 and figure 38). \hat{E} estimated by either of the average based approaches is mainly influenced by $\beta_{A_{c,i}}$ followed by $\overline{E_{c,i}}$ (see tables 63, 67 and figures 36, 37). The most important factors determining the estimates of \hat{A} based on either of the average based approaches are $\overline{\ln A_{c,i}}$ followed by $\beta_{A_{c,i}}$ (see tables 65, 69 and figures 36, 37).

The differences between simulated and average values of $\overline{\ln A_{c,i}} - \hat{A}$ and $\overline{E_{c,i}} - \hat{E}$ have a large variance for the average based approaches, which is in sharp contrast to the LMER approach with very little variance. In addition estimates of $\overline{E_{c,i}}$ by both average approaches seem on average substantially overestimated (see figure 34). This is in line with a considerable deviation of the density distribution of the simulated parameters compared to the estimated ones based on the average based approaches (see figure 35).

Thus, while the LMER approach estimates average values well, the estimates by the average based approaches are influenced by both the average parameter value but also by $\beta_{A_{c,i}}$, thus they neither reproduce the average nor the systematic changes in a systematic way.

8.3 Scenario six: Comparison between $\overline{E_{c,i}}$ and $\overline{\ln A_{c,i}}$ and \hat{E} and \hat{A} from the 3 different estimation approaches

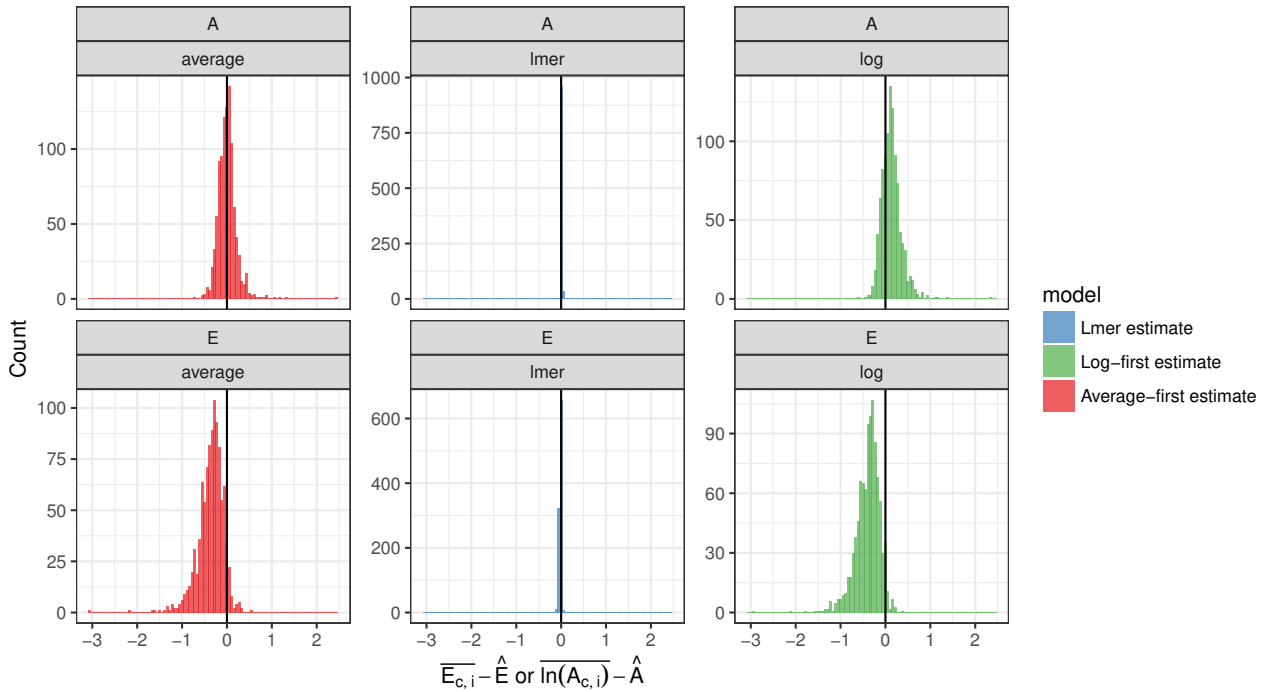


Figure 34: Scenario six: Comparison of $\overline{E_{c,i}} - \hat{E}$ and $\overline{\ln A_{c,i}} - \hat{A}$ for the 3 tested estimation approaches

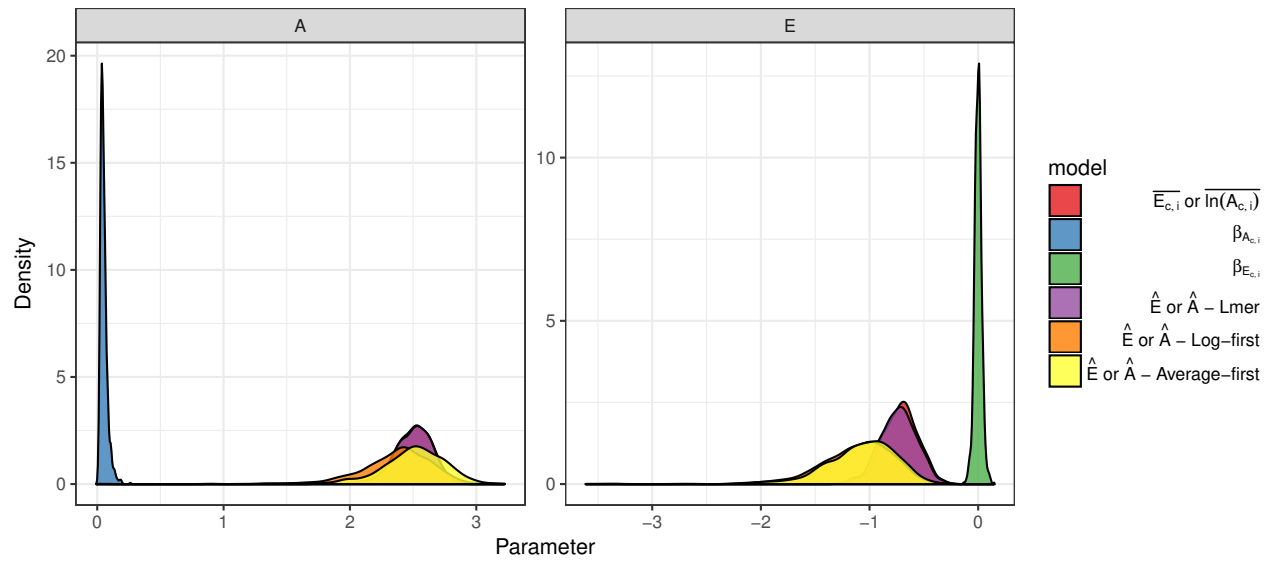


Figure 35: Scenario six: Comparison between simulated and estimated parameter

8.4 Scenario six: Detailed results on the influence of chance correlation of $\ln A_{c,i}$ $E_{c,i}$ with \bar{T}_c on the estimates of \hat{E} and \hat{A}

8.4.1 Log-first approach - Best model to explain \hat{E} and \hat{A} based on $\overline{E_{c,i}}$, $\overline{\ln A_{c,i}}$, $\beta_{E_{c,i}}$ and $\beta_{A_{c,i}}$

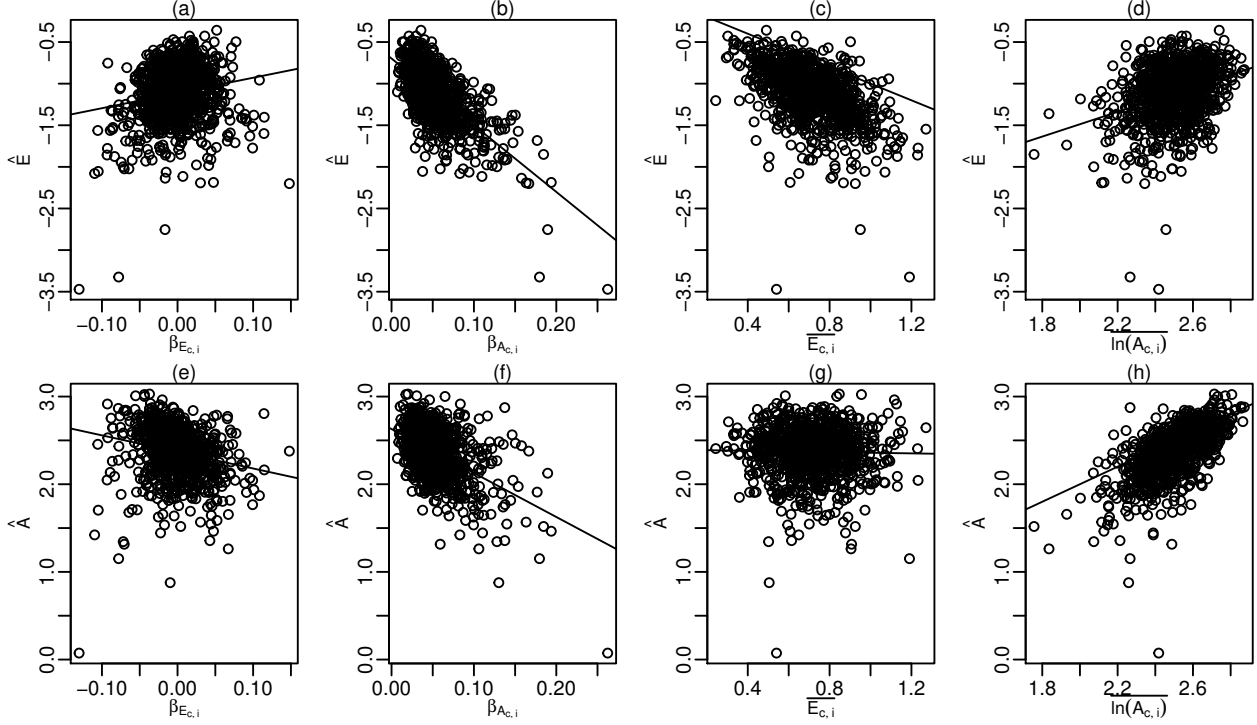


Figure 36: Scenario six - Log-first approach: Influence of $\beta_{E_{c,i}}$, $\beta_{A_{c,i}}$, $\overline{E_{c,i}}$, and $\overline{\ln A_{c,i}}$ on \hat{E} and \hat{A} . Solid lines depict linear regression relations for all plot except (c) and (h) where a bisection line is plotted since identity relations are expected.

Table 62: Scenario six - Log-first approach: Best model for \hat{E}

	Estimate	Std. Error	t.value	Pr(> t)
(Intercept)	-0.216	0.117	-1.841	0.066
$\overline{\ln A_{c,i}}$	0.086	0.044	1.974	0.049
$\beta_{A_{c,i}}$	-7.443	0.229	-32.504	0.000
$\beta_{E_{c,i}}$	1.062	0.326	3.255	0.001
$\overline{E_{c,i}}$	-1.017	0.035	-28.851	0.000
$\beta_{A_{c,i}} : \beta_{E_{c,i}}$	6.715	4.208	1.596	0.111

Table 63: Scenario six - Log-first approach: Relative importance of best model parameters to explain \hat{E}

	Rel. Importance
$\overline{\ln A_{c,i}}$	0.055
$\beta_{A_{c,i}}$	0.556
$\beta_{E_{c,i}}$	0.037
$\overline{E_{c,i}}$	0.351

Rel. Importance	
$\beta_{A_{c,i}} : \beta_{E_{c,i}}$	0.001

Table 64: Scenario six - Log-first approach: Best model for \hat{A}

	Estimate	Std. Error	t.value	Pr(> t)
(Intercept)	0.855	0.525	1.630	0.103
$\ln A_{c,i}$	0.705	0.199	3.538	0.000
$\beta_{A_{c,i}}$	-4.406	1.005	-4.383	0.000
$\beta_{E_{c,i}}$	-18.507	3.652	-5.067	0.000
$\overline{E_{c,i}}$	-1.443	0.726	-1.989	0.047
$\ln A_{c,i} : \beta_{E_{c,i}}$	4.470	1.371	3.261	0.001
$\ln A_{c,i} : \overline{E_{c,i}}$	0.502	0.276	1.823	0.069
$\beta_{A_{c,i}} : \beta_{E_{c,i}}$	56.063	4.932	11.367	0.000
$\beta_{A_{c,i}} : \overline{E_{c,i}}$	2.910	1.370	2.124	0.034
$\beta_{E_{c,i}} : \overline{E_{c,i}}$	2.020	1.072	1.884	0.060

Table 65: Scenario six - Log-first approach: Relative importance of best model parameters to explain \hat{A}

Rel. Importance	
$\ln A_{c,i}$	0.540
$\beta_{A_{c,i}}$	0.258
$\beta_{E_{c,i}}$	0.093
$\overline{E_{c,i}}$	0.001
$\ln A_{c,i} : \beta_{E_{c,i}}$	0.006
$\ln A_{c,i} : \overline{E_{c,i}}$	0.002
$\beta_{A_{c,i}} : \beta_{E_{c,i}}$	0.092
$\beta_{A_{c,i}} : \overline{E_{c,i}}$	0.006
$\beta_{E_{c,i}} : \overline{E_{c,i}}$	0.002

8.4.2 Average-first approach - Best model to explain \hat{E} and \hat{A} based on $\overline{E_{c,i}}$, $\overline{\ln A_{c,i}}$, $\beta_{E_{c,i}}$ and $\beta_{A_{c,i}}$

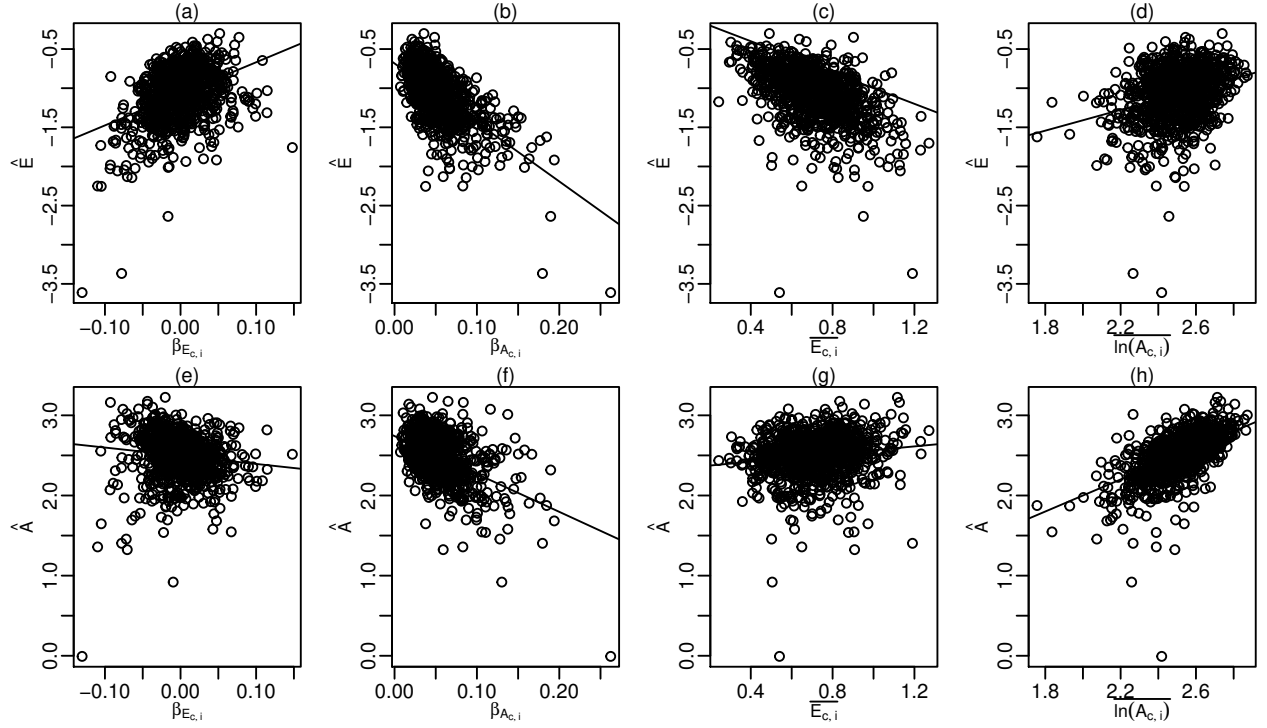


Figure 37: Scenario six - Average-first approach: Influence of $\beta_{E_{c,i}}$, $\beta_{A_{c,i}}$, $\overline{E_{c,i}}$, and $\overline{\ln A_{c,i}}$ on \hat{E} and \hat{A} . Solid lines depict linear regression relations for all plot except (c) and (h) where a bisection line is plotted since identity relations are expected.

Table 66: Scenario six - average-first approach: Best model for \hat{E}

	Estimate	Std. Error	t.value	Pr(> t)
(Intercept)	-0.027	0.025	-1.058	0.290
$\beta_{A_{c,i}}$	-7.111	0.189	-37.544	0.000
$\beta_{E_{c,i}}$	2.047	0.789	2.593	0.010
$\overline{E_{c,i}}$	-0.948	0.033	-28.861	0.000
$\beta_{A_{c,i}} : \beta_{E_{c,i}}$	6.319	3.895	1.622	0.105
$\beta_{E_{c,i}} : \overline{E_{c,i}}$	1.672	0.952	1.756	0.079

Table 67: Scenario six - average-first approach: Relative importance of best model parameters to explain \hat{E}

	Rel. Importance
$\beta_{A_{c,i}}$	0.502
$\beta_{E_{c,i}}$	0.195
$\overline{E_{c,i}}$	0.301
$\beta_{A_{c,i}} : \beta_{E_{c,i}}$	0.001
$\beta_{E_{c,i}} : \overline{E_{c,i}}$	0.001

Table 68: Scenario six - average-first approach: Best model for \hat{A}

	Estimate	Std. Error	t.value	Pr(> t)
(Intercept)	1.090	0.533	2.047	0.041
$\ln A_{c,i}$	0.586	0.202	2.896	0.004
$\beta_{A_{c,i}}$	-4.554	1.020	-4.464	0.000
$\beta_{E_{c,i}}$	-16.090	3.706	-4.341	0.000
$\overline{E_{c,i}}$	-1.376	0.737	-1.868	0.062
$\ln A_{c,i} : \beta_{E_{c,i}}$	3.806	1.391	2.737	0.006
$\ln A_{c,i} : \overline{E_{c,i}}$	0.580	0.280	2.075	0.038
$\beta_{A_{c,i}} : \beta_{E_{c,i}}$	52.194	5.005	10.429	0.000
$\beta_{A_{c,i}} : \overline{E_{c,i}}$	3.226	1.390	2.321	0.021
$\beta_{E_{c,i}} : \overline{E_{c,i}}$	2.533	1.088	2.329	0.020

Table 69: Scenario six - average-first approach: Relative importance of best model parameters to explain \hat{A}

	Rel. Importance
$\ln A_{c,i}$	0.550
$\beta_{A_{c,i}}$	0.264
$\beta_{E_{c,i}}$	0.034
$\overline{E_{c,i}}$	0.038
$\ln A_{c,i} : \beta_{E_{c,i}}$	0.006
$\ln A_{c,i} : \overline{E_{c,i}}$	0.003
$\beta_{A_{c,i}} : \beta_{E_{c,i}}$	0.093
$\beta_{A_{c,i}} : \overline{E_{c,i}}$	0.007
$\beta_{E_{c,i}} : \overline{E_{c,i}}$	0.004

8.4.3 LMER approach - Best model to explain \hat{E} and \hat{A} based on $\overline{E_{c,i}}$, $\overline{\ln A_{c,i}}$, $\beta_{E_{c,i}}$ and $\beta_{A_{c,i}}$

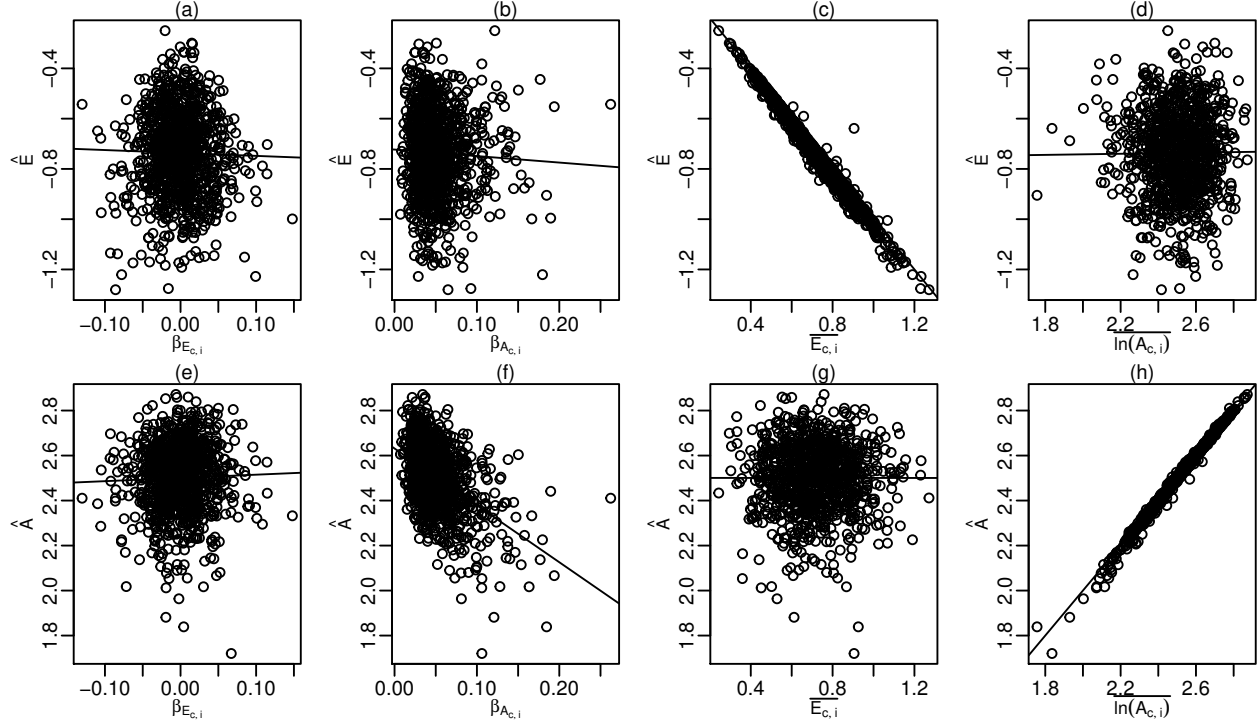


Figure 38: Scenario six - LMER approach: Influence of $\beta_{E_{c,i}}$, $\beta_{A_{c,i}}$, $\overline{E_{c,i}}$, and $\overline{\ln A_{c,i}}$ on \hat{E} and \hat{A} . Solid lines depict linear regression relations for all plot except (c) and (h) where a bisection line is plotted since identity relations are expected.

Table 70: Scenario six - lmer approach: Best model for \hat{E}

	Estimate	Std. Error	t.value	Pr(> t)
(Intercept)	-0.287	0.053	-5.444	0.000
$\overline{\ln A_{c,i}}$	0.115	0.021	5.471	0.000
$\beta_{A_{c,i}}$	1.647	0.300	5.486	0.000
$\beta_{E_{c,i}}$	0.885	0.416	2.129	0.033
$\overline{E_{c,i}}$	-0.839	0.071	-11.848	0.000
$\overline{\ln A_{c,i}} : \beta_{A_{c,i}}$	-0.657	0.124	-5.301	0.000
$\overline{\ln A_{c,i}} : \beta_{E_{c,i}}$	-0.522	0.156	-3.352	0.001
$\overline{\ln A_{c,i}} : \overline{E_{c,i}}$	-0.078	0.028	-2.749	0.006
$\beta_{A_{c,i}} : \beta_{E_{c,i}}$	1.025	0.551	1.860	0.063
$\beta_{E_{c,i}} : \overline{E_{c,i}}$	0.199	0.120	1.659	0.097

Table 71: Scenario six - lmer approach: Relative importance of best model parameters to explain \hat{E}

	Rel. Importance
$\overline{\ln A_{c,i}}$	0.000
$\beta_{A_{c,i}}$	0.001
$\beta_{E_{c,i}}$	0.001

	Rel. Importance
$\overline{E_{c,i}}$	0.997
$\ln A_{c,i} : \beta_{A_{c,i}}$	0.001
$\ln A_{c,i} : \beta_{E_{c,i}}$	0.000
$\ln A_{c,i} : \overline{E_{c,i}}$	0.000
$\beta_{A_{c,i}} : \beta_{E_{c,i}}$	0.000
$\beta_{E_{c,i}} : \overline{E_{c,i}}$	0.000

Table 72: Scenario six - lmer approach: Best model for \hat{A}

	Estimate	Std. Error	t.value	Pr(> t)
(Intercept)	-0.026	0.012	-2.099	0.036
$\ln A_{c,i}$	1.012	0.005	209.513	0.000
$\beta_{A_{c,i}}$	-0.642	0.166	-3.864	0.000
$\beta_{E_{c,i}}$	-0.851	0.195	-4.356	0.000
$\overline{E_{c,i}}$	-0.002	0.002	-1.077	0.282
$\ln A_{c,i} : \beta_{A_{c,i}}$	0.215	0.069	3.140	0.002
$\ln A_{c,i} : \beta_{E_{c,i}}$	0.388	0.076	5.090	0.000
$\beta_{E_{c,i}} : \overline{E_{c,i}}$	-0.185	0.067	-2.784	0.005

Table 73: Scenario six - lmer approach: Relative importance of best model parameters to explain \hat{A}

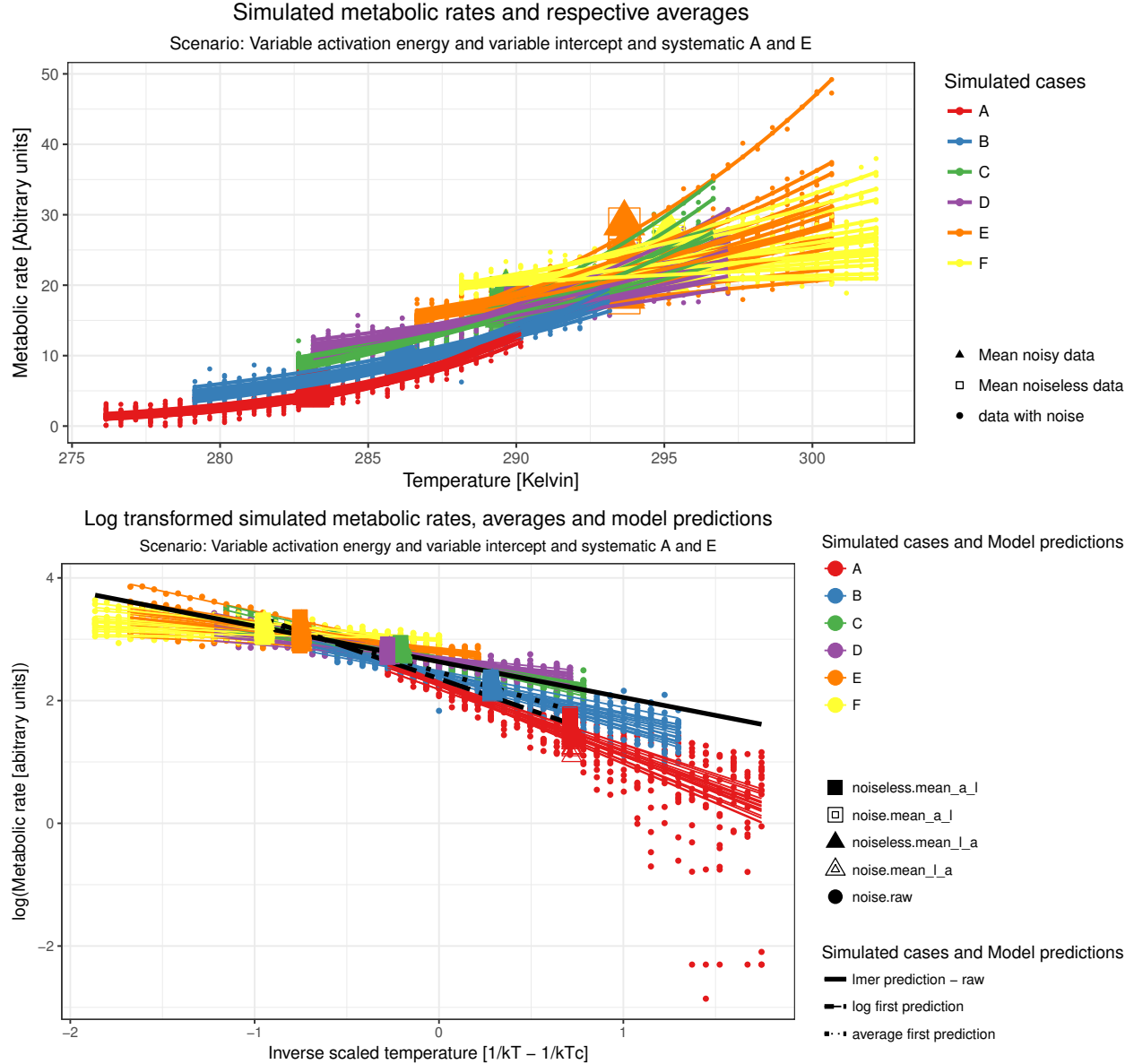
	Rel. Importance
$\ln A_{c,i}$	0.904
$\beta_{A_{c,i}}$	0.095
$\beta_{E_{c,i}}$	0.000
$\overline{E_{c,i}}$	0.000
$\ln A_{c,i} : \beta_{A_{c,i}}$	0.000
$\ln A_{c,i} : \beta_{E_{c,i}}$	0.000
$\beta_{E_{c,i}} : \overline{E_{c,i}}$	0.000

9 Scenario seven: All entities are allowed to have variable A_c and E_c which systematically increase respectively decrease with \bar{T}

9.1 Description and assumptions of scenario seven

In this scenario randomly drawn A_c and E_c are forced to systematically increase respectively decrease with increasing \bar{T}_c (see figure 39).

The temperature dependent changes in E_c and A_c raise the question if estimates of $\overline{\ln A_{c,i}}$ and $\overline{E_{c,i}}$ are of particular interest, or if rather the qualification and quantification of the increase of $E_c = \beta_{E_c} \cdot \bar{T}_c$ and $A_c = \beta_{A_c} \cdot \bar{T}_c$ are in the focus of interest particular under a climate change aspect.



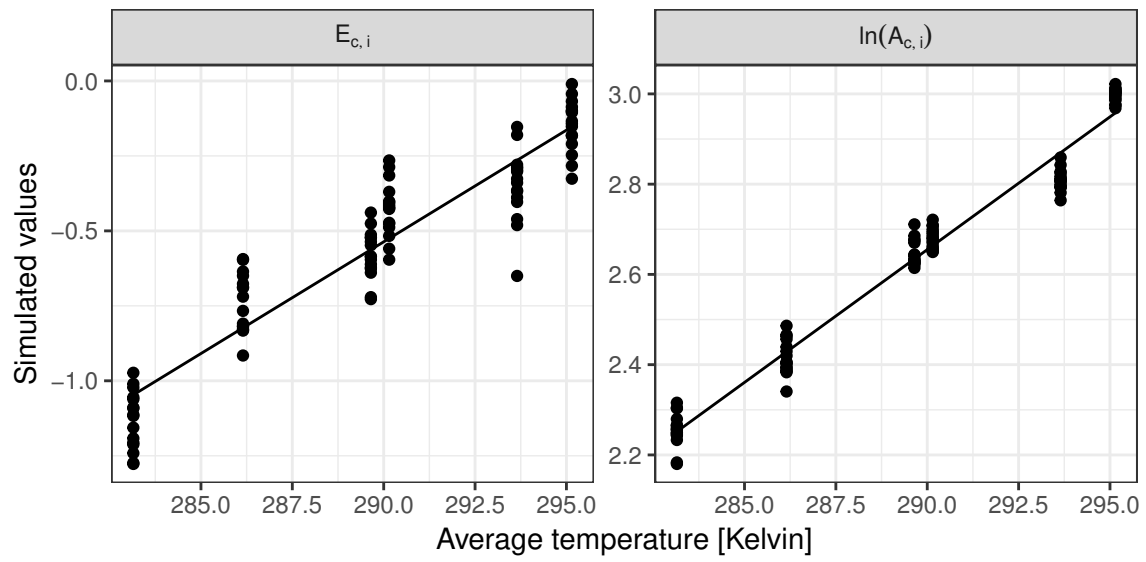


Figure 39: Scenario seven: Regression of $\ln A_{c,i}$ and $E_{c,i}$ vs. $\overline{T_c}$

9.2 Summary results scenario seven:

\hat{E} estimated by the LMER approach is predominately determined by $\overline{E_{c,i}}$, while the systematic increases of these averages, quantified in $\beta_{A_{c,i}}$ and $\beta_{E_{c,i}}$, only have very minor relevance (see table 83 and figure 44). Similar, \hat{A} estimated by the LMER approach is mainly determined by $\ln A_{c,i}$ and to a lesser extend also by $\beta_{A_{c,i}}$ (see table 85 and figure 44). Differences between simulated and estimated values, i.e. $\ln A_{c,i} - \hat{A}$ and $\overline{E_{c,i}} - \hat{E}$ are closely centered around zero (see figure 40) and estimated values resemble well the density distribution. \hat{E} , however, seems on average to be slightly overestimated (see figure 41). In comparison the estimates of \hat{E} is almost as much influenced by $\overline{E_{c,i}}$ than by $\beta_{A_{c,i}}$ this holds for both average approaches (see tables 75, 79 and figures 42, 43). \hat{A} estimated by the average approaches is determined by $\ln A_{c,i}$ followed by $\beta_{A_{c,i}}$ and for the average-first approach also $\beta_{E_{c,i}}$ (see tables 77, 77 and figures 42, 43). Both differences, $\ln A_{c,i} - \hat{A}$ and $\overline{E_{c,i}} - \hat{E}$, vary considerably for the average based approach. Both approaches tend to under estimate $\ln A_{c,i}$ but overestimate $\overline{E_{c,i}}$ considerably (see figures 40 and 41). In summary the LMER approach is the only one which reasonably produces average estimates and is rather insensitive to the systematic changes, on the other hand the average based approaches are sensitive to the systematic increases but are unable to quantify them in a useful way.

9.3 Scenario seven: Comparison between $\overline{E_{c,i}}$ and $\ln A_{c,i}$ and \hat{E} and \hat{A} from the 3 different estimation approaches

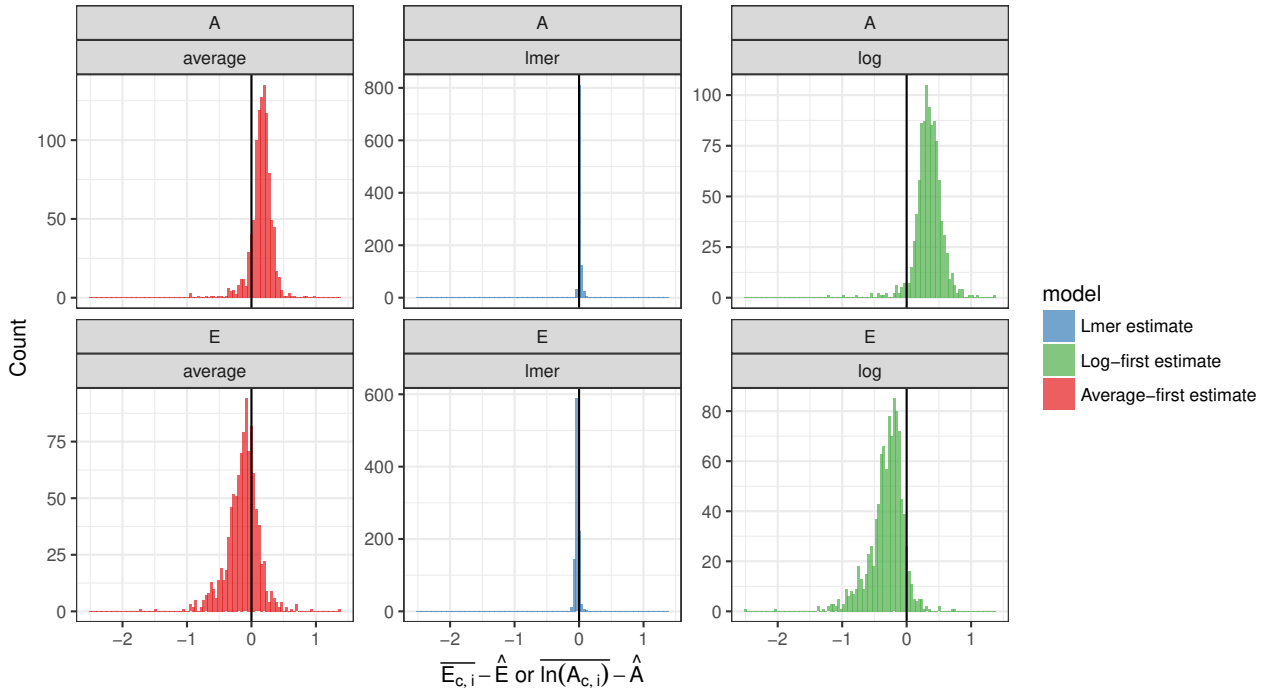


Figure 40: Scenario seven: Comparison of $\overline{E_{c,i}} - \hat{E}$ and $\ln A_{c,i} - \hat{A}$ for the 3 tested estimation approaches

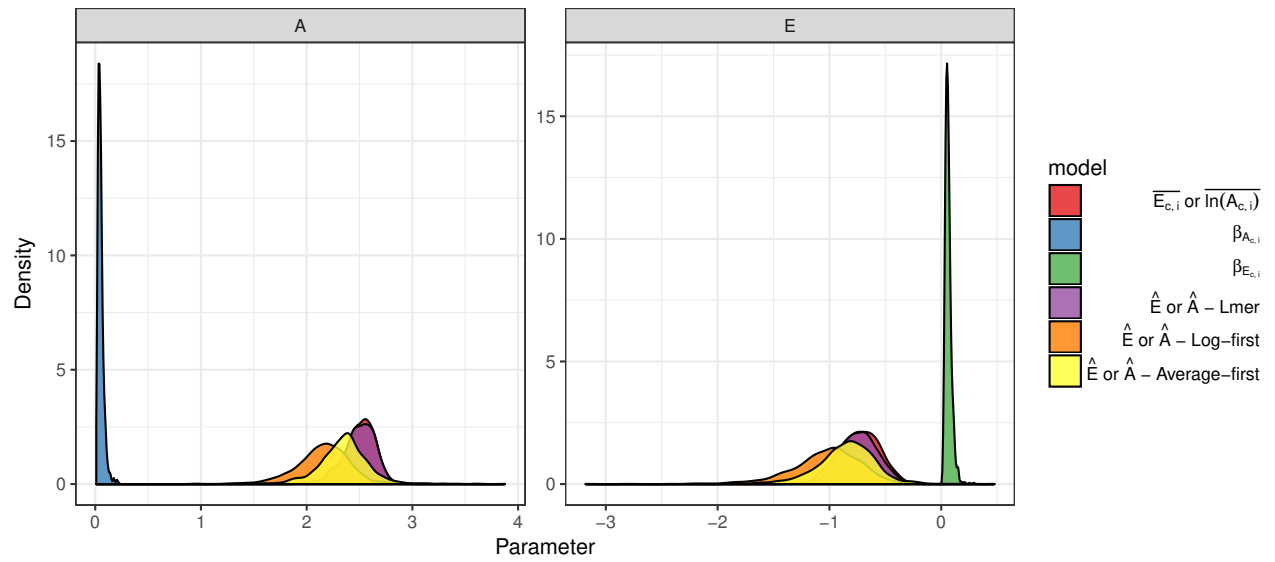


Figure 41: Scenario seven: Comparison between simulated and estimated parameter

9.4 Scenario seven: Detailed results on the influence of chance correlation of $\ln A_{c,i}$ $E_{c,i}$ with \bar{T}_c on the estimates of \hat{E} and \hat{A}

9.4.1 Log-first approach - Best model to explain \hat{E} and \hat{A} based on $\overline{E_{c,i}}$, $\overline{\ln A_{c,i}}$, $\beta_{E_{c,i}}$ and $\beta_{A_{c,i}}$

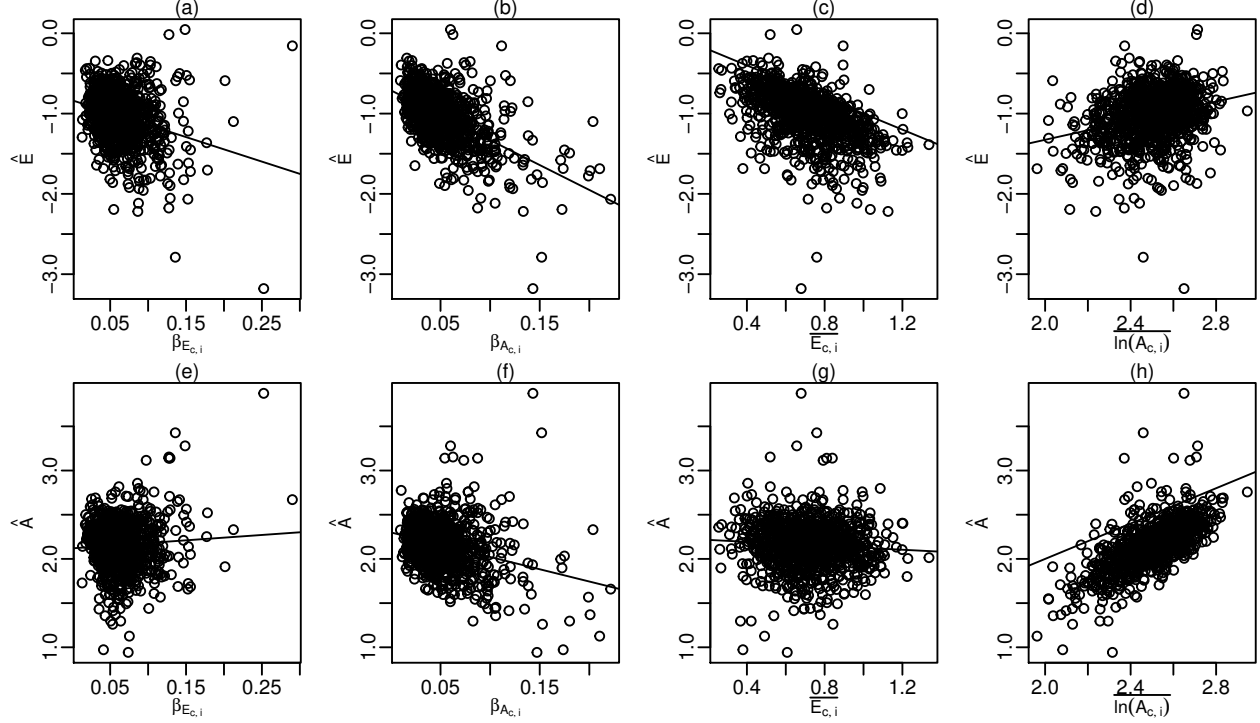


Figure 42: Scenario seven - Log-first approach: Influence of $\beta_{E_{c,i}}$, $\beta_{A_{c,i}}$, $\overline{E_{c,i}}$, and $\overline{\ln A_{c,i}}$ on \hat{E} and \hat{A} . Solid lines depict linear regression relations for all plot except (c) and (h) where a bisection line is plotted since identity relations are expected.

Table 74: Scenario seven - Log-first approach: Best model for \hat{E}

	Estimate	Std. Error	t.value	Pr(> t)
(Intercept)	-0.706	0.283	-2.496	0.013
$\overline{\ln A_{c,i}}$	0.299	0.108	2.761	0.006
$\beta_{A_{c,i}}$	-8.150	0.530	-15.365	0.000
$\beta_{E_{c,i}}$	12.958	3.789	3.420	0.001
$\overline{E_{c,i}}$	-0.987	0.040	-24.895	0.000
$\overline{\ln A_{c,i}} : \beta_{E_{c,i}}$	-5.170	1.471	-3.515	0.000
$\beta_{A_{c,i}} : \beta_{E_{c,i}}$	15.101	5.604	2.694	0.007

Table 75: Scenario seven - Log-first approach: Relative importance of best model parameters to explain \hat{E}

	Rel. Importance
$\overline{\ln A_{c,i}}$	0.062
$\beta_{A_{c,i}}$	0.430
$\beta_{E_{c,i}}$	0.066

	Rel. Importance
$\overline{E_{c,i}}$	0.419
$\ln A_{c,i} : \beta_{E_{c,i}}$	0.011
$\beta_{A_{c,i}} : \beta_{E_{c,i}}$	0.012

Table 76: Scenario seven - Log-first approach: Best model for \hat{A}

	Estimate	Std. Error	t.value	Pr(> t)
(Intercept)	0.521	0.276	1.886	0.060
$\ln A_{c,i}$	0.800	0.106	7.539	0.000
$\beta_{A_{c,i}}$	-17.013	2.953	-5.762	0.000
$\beta_{E_{c,i}}$	-6.767	3.695	-1.831	0.067
$\overline{E_{c,i}}$	-0.427	0.074	-5.738	0.000
$\ln A_{c,i} : \beta_{A_{c,i}}$	4.616	1.257	3.671	0.000
$\ln A_{c,i} : \beta_{E_{c,i}}$	2.392	1.435	1.667	0.096
$\beta_{A_{c,i}} : \beta_{E_{c,i}}$	23.623	5.356	4.411	0.000
$\beta_{A_{c,i}} : \overline{E_{c,i}}$	5.345	1.271	4.206	0.000

Table 77: Scenario seven - Log-first approach: Relative importance of best model parameters to explain \hat{A}

	Rel. Importance
$\ln A_{c,i}$	0.774
$\beta_{A_{c,i}}$	0.102
$\beta_{E_{c,i}}$	0.025
$\overline{E_{c,i}}$	0.019
$\ln A_{c,i} : \beta_{A_{c,i}}$	0.024
$\ln A_{c,i} : \beta_{E_{c,i}}$	0.003
$\beta_{A_{c,i}} : \beta_{E_{c,i}}$	0.031
$\beta_{A_{c,i}} : \overline{E_{c,i}}$	0.023

9.4.2 Average-first approach - Best model to explain \hat{E} and \hat{A} based on $\overline{E_{c,i}}$, $\overline{\ln A_{c,i}}$, $\beta_{E_{c,i}}$ and $\beta_{A_{c,i}}$

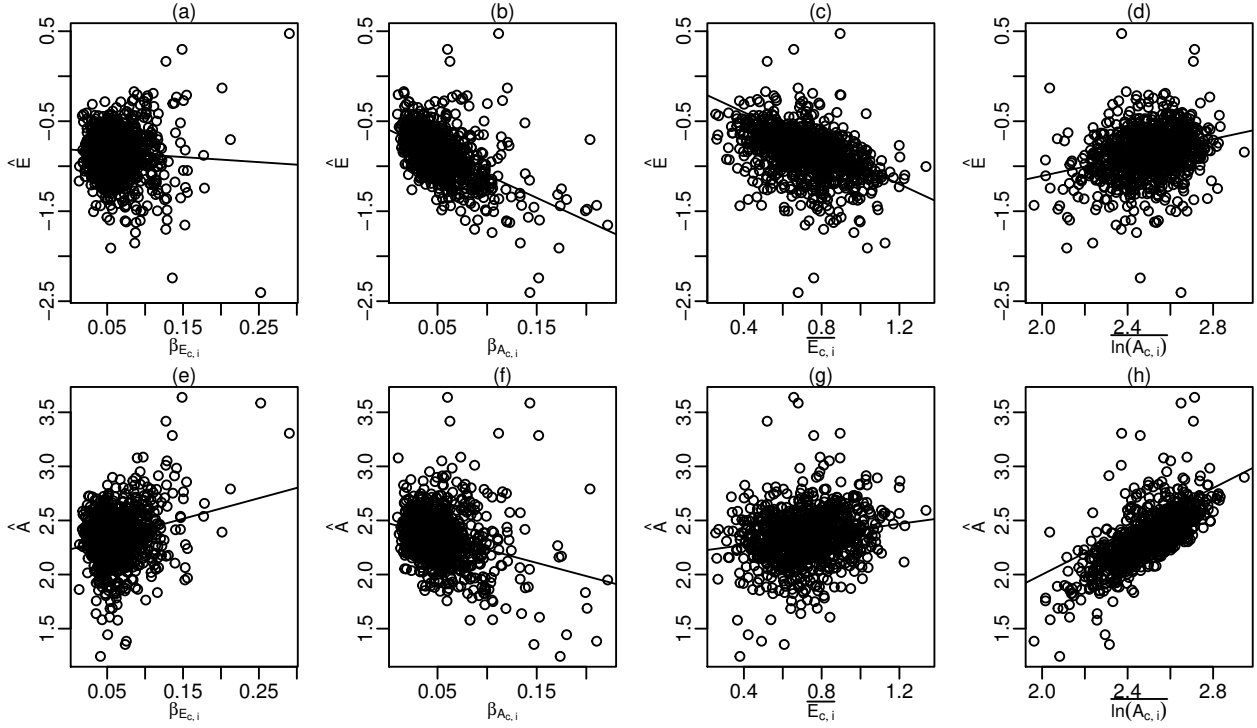


Figure 43: Scenario seven - Average-first approach: Influence of $\beta_{E_{c,i}}$, $\beta_{A_{c,i}}$, $\overline{E_{c,i}}$, and $\overline{\ln A_{c,i}}$ on \hat{E} and \hat{A} . Solid lines depict linear regression relations for all plot except (c) and (h) where a bisection line is plotted since identity relations are expected.

Table 78: Scenario seven - average-first approach: Best model for \hat{E}

	Estimate	Std. Error	t.value	Pr(> t)
(Intercept)	-0.749	0.257	-2.913	0.004
$\overline{\ln A_{c,i}}$	0.277	0.100	2.777	0.006
$\beta_{A_{c,i}}$	-1.756	2.750	-0.638	0.523
$\beta_{E_{c,i}}$	11.168	3.465	3.223	0.001
$\overline{E_{c,i}}$	-0.811	0.034	-23.635	0.000
$\overline{\ln A_{c,i}} : \beta_{A_{c,i}}$	-2.522	1.170	-2.154	0.031
$\overline{\ln A_{c,i}} : \beta_{E_{c,i}}$	-3.548	1.344	-2.641	0.008
$\beta_{A_{c,i}} : \beta_{E_{c,i}}$	14.084	4.990	2.822	0.005

Table 79: Scenario seven - average-first approach: Relative importance of best model parameters to explain \hat{E}

	Rel. Importance
$\overline{\ln A_{c,i}}$	0.068
$\beta_{A_{c,i}}$	0.483
$\beta_{E_{c,i}}$	0.046
$\overline{E_{c,i}}$	0.378

	Rel. Importance
$\overline{\ln A_{c,i}} : \beta_{A_{c,i}}$	0.004
$\ln A_{c,i} : \beta_{E_{c,i}}$	0.010
$\beta_{A_{c,i}} : \beta_{E_{c,i}}$	0.013

Table 80: Scenario seven - average-first approach: Best model for \hat{A}

	Estimate	Std. Error	t.value	Pr(> t)
(Intercept)	0.073	0.163	0.444	0.657
$\overline{\ln A_{c,i}}$	0.919	0.064	14.400	0.000
$\beta_{A_{c,i}}$	-13.071	2.286	-5.718	0.000
$\beta_{E_{c,i}}$	0.357	0.349	1.024	0.306
$\overline{E_{c,i}}$	-0.036	0.060	-0.611	0.541
$\ln A_{c,i} : \beta_{A_{c,i}}$	3.484	0.955	3.648	0.000
$\beta_{A_{c,i}} : \beta_{E_{c,i}}$	19.422	4.155	4.675	0.000
$\beta_{A_{c,i}} : \overline{E_{c,i}}$	3.903	1.018	3.833	0.000

Table 81: Scenario seven - average-first approach: Relative importance of best model parameters to explain \hat{A}

	Rel. Importance
$\overline{\ln A_{c,i}}$	0.706
$\beta_{A_{c,i}}$	0.107
$\beta_{E_{c,i}}$	0.100
$\overline{E_{c,i}}$	0.033
$\ln A_{c,i} : \beta_{A_{c,i}}$	0.014
$\beta_{A_{c,i}} : \beta_{E_{c,i}}$	0.025
$\beta_{A_{c,i}} : \overline{E_{c,i}}$	0.015

9.4.3 LMER approach - Best model to explain \hat{E} and \hat{A} based on $\overline{E_{c,i}}$, $\overline{\ln A_{c,i}}$, $\beta_{E_{c,i}}$ and $\beta_{A_{c,i}}$

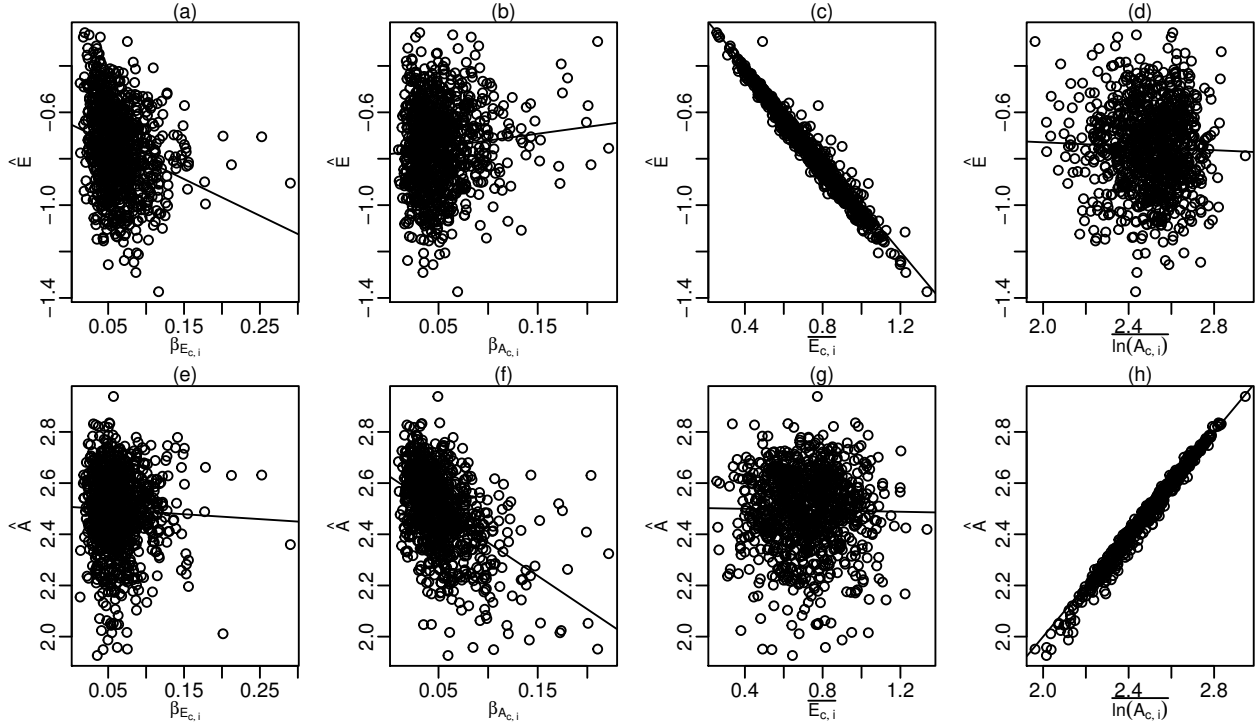


Figure 44: Scenario seven - LMER approach: Influence of $\beta_{E_{c,i}}$, $\beta_{A_{c,i}}$, $\overline{E_{c,i}}$, and $\overline{\ln A_{c,i}}$ on \hat{E} and \hat{A} . Solid lines depict linear regression relations for all plot except (c) and (h) where a bisection line is plotted since identity relations are expected.

Table 82: Scenario seven - lmer approach: Best model for \hat{E}

	Estimate	Std. Error	t.value	Pr(> t)
(Intercept)	-0.532	0.084	-6.313	0.000
$\overline{\ln A_{c,i}}$	0.212	0.032	6.571	0.000
$\beta_{A_{c,i}}$	4.178	0.454	9.197	0.000
$\beta_{E_{c,i}}$	-1.510	0.585	-2.580	0.010
$\overline{E_{c,i}}$	-0.543	0.110	-4.929	0.000
$\overline{\ln A_{c,i}} : \beta_{A_{c,i}}$	-1.679	0.187	-8.989	0.000
$\overline{\ln A_{c,i}} : \beta_{E_{c,i}}$	0.529	0.218	2.429	0.015
$\overline{\ln A_{c,i}} : \overline{E_{c,i}}$	-0.214	0.042	-5.071	0.000
$\beta_{A_{c,i}} : \beta_{E_{c,i}}$	-1.653	0.793	-2.084	0.037
$\beta_{A_{c,i}} : \overline{E_{c,i}}$	0.394	0.226	1.741	0.082
$\beta_{E_{c,i}} : \overline{E_{c,i}}$	0.507	0.201	2.524	0.012

Table 83: Scenario seven - lmer approach: Relative importance of best model parameters to explain \hat{E}

	Rel. Importance
$\overline{\ln A_{c,i}}$	0.001
$\beta_{A_{c,i}}$	0.011

	Rel. Importance
$\beta_{E_{c,i}}$	0.038
$\overline{E_{c,i}}$	0.947
$\ln A_{c,i} : \beta_{A_{c,i}}$	0.002
$\ln A_{c,i} : \beta_{E_{c,i}}$	0.000
$\ln A_{c,i} : \overline{E_{c,i}}$	0.001
$\beta_{A_{c,i}} : \beta_{E_{c,i}}$	0.001
$\beta_{A_{c,i}} : \overline{E_{c,i}}$	0.000
$\beta_{E_{c,i}} : \overline{E_{c,i}}$	0.000

Table 84: Scenario seven - lmer approach: Best model for \hat{A}

	Estimate	Std. Error	t.value	Pr(> t)
(Intercept)	0.148	0.044	3.382	0.001
$\ln A_{c,i}$	0.949	0.017	55.218	0.000
$\beta_{A_{c,i}}$	-1.167	0.260	-4.487	0.000
$\beta_{E_{c,i}}$	0.745	0.344	2.165	0.031
$\overline{E_{c,i}}$	-0.362	0.054	-6.709	0.000
$\ln A_{c,i} : \beta_{A_{c,i}}$	0.336	0.110	3.045	0.002
$\ln A_{c,i} : \beta_{E_{c,i}}$	-0.309	0.129	-2.395	0.017
$\ln A_{c,i} : \overline{E_{c,i}}$	0.143	0.021	6.665	0.000
$\beta_{A_{c,i}} : \beta_{E_{c,i}}$	2.575	0.465	5.537	0.000
$\beta_{E_{c,i}} : \overline{E_{c,i}}$	-0.283	0.114	-2.487	0.013

Table 85: Scenario seven - lmer approach: Relative importance of best model parameters to explain \hat{A}

	Rel. Importance
$\ln A_{c,i}$	0.884
$\beta_{A_{c,i}}$	0.108
$\beta_{E_{c,i}}$	0.004
$\overline{E_{c,i}}$	0.001
$\ln A_{c,i} : \beta_{A_{c,i}}$	0.000
$\ln A_{c,i} : \beta_{E_{c,i}}$	0.000
$\ln A_{c,i} : \overline{E_{c,i}}$	0.000
$\beta_{A_{c,i}} : \beta_{E_{c,i}}$	0.002
$\beta_{E_{c,i}} : \overline{E_{c,i}}$	0.000